

PHASE RETRIEVAL FROM CONTINUOUS AND DISCRETE
PTYCHOGRAPHIC MEASUREMENTS

By

Sami Eid Merhi

A DISSERTATION

Submitted to
Michigan State University
in partial fulfillment of the requirements
for the degree of

Mathematics — Doctor of Philosophy

2019

ABSTRACT

PHASE RETRIEVAL FROM CONTINUOUS AND DISCRETE PTYCHOGRAPHIC MEASUREMENTS

By

Sami Eid Merhi

In this dissertation, we present and study two novel approaches to phase retrieval – an inverse problem in which one attempts to reconstruct a complex-valued function (or vector) from phaseless (or magnitude-only) measurements. Phase retrieval arises in several scientific areas including bio-chemistry, optics, astronomy, quantum mechanics, and speech signal processing. Early solutions to phase retrieval, although practical, lacked robustness guarantees. To this day, practitioners in scientific imaging are still seeking demonstrably stable and robust recovery algorithms.

Ptychography is a form of coherent diffractive imaging where diffraction patterns are processed by algorithms to recover an image of a specimen. More specifically, small regions of a specimen are illuminated one-at-a-time, and a detector captures the intensities of the resulting diffraction patterns. As such, the measurements are *local* and *phaseless*. In this work, we present two algorithms to recover signals from ptychographic measurements. The first algorithm aims to recover a discrete one-dimensional signal from discrete spectrogram measurements via a modified Wigner distribution deconvolution (WDD) method. While the method is known to practitioners of scientific imaging, robustness and recovery guarantees are lacking, if not absent; our contribution is to supply such guarantees.

The second algorithm aims to approximately recover a compactly supported function from continuous spectrogram measurements via lifting and angular synchronization. This setup can be interpreted as the infinite-dimensional equivalent of discrete ptychographic imaging.

Our contribution is a model which assumes infinite-dimensional signals and measurements *ab initio*, as opposed to most recent algorithms in which discrete models are a necessity.

Finally, we consider the worst-case noise robustness of any phase retrieval algorithm which aims to reconstruct all nonvanishing vectors from the magnitudes of an arbitrary collection of local correlation measurements. The robustness results provided therein apply to a wide range of ptychographic imaging scenarios. In particular, our contribution is to show that stable recovery of high-resolution images of extremely large samples is likely to require a vast number of measurements, independent of the recovery algorithm employed.

The first chapter introduces the phase retrieval problem and presents historical context, as well as applications in which phase retrieval manifests. In addition, we introduce ptychography, discuss existing WDD formulations, and compare these to our contribution in the discrete setting. Chapter 2 provides recovery guarantees for using aliased WDD methods to solve the phase retrieval problem in a discrete setting with sub-sampled measurements. In Chapter 3 we provide lower Lipschitz bounds for generic phase retrieval algorithms from locally supported measurements. Finally, Chapter 4 presents a numerical method to recover compactly supported functions from local measurements via lifting and angular synchronization.

This dissertation is dedicated to my loving parents, Antoinette Asmar and Eid Merhi.

For even as He loves the arrow that flies, so He loves also the bow that is stable.

- Gibran Khalil Gibran, The Prophet

ACKNOWLEDGMENTS

When you part from your friend, you grieve not; for that which you love most in him may be clearer in his absence, as the mountain to the climber is clearer from the plain.

- Gibran Khalil Gibran, The Prophet

This dissertation is the fruit of wonderful relationships established during my years of study at Michigan State University. On a personal level, the camaraderie I enjoyed with fellow doctoral students helped ease the frustration of graduate school. Professionally, the mentorship and guidance I received from my advisor and collaborators set me up for academic fulfillment. I would like to dedicate a few paragraphs to thank the people who unequivocally contributed to my well-being and success.

First and foremost, I would like to thank my advisor, Dr. Mark Iwen, for all he has done for me during my years at Michigan State University. Your class on compressive sensing showed me how practical harmonic analysis can be, and how fun pages and pages of computations are. Whenever we hit a research wall, somehow you managed to find a way around it. Your tenacity is infectious. I appreciate how dedicated you are not only to your work and your career, but also to the success of your students and collaborators. To say I have had the pleasure to work with you is an understatement. Thank you for your time, your guidance, and your understanding.

I would also like to thank Aditya Viswanathan, who collaborated on my research both as a postdoctoral fellow and assistant professor. Your experience in programming and computation were invaluable to me, and I learned more from reading your scripts than from any other source. Your readiness to answer questions and debug problems is appreciated. You have been great help to me, and for that I'm forever grateful. While on the topic of

co-authorship, I would also like to thank Michael Perlmutter for his collaboration on my research, and for the valuable feedback he's provided.

My years of studying and teaching at MSU were made enjoyable thanks to an amazing staff, good friends, and wonderful teachers. I would specifically like to thank Tsveta Sendova and Andrew Krause for giving me the opportunity to mentor fellow graduate students, and to grow in leadership. I'm grateful to Ryan Maccombs for making the tedious aspects of setting up courses disappear. I couldn't possibly thank all the friends I made at MSU, for they are many. And yet, I would like to mention those who shared in my accomplishments and helped me through the difficult times. Rami, Wenzhao, Charlotte, Paata, Nick, Andy, Tyler, Guillermo, Reshma, Hitesh, Max, and Arman: thank you for being a memorable part of my story. I am deeply thankful and grateful for Megan; you have been such a great companion over the past two years, and have brought so much happiness and joy into my life. Thank you for running this race and for celebrating with me at the finish line.

Many of the faculty at MSU helped nourish my interest in applied mathematics generally, and applied harmonic analysis specifically. I would like to thank Dr. Yingda Cheng for running a pleasurable class in applied methods for ODEs, and Dr. Selin Aviyente for her invaluable class in wavelets and time-frequency analysis. Both Dr. Cheng and Dr. Aviyente served on my comprehensive exam committee, and with Dr. Zhengfang Zhou, also served on my dissertation committee; for that I'm deeply grateful.

My mathematical journey started at Western Connecticut State University, and I would be remiss if I didn't mention, and thank, Dr. Xiaodi Wang, who played an exceptional role in introducing me to research in applied math. You were instrumental in guiding me and preparing me for a graduate track. WCSU hosted a group of influential educators who, in one way or another, prepared me for teaching at MSU. Thanks are due to Dr. Lubell, Dr.

Rocca, Dr. Novozhilova, Dr. Burns, Dr. Mittag, Dr. Lightwood, and Dr. Hamer, for the wonderful experiences I had in your classrooms. I would also like to thank Pierce O'Donnell, who, along with being my first collaborator, has been my best friend and close confidant for years. Your friendship has been indispensable to me.

Lastly, but most importantly, I am forever grateful for having a supportive family. I couldn't have asked for better siblings; Celina and Anthony, thank you for laughing at my silly jokes, and for listening when no one else could. Mom and Dad, you are the kind of parents everyone wishes they had. Your support and encouragement helped me along the way, and the prospect of making you proud got me to the finish line. We did it!

TABLE OF CONTENTS

LIST OF FIGURES	x
KEY TO SYMBOLS	xi
KEY TO ABBREVIATIONS	xii
Chapter 1 History of Phase Retrieval and Ptychography	1
1.1 Problem Definition and Applications	1
1.2 Existing Solutions to Phase Retrieval	3
1.2.1 Alternating Projections	3
1.2.2 PhaseLift	5
1.2.3 Wirtinger Flow	6
1.3 Ptychography	8
1.3.1 Experimental Setup	8
1.3.2 Ptychography and Continuous Wigner Distribution Deconvolution	9
1.3.3 Ptychography via Discrete Wigner Distribution Deconvolution	13
1.3.3.1 Notation and Basic Properties of the DFT	13
1.3.3.2 Wigner Distribution Deconvolution in the Discrete Setting	17
Chapter 2 Phase Retrieval via Aliased Wigner Distribution Deconvolution and Angular Synchronization	19
2.1 Aliased WDD for Phase Retrieval	21
2.1.1 Sub-sampling in Frequency	22
2.1.2 Sub-sampling in Frequency and Space	24
2.1.3 Recovering Diagonals of $\widehat{\mathbf{x}}\widehat{\mathbf{x}}^*$	26
2.1.3.1 A Special Case of Theorem 2.1.1	37
2.1.4 Other Support Conditions	40
2.1.4.1 A Special Case of Lemma 2.1.6.	43
2.2 Numerical Results	51
2.2.1 Empirical Validation of Theorem 2.1.1 (Algorithm 1)	53
2.2.2 Empirical Validation of Lemma 2.1.5	58
2.2.3 Empirical Validation of Theorem 2.1.2 (Algorithm 2)	62
Chapter 3 Lower Lipschitz Bounds for Phase Retrieval from Locally Supported Measurements	63
3.1 Introduction and Statement of Results	64
3.1.1 Related Work and Implications	67
3.1.2 Main Results	70
3.2 The Proofs of Theorem 3.1.1 and Theorem 3.1.2	72
3.3 Examples: Lower Bounds for Specific Measurement Masks	77
3.3.1 Windowed Fourier Measurement Masks	77

3.3.2	Two-Shot Measurement Masks	81
3.4	Discussion and Future Work	84
Chapter 4	Recovery of Compactly Supported Functions from Spectro-	
	gram Measurements via Lifting	86
4.1	Introduction	87
4.1.1	The Problem Statement and Specifications	88
4.1.2	The Proposed Numerical Approach	89
4.2	Our Lifted Formulation	90
4.2.1	Obtaining a Truncated, Finite Lifted Linear System	93
4.3	Numerical Results	97
4.4	Future Work	100
APPENDIX	101
REFERENCES	105

LIST OF FIGURES

Figure 1.3.1: Experimental setup for fly-scan ptychography. Adapted from “Fly-scan ptychography”, Huang et al., Scientific Reports 5 (9074), 2015.	8
Figure 2.2.1: Selection of HIO+ER iteration parameters. $(\text{HIO}, \text{ER}) = (x, y)$ indicates that every set of x iterations of the HIO algorithm was followed by a set of y iterations of the ER algorithm.	52
Figure 2.2.2: Reconstruction accuracy with and without HIO+ER (60 iterations) post-processing, improved magnitude estimation.	54
Figure 2.2.3: Reconstruction accuracy vs. number of shifts L	55
Figure 2.2.4: Reconstruction accuracy vs. added noise.	57
Figure 2.2.5: Execution time vs. signal size d	57
Figure 2.2.6: Reconstruction accuracy with and without HIO+ER (60 iterations) post-processing, improved magnitude estimation, and comparison with results from [36].	59
Figure 2.2.7: Reconstruction accuracy vs. number of Fourier modes K	60
Figure 2.2.8: Reconstruction accuracy vs. added noise.	61
Figure 2.2.9: Execution time versus signal size d	61
Figure 2.2.10: Reconstruction accuracy vs. added noise.	62
Figure 4.3.1: Modulated Gaussian signal and 11 shifts of a Gaussian window.	97
Figure 4.3.2: True Gaussian signal and its reconstruction.	97
Figure 4.3.3: True modulated Gaussian signal and its reconstruction.	98
Figure 4.3.4: Characteristic function and its reconstruction.	98
Figure 4.3.5: Piecewise continuous function and its reconstruction.	98

KEY TO SYMBOLS

The following is a list of some of the notation used throughout this paper.

- For $d \in \mathbb{N}$, $[d]_0 := \{0, 1, \dots, d-1\}$ is the set of remainders modulo d .
- For $d \in \mathbb{N}$, $[d] := \{1\} + [d]_0 = \{1, 2, \dots, d\}$.
- $L^1(\mathbb{R})$, the set of integrable functions on \mathbb{R} .
- $L^2(\mathbb{R})$, the set of square-integrable functions on \mathbb{R} .
- $\|\cdot\|_2, \|\cdot\|_F, \|\cdot\|_\infty$, the Euclidean, Frobenius, and supremum norms, respectively.
- $\|\cdot\|_{L^2} := \|\cdot\|_{L^2(\mathcal{H})}$, the L^2 norm on the Hilbert space \mathcal{H} .
- $\langle \mathbf{x}, \mathbf{y} \rangle$, the complex inner product of $\mathbf{x}, \mathbf{y} \in \mathbb{C}^d$.
- \mathcal{F} , the Fourier transform on $L^2(\mathbb{R})$.
- F_d , the $d \times d$ Fourier transform matrix; also denoted F when dimension is clear.
- $*$, the continuous convolution operator on $L^2(\mathbb{R}) \times L^2(\mathbb{R})$.
- $*_d$, the discrete convolution operator on $\mathbb{C}^d \times \mathbb{C}^d$.
- \circ , the componentwise Hadamard product.
- I , the identity matrix.
- M^* , the Hermitian (conjugate) transpose of matrix M .
- $\text{diag}(M)$, the diagonal of matrix M .
- $\sigma_{\min}(M)$, the smallest singular value of matrix M .
- $M \succeq 0$ denotes a positive semi-definite matrix M .
- $|S|$, the cardinality of set S .
- χ_S , the characteristic (or indicator) function of set S .
- $\mathbf{x}|_S$, the restriction of vector \mathbf{x} to the index set S .
- ∇f , the gradient of function f .
- $\mathcal{N}(0, 1)$, the standard normal distribution.
- $\text{sinc}(x) := \sin(x)/x$, the unnormalized sinc function at x .

KEY TO ABBREVIATIONS

- AP, the Alternating Projections algorithm.
- CCD, charge-coupled device.
- DFT, the discrete Fourier transform.
- ePIE, the extended Ptychographic Iterative Engine.
- FFT, the Fast Fourier transform.
- HIO+ER, the Hybrid Input-Output + Error Reduction algorithm.
- PIE, the Ptychographic Iterative Engine.
- SNR, signal-to-noise ratio.
- STFT, the short-time Fourier transform.
- WDD, the Wigner distribution deconvolution.
- WDF, the Wigner distribution function.
- WF, the Wirtinger Flow algorithm.

Chapter 1

History of Phase Retrieval and Ptychography

1.1 Problem Definition and Applications

Phase retrieval in the discrete setting is the process of algorithmically recovering an estimate to a vector $\mathbf{x} \in \mathbb{C}^d$ from D (possibly noisy) measurements of the form

$$\mathbf{y} = |B\mathbf{x}|^2 + \eta \in \mathbb{C}^D. \quad (1.1.1)$$

Here, $B \in \mathbb{C}^{D \times d}$ is (usually) a known measurement matrix, and $\eta \in \mathbb{C}^D$ is an additive noise vector. The operator $|\cdot|^2$ represents the componentwise magnitude squared operation, so that

$$\left(|\mathbf{u}|^2\right)_n := |u_n|^2 \quad \forall \mathbf{u} := (u_0, \dots, u_{d-1})^T \in \mathbb{C}^d.$$

A simple inspection of (1.1.1) shows that any solution to the phase retrieval problem is only possibly unique up to a global phase factor. More precisely, if $\mathbf{x}_0 \in \mathbb{C}^d$ solves (1.1.1), then so does $e^{i\theta}\mathbf{x}_0$ for any $\theta \in [0, 2\pi)$. This phase ambiguity means that any phase retrieval

algorithm aims to find a unique solution to (1.1.1) under the equivalence relation

$$\mathbf{u} \sim \mathbf{v} \iff \mathbf{u} = \lambda \mathbf{v}$$

for some $\lambda \in \mathbb{C}$ with $|\lambda| = 1$.

Phase retrieval originates from the fact that light detectors, such as photographic plates or charge-coupled devices (CCDs), can often times only measure the intensity of incident light. This is because these devices respond only to the number and energy of photons arriving at their surface. More specifically, these detectors record the squared magnitude of the Fresnel or Fraunhofer diffraction pattern of the radiation that is scattered from an object. These measurements are therefore incomplete, because a light wave has not only an amplitude (related to the intensity), but also a phase, which is systematically lost in a measurement. It is important to note that the phase part of the wave often encodes relevant information about the specimen of interest, especially in diffraction or microscopy experiments.

Historically, the first application of phase retrieval is X-ray crystallography [29, 45], a technique used for determining the atomic structure of a crystal, in which the crystalline arrangement causes a beam of incident X-rays to diffract into many specific directions. X-ray crystallography is still the primary method for characterizing the atomic structure of new materials and in discerning materials that appear similar by other experiments.

Other areas of imaging science in which phase retrieval is employed include diffraction imaging [11, 52], optics [59], electron microscopy [32], astronomy [21], and X-ray tomography [19], to name a few. Phase retrieval also appears in solutions to problems in quantum mechanics [18], speech recognition and audio processing [46, 4, 56], and self-calibration [40].

1.2 Existing Solutions to Phase Retrieval

Prior to algorithmic solutions to phase retrieval, practitioners had to invent, and contend with, *ad hoc* methods to resolve their phaseless imaging experiments. Indeed, the 1915 Nobel Prize in Physics was awarded jointly to Sir William Henry Bragg and his son, William Lawrence Bragg, for their geometric analysis of crystal structures by means of X-rays. It was not until the 1970s that a systematic method for phase retrieval came to the scene, and showed promise outside the X-ray crystallography regimen. The method, called *Alternating Projections* (AP), was proposed by Gerchberg and Saxton in 1971 [24], and later refined and improved. In the sections below, we provide brief outlines of the generic AP algorithm, as well as more recent numerical methods for phase retrieval which enjoy theoretical recovery guarantees.

1.2.1 Alternating Projections

By and large, the most popular methods for phase retrieval from over-sampled data are alternating projections (AP) algorithms pioneered by Gerchberg and Saxton [24] and Fienup [22, 23]. AP algorithms provided great improvements over *ad hoc* methods, since they could be applied to fairly general data, with very minimal assumptions made on the structure of the specimen being imaged.

A typical AP algorithm works in the following manner. Suppose one has to recover $\mathbf{x} \in \mathbb{C}^d$ from the measurements $\mathbf{y} = |\mathbf{A}\mathbf{x}|$, where the D rows of $A \in \mathbb{C}^{D \times d}$ are a frame, and $D \geq d$. Two pieces of information are available concerning the solution of this phase retrieval problem: the solution has amplitude \mathbf{y} and is located on the range of A , denoted

R_A . One then defines a *phase correction* operator $P_A : \mathbb{C}^D \rightarrow \mathbb{C}^D$ as

$$P_A := A(A^*A)^{-1}A^*,$$

which projects a complex vector to R_A , and an *amplitude correction* operator $P_{\mathbf{y}} : \mathbb{C}^d \rightarrow \mathbb{C}^d$, defined for all $\mathbf{u} \in \mathbb{C}^D$ componentwise by

$$(P_{\mathbf{y}}\mathbf{u})_j := y_j \frac{u_j}{|u_j|} \chi_{u_j} + y_j (1 - \chi_{u_j}).$$

As such, $P_{\mathbf{y}}$ substitutes the amplitude u_j by y_j and preserves phase information.

With the notation above, solving the phase retrieval problem amounts to finding a vector $\mathbf{x}_0 \in \mathbb{C}^D$ which is a fixed point of both operators P_A and $P_{\mathbf{y}}$; that is, \mathbf{x}_0 satisfies the two conditions

$$\|(\mathbf{x}_0 - P_A\mathbf{x}_0)\| = 0 \text{ and } \|\mathbf{x}_0 - P_{\mathbf{y}}\mathbf{x}_0\| = 0.$$

The unknown \mathbf{x} may then be estimated as $(A^*A)^{-1}A^*\mathbf{x}_0$.

The AP algorithm gets its name from the iterative scheme used to find the fixed point \mathbf{x}_0 :

$$\mathbf{g}_{j+1/2} := P_{\mathbf{y}}\mathbf{g}_j, \quad \mathbf{g}_{j+1} := P_A\mathbf{g}_{j+1/2},$$

where j ranges over \mathbb{N} and \mathbf{g}_0 is the initial guess.

Marchesini and his collaborators proved in 2015 that AP algorithms using generic measurements are guaranteed to converge when provided with a sufficiently accurate initial guess [43]. To this day, no global recovery guarantees exist for AP algorithms in the case of local measurements. These algorithms will converge when provided with an accurate enough

initialization; however, the geometry of the basin of attraction is unknown. Although easy to state and explain, Marchesini et al. argue that AP algorithms often require careful exploitation of signal constraints and delicate parameter selection to increase the likelihood of convergence. For instance, our knowledge may be that the signal is real-valued, positive, band-limited, or spatially-limited. More can be said about AP algorithms when the measurements are Gaussian. For example, Waldspurger has argued that when provided with Gaussian measurements, spectral initialization is sufficiently accurate for AP algorithms [58].

1.2.2 PhaseLift

In 2011, Emmanuel J. Candès and his collaborators proposed *PhaseLift*, an algorithm based on convex programming, to solve the phase retrieval problem [14]. Their approach included two main components: *multiple structured illuminations*, as is the case in ptychographic imaging, and the formulation of phase recovery as a *matrix completion problem*.

To summarize the PhaseLift algorithm, let us pose the phase retrieval problem as

$$\text{Find } \mathbf{x} \in \mathbb{C}^d \text{ satisfying } |\langle \mathbf{x}, \mathbf{a}_k \rangle|^2 = y_k \quad \forall k \in [D]_0 := \{0, 1, \dots, D-1\}. \quad (1.2.1)$$

Let us now denote by X the rank-one matrix $\mathbf{x}\mathbf{x}^*$, and by A_k the rank-one matrix $\mathbf{a}_k\mathbf{a}_k^*$. Moreover, let \mathcal{A} denote the linear operator mapping positive semi-definite matrices into $\{\text{Tr}(A_k X) : k \in [D]_0\}$. Then the phase retrieval problem is equivalent to

$$\begin{array}{ll} \text{find} & X \\ \text{subject to} & \begin{cases} \mathcal{A}(X) = \mathbf{y} \\ X \succeq 0 \\ \text{rank}(X) = 1 \end{cases} \end{array} \iff \begin{array}{ll} \text{minimize} & \text{rank}(X) \\ \text{subject to} & \begin{cases} \mathcal{A}(X) = \mathbf{y} \\ X \succeq 0. \end{cases} \end{array}$$

Once the left-hand side of the problem above is solved, the rank-one solution X can

be factorized as $\mathbf{x}\mathbf{x}^*$, hence finding solutions to the phase retrieval problem up to a global phase, if the linear operator \mathcal{A} is well-behaved. The problem above is a rank minimization problem over an affine slice of the positive semi-definite cone. As such, it falls in the realm of low-rank matrix completion or matrix recovery.

Since the minimization problem above is NP hard, the authors propose using the trace norm as a convex surrogate for the rank functional, giving the semi-definite program

$$\begin{aligned} & \text{minimize} && \text{Trace}(X) \\ & \text{subject to} && \begin{cases} \mathcal{A}(X) = \mathbf{y} \\ X \succeq 0. \end{cases} \end{aligned}$$

One should note that while SDP based relaxation methods provide tractable solutions, they become computationally prohibitive as the dimension d of the signal increases.

1.2.3 Wirtinger Flow

In 2015, Candès, Li, and Soltanolkotabi developed a non-convex formulation of the phase retrieval problem, and proposed a solution algorithm [13]. The algorithm, referred to as *Wirtinger Flow* (WF), relies on a spectral initialization and update rules of low computational complexity.

The WF algorithm works as follows. Consider the phase retrieval problem as stated in (1.2.1). Set

$$\lambda^2 = d \frac{\sum_k y_k}{\sum_k \|\mathbf{a}_k\|^2}.$$

Then the initial guess, \mathbf{g}_0 , is the leading eigenvector (normalized so that $\|\mathbf{g}_0\| = \lambda$) of the matrix

$$Y = \frac{1}{D} \sum_{k=1}^D y_k \mathbf{a}_k \mathbf{a}_k^*.$$

The guess is updated via the following steepest-descent recursion:

$$\mathbf{g}_{j+1} = \mathbf{g}_j - \frac{\alpha_{j+1}}{\|\mathbf{g}_0\|^2} \nabla f(\mathbf{g}_j),$$

where α_{j+1} is the step size, and $f : \mathbb{C}^d \rightarrow \mathbb{R}$ is the loss function

$$f(\mathbf{u}) := \frac{1}{2D} \sum_{k=1}^D \left(y_k - |\mathbf{a}_k^* \mathbf{u}|^2 \right)^2.$$

The authors in [13] motivate the spectral initialization step by considering the simple case where everything is real-valued, and the measurement vectors \mathbf{a}_k are i.i.d. $\mathcal{N}(0, I)$. In this case, the matrix Y is equal to $I + 2\mathbf{x}\mathbf{x}^*$ in the limit of large samples. Moreover, the top eigenvector of $I + 2\mathbf{x}\mathbf{x}^*$ is of the form $\lambda\mathbf{x}$ for some positive scalar λ . This means that \mathbf{x} can be recovered perfectly by the initialization step, up to a global sign ± 1 .

Both PhaseLift [15, 28] and Wirtinger Flow [13] achieve recovery guarantees with high probability when using $\mathcal{O}(d \log^4 d)$ masked Fourier coded diffraction pattern measurements, but stop short, however, of providing guarantees when the measurements are not randomized.

We end this section by noting that the methods aforementioned do not provide theoretical recovery guarantees for locally supported and deterministic measurements of the type encountered in ptychography.

1.3 Ptychography

1.3.1 Experimental Setup

Ptychography is a computational method of microscopic imaging, in which images are generated by processing a large number of coherent diffraction patterns that have been scattered from a specimen of interest. The interference patterns are generated by a constant function, say a field of illumination, moving laterally by a known amount with respect to the specimen. As such, ptychography is translation-invariant. The interference patterns are captured by a detector, some distance away from the specimen, so that the scattered waves fold into one another. This explains the origin of the name: *ptycho* in Greek means *to fold*.

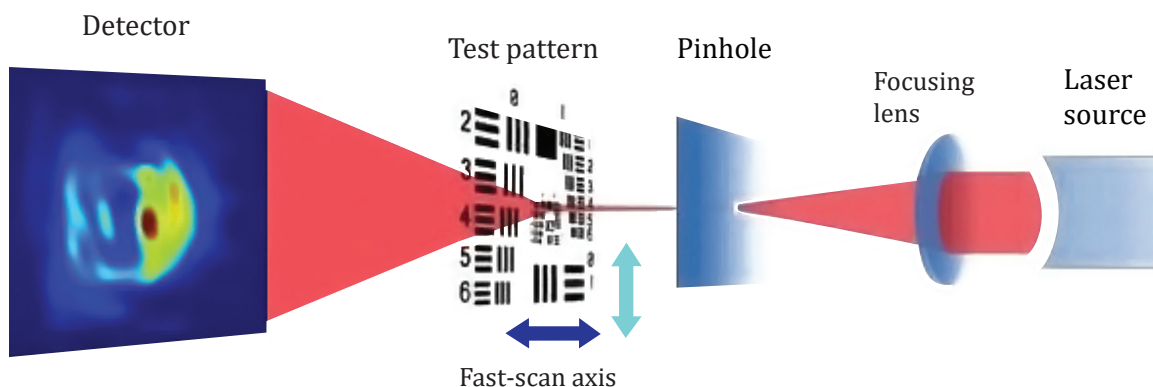


Figure 1.3.1: Experimental setup for fly-scan ptychography. Adapted from “Fly-scan ptychography”, Huang et al., Scientific Reports 5 (9074), 2015.

The name “ptychography” was coined by Hegerl and Hoppe in 1972 [30] to describe a solution to the crystallographic phase problem first suggested by Hoppe in 1969 [31]. In this early stage, the concept required the specimen to be a crystal, and to be exposed to a precisely engineered wave, so that only two pairs of diffraction peaks interfere with one another at a time. The Fourier shift theorem implies that a shift in the illumination changes the interference condition. This means that two ptychographic measurements can

be used to solve for phase differences between the diffraction peaks, by breaking a complex-conjugate ambiguity that would otherwise exist [52]. In non-crystalline objects, millions of beams interfere at the same time, making the phase differences inseparable; for this reason, crystalline ptychography could not be used to image continuous media.

Between the years 1989 and 2007 Rodenburg and his colleagues created multiple inversion methods for the general ptychographic phase problem, including Wigner distribution deconvolution (WDD) [49], SSB [50], the *PIE* iterative method [51] (a precursor of the *ePIE* algorithm [41]), demonstrating proof-of-principles at different wavelengths. Chapman used Wigner deconvolution to demonstrate the first implementation of X-ray ptychography in 1996 [17]. The poor quality of detectors and rudimentary computing abilities of the time may account for the limited adoption of ptychography by other practitioners.

1.3.2 Ptychography and Continuous Wigner Distribution Deconvolution

In this section, we introduce the method of Wigner distribution deconvolution as presented by Rodenburg and Bates [49], discuss how it applies to phase retrieval in the continuous setting, and present novel ideas in the case of discrete measurements. A more thorough discussion on WDD, and a further expansion of the method, are the subject of Chapter 2.

Let $\mathcal{F} : L^2(\mathbb{R}) \rightarrow L^2(\mathbb{R})$ denote the continuous Fourier transform, defined via:

$$\mathcal{F}\{h\}(\omega) := \int_{-\infty}^{\infty} h(t) e^{-2\pi i \omega t} dt. \quad (1.3.1)$$

Let $f : \mathbb{R} \rightarrow \mathbb{C}$ denote an unknown specimen, and $g : \mathbb{R} \rightarrow \mathbb{C}$ denote a known *mask* or *window* function. The short-time Fourier transform of f at a physical shift $\ell \in \mathbb{R}$ and

frequency $\omega \in \mathbb{R}$, given the window function g , is defined as

$$STFT\{f, g\}(\ell, \omega) := \mathcal{F}\{f \cdot S_{-\ell}g\}(\omega), \quad (1.3.2)$$

where S_t is the shift operator defined so that $(S_t g)(x) = g(x + t)$. To each STFT measurement $STFT\{f, g\}(\ell, \omega)$ corresponds a *spectrogram* measurement $b(\ell, \omega)$ formed by squaring the absolute value:

$$b(\ell, \omega) := |STFT\{f, g\}(\ell, \omega)|^2. \quad (1.3.3)$$

Spectrogram measurements are ptychographic in nature, since the mask or window function g may be seen as a spatially-limited probe function, the function f represents an unknown specimen, and $b(\ell, \omega)$ represents a phaseless intensity measurement as captured by a detector. One is then interested in recovering f from a finite number of such spectrogram measurements. The WDD method does so due to the following equality:

$$\mathcal{F}\{\mathcal{F}\{b\}(\omega')\}(\ell') = \mathcal{F}\{f \cdot \overline{S_{\omega'}f}\}(\ell') \cdot \mathcal{F}\{g \cdot \overline{S_{-\omega'}g}\}(\ell') \quad (1.3.4)$$

for all $(\ell', \omega') \in \mathbb{R} \times \mathbb{R}$. In simple terms, applying the continuous Fourier transform twice to the spectrogram measurements, first in the frequency variable and then in the spacial variable, leads to a *decoupling* of the unknown function f from the known mask g .

For the sake of completeness, we present a computational proof of (1.3.4). The proof uses the following elementary properties of the Fourier transform as defined in (1.3.1), which hold for any $h : \mathbb{R} \rightarrow \mathbb{C}$:

$$|\mathcal{F}\{h\}|^2 = \mathcal{F}\{h * \overline{\tilde{h}}\},$$

$$\mathcal{F}\{\mathcal{F}\{h\}\} = \tilde{h},$$

where $*$ denotes the convolution operator, and \tilde{h} is the reversal of h about zero, so that $\tilde{h}(t) = h(-t)$ for all $t \in \mathbb{R}$. Now observe that for $(\ell, \omega) \in \mathbb{R} \times \mathbb{R}$,

$$\begin{aligned} b(\ell, \omega) &= \left| \int_{-\infty}^{\infty} f(t) g(t - \ell) e^{-2\pi i \omega t} dt \right|^2 \\ &= |\mathcal{F}\{f \cdot S_{-\ell} g\}(\omega)|^2 \\ &= \mathcal{F}\left\{(f \cdot S_{-\ell} g) * \left(\tilde{f} \cdot \overline{S_{-\ell} g}\right)\right\}(\omega). \end{aligned}$$

Upon taking a Fourier transform in the ω variable, at ω' , one gets

$$\begin{aligned} \mathcal{F}\{b(\ell, \cdot)\}(\omega') &= \mathcal{F}\left\{\mathcal{F}\left\{(f \cdot S_{-\ell} g) * \left(\tilde{f} \cdot \overline{S_{-\ell} g}\right)\right\}\right\}(\omega') \\ &= \left((f \cdot S_{-\ell} g) * \left(\tilde{f} \cdot \overline{S_{-\ell} g}\right)\right)(-\omega') \\ &= \int_{-\infty}^{\infty} f(t) g(t - \ell) \left(\tilde{f} \cdot \overline{S_{-\ell} g}\right)(-t - \omega') dt \\ &= \int_{-\infty}^{\infty} f(t) g(t - \ell) \overline{f(t + \omega') \cdot g(t - \ell + \omega')} dt \\ &= \int_{-\infty}^{\infty} f(t) S_{\omega'} \bar{f}(t) g(t - \ell) S_{\omega'} \bar{g}(t - \ell) dt \\ &= \int_{-\infty}^{\infty} (f \cdot S_{\omega'} \bar{f})(t) \cdot \left(\tilde{g} \cdot S_{-\omega'} \bar{\tilde{g}}\right)(\ell - t) dt \\ &= \int_{-\infty}^{\infty} f_{\omega'}(t) g_{-\omega'}(\ell - t) dt, \end{aligned}$$

where

$$\begin{aligned} f_{\omega'}(t) &:= (f \cdot S_{\omega'} \bar{f})(t), \\ g_{-\omega'}(t) &:= \left(\tilde{g} \cdot S_{-\omega'} \bar{\tilde{g}}\right)(t). \end{aligned}$$

Therefore, we have

$$\begin{aligned}
\mathcal{F}\{b(\ell, \cdot)\}(\omega') &= \int_{-\infty}^{\infty} f_{\omega'}(t) g_{-\omega'}(\ell - t) dt \\
&= (f_{\omega'} * g_{-\omega'}) (\ell) \\
&= \left((f \cdot S_{\omega'} \bar{f}) * (\tilde{g} \cdot S_{-\omega'} \tilde{\bar{g}}) \right) (\ell).
\end{aligned}$$

Taking a Fourier transform one last time, in the ℓ variable, at ℓ' , yields

$$\mathcal{F}\{\mathcal{F}\{b\}(\omega')\}(\ell') = \mathcal{F}\{f \cdot S_{\omega'} \bar{f}\}(\ell') \cdot \mathcal{F}\{\tilde{g} \cdot S_{-\omega'} \tilde{\bar{g}}\}(\ell'),$$

by the Convolution Theorem. This proves (1.3.4).

The WDD method gets its name from observing that each of the Fourier transforms on the right-hand side of (1.3.4) is a *Wigner distribution function*. Namely,

$$\mathcal{F}\{f \cdot S_{\omega'} \bar{f}\}(\ell') = WDF_f(\omega', \ell'), \tag{1.3.5}$$

$$\mathcal{F}\{\tilde{g} \cdot S_{-\omega'} \tilde{\bar{g}}\}(\ell') = WDF_{\tilde{g}}(-\omega', \ell'), \tag{1.3.6}$$

where the Wigner distribution function of h at (u, v) is defined as

$$WDF_h(u, v) := \int_{-\infty}^{\infty} h(t) \overline{h(t+u)} e^{-2\pi i vt} dt. \tag{1.3.7}$$

In Chapter 4, we propose a different approach to recover compactly supported functions from their spectrograms. The method does not require applications of Fourier transforms, but rather a rewriting of the phaseless measurements in a lifted form. Angular synchronization is then used to solve for a vectorized version of the infinite dimensional specimen.

1.3.3 Ptychography via Discrete Wigner Distribution Deconvolution

In this section, we define a discrete Wigner distribution deconvolution method for recovering a discrete signal from its spectrogram measurements. To be precise, we define such (noiseless) measurements as follows. Let $\mathbf{x}, \mathbf{m} \in \mathbb{C}^{d \times 1}$ denote specimen and mask, respectively. The spectrogram of \mathbf{x} given mask \mathbf{m} at a physical shift $\ell \in [d]_0$ and Fourier mode $k \in [d]_0$ is the phaseless quantity

$$\left| \sum_{n=0}^{d-1} x_n m_{n-\ell} e^{-\frac{2\pi i n k}{d}} \right|^2. \quad (1.3.8)$$

The approach below is the discrete equivalent of the WDD method introduced by Rodenburg and Bates in 1992 [49]. Specifically, the mask, specimen, and measurements are assumed to be discrete ab initio. Before discussing this approach in detail, we introduce some notation and basic properties of the discrete Fourier transform (DFT).

1.3.3.1 Notation and Basic Properties of the DFT

Let $\mathbf{x} = (x_0, x_1, \dots, x_{d-1})^T \in \mathbb{C}^{d \times 1}$. Recall that $[d]_0 = \{0, 1, \dots, d-1\}$ is the set of remainders modulo d . We denote by $\text{supp}(\mathbf{x})$ the index set corresponding to the nonzero entries of \mathbf{x} ; that is,

$$\text{supp}(\mathbf{x}) := \{n \in [d]_0 \mid x_n \neq 0\}.$$

The Fourier transform of \mathbf{x} , denoted by $\widehat{\mathbf{x}} \in \mathbb{C}^{d \times 1}$, is defined componentwise via

$$\widehat{x}_k := (F_d \mathbf{x})_k = \sum_{n=0}^{d-1} x_n e^{-\frac{2\pi i n k}{d}},$$

where $F_d \in \mathbb{C}^{d \times d}$ denotes the $d \times d$ DFT matrix with entries

$$(F_d)_{\ell,k} = e^{-\frac{2\pi i \ell k}{d}} \quad \forall (\ell, k) \in [d]_0 \times [d]_0.$$

With this definition one can invert the Fourier transform via

$$x_n = \left(F_d^{-1} \widehat{\mathbf{x}} \right)_n = \frac{1}{d} \sum_{k=0}^{d-1} \widehat{x}_k e^{\frac{2\pi i k n}{d}}.$$

Given a vector $\mathbf{u} \in \mathbb{C}^{d \times 1}$, denote by $\widetilde{\mathbf{u}}$ the reversal of \mathbf{u} about its first entry so that its components are

$$\widetilde{u}_n := u_{-n \bmod d} \quad \forall n \in [d]_0.$$

Given $\ell \in [d]_0$, define the circular shift operator $S_\ell : \mathbb{C}^{d \times 1} \rightarrow \mathbb{C}^{d \times 1}$ componentwise via

$$(S_\ell \mathbf{u})_n = u_{(\ell+n) \bmod d} \quad \forall n \in [d]_0.$$

Similarly, given $k \in [d]_0$, define the modulation operator $W_k : \mathbb{C}^{d \times 1} \rightarrow \mathbb{C}^{d \times 1}$ componentwise via

$$(W_k \mathbf{u})_n = u_n e^{\frac{2\pi i k n}{d}} \quad \forall n \in [d]_0.$$

We summarize some properties of the DFT and the operators above in the lemma below.

The interested reader may refer to the Appendix for a complete proof.

Lemma 1.3.1. *The following equalities hold for any $\mathbf{x} \in \mathbb{C}^{d \times 1}$ and for all $\ell \in [d]_0$:*

1. $F_d \widehat{\mathbf{x}} = d \cdot \widetilde{\mathbf{x}}$.
2. $F_d (W_\ell \mathbf{x}) = S_{-\ell} \widehat{\mathbf{x}}$.

$$3. F_d(S_\ell \mathbf{x}) = W_\ell \widehat{\mathbf{x}}.$$

$$4. W_{-\ell} F_d(S_\ell \widetilde{\mathbf{x}}) = \widetilde{\mathbf{x}}.$$

$$5. \widetilde{\widetilde{\mathbf{x}}} = S_{-\ell} \widetilde{\mathbf{x}}.$$

$$6. F_d \overline{\mathbf{x}} = \overline{F_d \widetilde{\mathbf{x}}}.$$

$$7. \widetilde{\widetilde{\mathbf{x}}} = F_d \widetilde{\mathbf{x}}.$$

Let $*_d$ and \circ denote the circular convolution operator and the Hadamard product in $\mathbb{C}^{d \times 1}$, respectively. More precisely, given $\mathbf{x}, \mathbf{y} \in \mathbb{C}^{d \times 1}$ and $\ell \in [d]_0$, we define

$$(\mathbf{x} *_d \mathbf{y})_\ell := \sum_{n=0}^{d-1} x_n y_{(\ell-n) \bmod d},$$

$$(\mathbf{x} \circ \mathbf{y})_\ell := x_\ell y_\ell.$$

The discrete version of the Convolution Theorem may be stated as follows:

Lemma 1.3.2. (*Convolution Theorem*) For all $\mathbf{x}, \mathbf{y} \in \mathbb{C}^{d \times 1}$ one has

$$F_d^{-1}(\widehat{\mathbf{x}} \circ \widehat{\mathbf{y}}) = \mathbf{x} *_d \mathbf{y}$$

and

$$(F_d \mathbf{x}) *_d (F_d \mathbf{y}) = d \cdot F_d(\mathbf{x} \circ \mathbf{y}).$$

We also introduce some technical lemmas below, which will be used in the proofs of lemmas and theorems throughout this chapter, as well as in Chapter 2.

Lemma 1.3.3. *Let $\mathbf{x}, \mathbf{y} \in \mathbb{C}^{d \times 1}$ and $\ell, k \in [d]_0$. Then*

$$\left((\mathbf{x} \circ S_{-\ell} \mathbf{y}) *_d \left(\widetilde{\mathbf{x}} \circ S_{\ell} \widetilde{\mathbf{y}} \right) \right)_k = \left((\mathbf{x} \circ S_{-k} \overline{\mathbf{x}}) *_d \left(\widetilde{\mathbf{y}} \circ S_k \widetilde{\mathbf{y}} \right) \right)_\ell.$$

Proof. Let $\mathbf{x}, \mathbf{y} \in \mathbb{C}^{d \times 1}$ and $\ell, k \in [d]_0$ be arbitrary. We calculate

$$\begin{aligned} \left((\mathbf{x} \circ S_{-\ell} \mathbf{y}) *_d \left(\widetilde{\mathbf{x}} \circ S_{\ell} \widetilde{\mathbf{y}} \right) \right)_k &= \sum_{n=0}^{d-1} (\mathbf{x} \circ S_{-\ell} \mathbf{y})_n \left(\widetilde{\mathbf{x}} \circ S_{\ell} \widetilde{\mathbf{y}} \right)_{k-n} && \text{(by definition of } *_d) \\ &= \sum_{n=0}^{d-1} x_n y_{n-\ell} \widetilde{x}_{k-n} \widetilde{y}_{\ell+k-n} && \text{(by definition of } \circ) \\ &= \sum_{n=0}^{d-1} x_n \overline{x}_{n-k} \widetilde{y}_{\ell-n} \widetilde{y}_{\ell-(n-k)} && \text{(by definition of } \widetilde{\cdot}) \\ &= \left((\mathbf{x} \circ S_{-k} \overline{\mathbf{x}}) *_d \left(\widetilde{\mathbf{y}} \circ S_k \widetilde{\mathbf{y}} \right) \right)_\ell. && \text{(by definition of } *_d) \end{aligned}$$

□

Lemma 1.3.4. *For any $\mathbf{x} \in \mathbb{C}^{d \times 1}$, one has*

$$|F_d \mathbf{x}|^2 = F_d \left(\mathbf{x} *_d \widetilde{\mathbf{x}} \right).$$

Proof. Let $\mathbf{x} \in \mathbb{C}^{d \times 1}$ be arbitrary. Then

$$\begin{aligned} |F_d \mathbf{x}|^2 &= (F_d \mathbf{x}) \circ \overline{(F_d \mathbf{x})} \\ &= (F_d \mathbf{x}) \circ \left(F_d \widetilde{\mathbf{x}} \right) && \text{(by Lemma 1.3.1(4) with } \ell = 0) \\ &= F_d \left(\mathbf{x} *_d \widetilde{\mathbf{x}} \right). && \text{(by Lemma 1.3.2)} \end{aligned}$$

□

1.3.3.2 Wigner Distribution Deconvolution in the Discrete Setting

We are now ready to provide the equivalent of (1.3.4) in the discrete, noisy setting. Let $\mathbf{x}, \mathbf{m} \in \mathbb{C}^{d \times 1}$ denote the unknown specimen and known mask, respectively. Assume we have d^2 noisy spectrogram measurements of the form

$$(\mathbf{y}_\ell)_k = \left| \sum_{n=0}^{d-1} x_n m_{n-\ell} e^{-\frac{2\pi i n k}{d}} \right|^2 + (\eta_\ell)_k, \quad (\ell, k) \in [d]_0 \times [d]_0. \quad (1.3.9)$$

Let these measurements populate a matrix $Y \in \mathbb{R}^{d \times d}$, whose ℓ^{th} column we will denote by $\mathbf{y}_\ell \in \mathbb{C}^{d \times 1}$, for $\ell \in [d]_0$. Similarly, let the noise measurements $(\eta_\ell)_k$ populate a matrix $N \in \mathbb{C}^{d \times d}$, whose ℓ^{th} column we will denote by $\eta_\ell \in \mathbb{C}^{d \times 1}$. We have the following lemma.

Lemma 1.3.5. *Let $\mathbf{x} \in \mathbb{C}^{d \times 1}$ denote an unknown specimen, and let $\mathbf{m} \in \mathbb{C}^{d \times 1}$ denote a known mask (or window). Let $Y \in \mathbb{R}^{d \times d}$ be the matrix of noisy spectrogram measurements as in (1.3.9). Then for any $k \in [d]_0$,*

$$F_d \left((Y - N)^T F_d^T \right)_k = d \cdot F_d(\mathbf{x} \circ S_k \bar{\mathbf{x}}) \circ F_d(\tilde{\mathbf{m}} \circ S_{-k} \overline{\tilde{\mathbf{m}}}). \quad (1.3.10)$$

Proof. By Lemma 1.3.4, we may write for any $\ell \in [d]_0$,

$$\begin{aligned} \mathbf{y}_\ell &= |F_d(\mathbf{x} \circ S_{-\ell} \mathbf{m})|^2 + \eta_\ell \\ &= F_d \left((\mathbf{x} \circ S_{-\ell} \mathbf{m}) *_d (\bar{\mathbf{x}} \circ S_\ell \overline{\mathbf{m}}) \right) + \eta_\ell. \end{aligned} \quad (1.3.11)$$

Taking a Fourier transform of \mathbf{y}_ℓ at $k \in [d]_0$ yields

$$(F_d \mathbf{y}_\ell)_k = d \cdot \left((\mathbf{x} \circ S_{-\ell} \mathbf{m}) *_d (\bar{\mathbf{x}} \circ S_\ell \overline{\mathbf{m}}) \right)_{-k} + (F_d \eta_\ell)_k,$$

by Lemma 1.3.1(1); by Lemma 1.3.3, we get

$$(F_d \mathbf{y}_\ell)_k = d \cdot \left((\mathbf{x} \circ S_k \bar{\mathbf{x}}) *_d \left(\tilde{\mathbf{m}} \circ S_{-k} \widetilde{\mathbf{m}} \right) \right)_\ell + (F_d \eta_\ell)_k. \quad (1.3.12)$$

For a given $\ell \in [d]_0$, the vector $F_d \mathbf{y}_\ell \in \mathbb{C}^{d \times 1}$ is the ℓ^{th} column of the matrix $F_d Y$; its transpose, $\mathbf{y}_\ell^T F_d^T \in \mathbb{C}^{1 \times d}$ is the ℓ^{th} row of the matrix $(F_d Y)^T$. Similarly, the vector $F_d \eta_\ell \in \mathbb{C}^{d \times 1}$ is the ℓ^{th} column of the matrix $F_d N$; its transpose, $\eta_\ell^T F_d^T \in \mathbb{C}^{1 \times d}$ is the ℓ^{th} row of the matrix $(F_d N)^T$. We may thus write

$$\left(\left(Y^T F_d^T \right)_k \right)_\ell = d \cdot \left((\mathbf{x} \circ S_k \bar{\mathbf{x}}) *_d \left(\tilde{\mathbf{m}} \circ S_{-k} \widetilde{\mathbf{m}} \right) \right)_\ell + \left(\left(N^T F_d^T \right)_k \right)_\ell,$$

so that for any $k \in [d]_0$, the vector $\left(\left(Y^T - N^T \right) F_d^T \right)_k \in \mathbb{C}^{d \times 1}$ may be computed as a convolution:

$$\left(\left(Y^T - N^T \right) F_d^T \right)_k = d \cdot (\mathbf{x} \circ S_k \bar{\mathbf{x}}) *_d \left(\tilde{\mathbf{m}} \circ S_{-k} \widetilde{\mathbf{m}} \right).$$

Taking a final Fourier transform now yields

$$F_d \left(\left(Y - N \right)^T F_d^T \right)_k = d \cdot F_d (\mathbf{x} \circ S_k \bar{\mathbf{x}}) \circ F_d \left(\tilde{\mathbf{m}} \circ S_{-k} \widetilde{\mathbf{m}} \right),$$

by Lemma 1.3.2. □

The result of Lemma 1.3.5 can be interpreted as the discrete analogue to (1.3.4). In (1.3.10), the unknown specimen \mathbf{x} and the known mask \mathbf{m} are decoupled. This allows for the recovery of \mathbf{x} via angular synchronization, which is discussed in Chapter 2.

Chapter 2

Phase Retrieval via Aliased Wigner

Distribution Deconvolution and Angular

Synchronization

In Chapter 1, we discussed how the Wigner distribution deconvolution method could be applied to d^2 discrete ptychographic measurements in order to recover a vector $\mathbf{x} \in \mathbb{C}^d$. The method consisted of applying two consecutive Fourier transforms to the matrix of measurements, yielding the product of two Wigner distribution functions, one for the specimen and one for the mask.

In practice, one is interested in collecting as few measurements as possible, while maintaining robust recovery guarantees. This amounts to shifting the mask by a fixed step-size larger than 1, while maintaining spatial overlap between consecutive shifted masks. Another form of sub-sampling takes place in the Fourier domain, where the spectrogram measurements may be collected at a subset of equally spaced Fourier modes. One could also combine both forms of sub-sampling, thus reducing the number of measurements drastically.

In what follows, we discuss phase retrieval from sub-sampled short-time Fourier transform (STFT) magnitude measurements of a vector $\mathbf{x} \in \mathbb{C}^d$ based on a two-step approach: first, a modified Wigner distribution deconvolution approach is used to solve for a portion of the

lifted rank-one signal $\widehat{\mathbf{x}\mathbf{x}}^* \in \mathbb{C}^{d \times d}$. Second, an angular synchronization approach is used to recover $\widehat{\mathbf{x}}$ (and then, by Fourier inversion, \mathbf{x}) from the known portion of $\widehat{\mathbf{x}\mathbf{x}}^*$. In addition to being computationally efficient, the proposed method also gives insight into the design of good window (or probe) functions.

Before discussing aliased WDD methods, we introduce some additional notation to that in Chapter 1. Let $\text{sgn} : \mathbb{C} \rightarrow \mathbb{C}$ be the normalization mapping

$$\text{sgn}(z) = \begin{cases} \frac{z}{|z|}, & \text{if } z \neq 0, \\ 1, & \text{if } z = 0. \end{cases}$$

For a given $n \in \mathbb{N}$, we introduce the operator $C_{2n-1} : \mathbb{C}^{d \times (2n-1)} \rightarrow \mathbb{C}^{d \times d}$ defined via

$$(C_{2n-1}(M))_{j,k} = \begin{cases} M_{j, n-1+(k-j) \bmod d}, & \text{if } |j-k| < n \text{ or } |j-k| > d-n, \\ 0, & \text{otherwise.} \end{cases} \quad (2.0.1)$$

We note, in particular, that this operator preserves the Frobenius norm. With the definition above, $C_{2n-1}(M) \in \mathbb{C}^{d \times d}$ is a circulant version of $M \in \mathbb{C}^{d \times (2n-1)}$, in such a way that column $n-1$ of M (the middle column) is the diagonal of $C_{2n-1}(M)$. For example,

$$C_3 \left(\begin{bmatrix} a_{0,0} & a_{0,1} & a_{0,2} \\ a_{1,0} & a_{1,1} & a_{1,2} \\ \vdots & \vdots & \vdots \\ a_{d-2,0} & a_{d-2,1} & a_{d-2,2} \\ a_{d-1,0} & a_{d-1,1} & a_{d-1,2} \end{bmatrix} \right) = \begin{bmatrix} a_{0,1} & a_{0,2} & \cdots & 0 & a_{0,0} \\ a_{1,0} & a_{1,1} & a_{1,2} & & 0 \\ \vdots & \ddots & \ddots & \ddots & \vdots \\ 0 & & a_{d-2,0} & a_{d-2,1} & a_{d-2,2} \\ a_{d-1,2} & 0 & \cdots & a_{d-1,0} & a_{d-1,1} \end{bmatrix}.$$

Given a natural number s which divides d , we introduce the sub-sampling operator

$$Z_s : \mathbb{C}^{d \times 1} \rightarrow \mathbb{C}^{\frac{d}{s} \times 1},$$

defined componentwise via

$$(Z_s \mathbf{u})_n := u_{n \cdot s} \quad \forall n \in \left[\frac{d}{s} \right]_0.$$

Fourier transforms of sub-sampled vectors have an aliasing effect which is described in the lemma below. A proof is provided in the Appendix.

Lemma 2.0.1. (*Aliasing*) For any $d \in \mathbb{N}$ and $s \in \mathbb{N}$ that divides d , and for any $\mathbf{u} \in \mathbb{C}^{d \times 1}$ and $\omega \in \left[\frac{d}{s} \right]_0$, one has

$$\left(F_{\frac{d}{s}} (Z_s \mathbf{u}) \right)_\omega = \frac{1}{s} \sum_{r=0}^{s-1} \hat{u}_{\omega - r \frac{d}{s}}.$$

Finally, we provide a technical lemma which provides an equivalence between the Fourier transform of an autocorrelation of a vector \mathbf{x} and that of its Fourier transform, $\hat{\mathbf{x}}$. A proof is provided in the Appendix.

Lemma 2.0.2. Let $\mathbf{x} \in \mathbb{C}^{d \times 1}$ and $\alpha, \omega \in [d]_0$. Then

$$(F_d (\mathbf{x} \circ S_\omega \bar{\mathbf{x}}))_\alpha = \frac{1}{d} e^{\frac{2\pi i \omega \alpha}{d}} \left(F_d (\hat{\mathbf{x}} \circ S_{-\alpha} \bar{\hat{\mathbf{x}}}) \right)_\omega.$$

2.1 Aliased WDD for Phase Retrieval

In this section, we expand on the classical WDD method to include sub-sampling. Specifically, in Section 2.1.1, we provide a WDD formulation for the case when one collects measurements on a small subset of all d Fourier modes in $[d]_0$. Next, in Section 2.1.2, we explore

further to include the case where one shifts the mask \mathbf{m} at a subset of all d possible shifts in $[d]_0$. We then provide two algorithms in Section 2.1.3 which allow for the recovery of a specimen \mathbf{x} from sub-sampled measurements via aliased WDD formulations and angular synchronization. Recovery guarantees are then provided for Algorithms 1 and 2.

2.1.1 Sub-sampling in Frequency

Let K be a positive integer which divides d , and assume that the data is measured at K equally spaced Fourier modes. As such, we restrict the Fourier modes of step-size $\frac{d}{K}$ to

$$\mathcal{K} = \frac{d}{K} [K]_0 = \left\{ 0, \frac{d}{K}, \frac{2d}{K}, \dots, d - \frac{d}{K} \right\}. \quad (2.1.1)$$

Definition. Given a matrix $A \in \mathbb{C}^{d \times d}$ with columns \mathbf{a}_j , and an integer K which divides d , we denote by $A_{K,d} \in \mathbb{C}^{K \times d}$ the submatrix of A whose ℓ^{th} column is equal to $Z_{\frac{d}{K}}(\mathbf{a}_\ell)$.

The following lemma is a generalization of Lemma 1.3.5.

Lemma 2.1.1. *Suppose that the measurements in (1.3.9) are collected on a subset $\mathcal{K} \subseteq [d]_0$ of K equally spaced Fourier modes. Then for any $\omega \in [K]_0$,*

$$F_d \left((Y_{K,d} - N_{K,d})^T F_K^T \right)_\omega = K \sum_{r=0}^{\frac{d}{K}-1} F_d(\mathbf{x} \circ S_{\omega-rK}\bar{\mathbf{x}}) \circ F_d(\tilde{\mathbf{m}} \circ S_{rK-\omega}\tilde{\mathbf{m}}),$$

where $(Y_{K,d} - N_{K,d}) \in \mathbb{C}^{K \times d}$ is the matrix of sub-sampled noiseless $K \cdot d$ measurements.

Before providing a proof, we note that in the special case where one collects data at all d frequencies in $[d]_0$, i.e., when $K = d$, the lemma above reduces to (1.3.12):

$$\left(F_K \left(Z_{\frac{d}{K}}(\mathbf{y}_\ell - \eta_\ell) \right) \right)_\omega = (F_d(\mathbf{y}_\ell - \eta_\ell))_\omega = d \cdot \left((\mathbf{x} \circ S_\omega \bar{\mathbf{x}}) *_d (\tilde{\mathbf{m}} \circ S_{-\omega} \tilde{\mathbf{m}}) \right)_\ell.$$

Proof. Let us recall from (1.3.11) that for $\ell \in [d]_0$, the ℓ^{th} column of the matrix $Y - N$ is

$$\mathbf{y}_\ell - \eta_\ell = F_d \left((\mathbf{x} \circ S_{-\ell} \mathbf{m}) *_d \left(\widetilde{\mathbf{x}} \circ S_\ell \widetilde{\mathbf{m}} \right) \right).$$

We may write, for any $\alpha \in [K]_0$,

$$\left(Z_{\frac{d}{K}} (\mathbf{y}_\ell - \eta_\ell) \right)_\alpha = \left(F_d \left((\mathbf{x} \circ S_{-\ell} \mathbf{m}) *_d \left(\widetilde{\mathbf{x}} \circ S_\ell \widetilde{\mathbf{m}} \right) \right) \right)_{\alpha \frac{d}{K}}.$$

Upon taking a Fourier transform at $\omega \in [K]_0$, we get

$$\begin{aligned} \left(F_K \left(Z_{\frac{d}{K}} (\mathbf{y}_\ell - \eta_\ell) \right) \right)_\omega &= \frac{K}{d} \sum_{r=0}^{\frac{d}{K}-1} (\widehat{\mathbf{y}}_\ell - \widehat{\eta}_\ell)_{\omega - rK} && \text{(by Lemma 2.0.1)} \\ &= d \cdot \frac{K}{d} \sum_{r=0}^{\frac{d}{K}-1} \left((\mathbf{x} \circ S_{\omega - rK} \overline{\mathbf{x}}) *_d \left(\widetilde{\mathbf{m}} \circ S_{rK - \omega} \widetilde{\mathbf{m}} \right) \right)_\ell. \\ &&& \text{(by (1.3.12))} \end{aligned}$$

Note that the ℓ^{th} column of $(Y_{K,d} - N_{K,d}) \in \mathbb{C}^{K \times d}$ is equal to $Z_{\frac{d}{K}} (\mathbf{y}_\ell - \eta_\ell)$. Then the ω^{th} column of $(Y_{K,d} - N_{K,d})^T F_K^T \in \mathbb{C}^{d \times K}$, for any $\omega \in [K]_0$, may be computed as

$$\left((Y_{K,d} - N_{K,d})^T F_K^T \right)_\omega = K \sum_{r=0}^{\frac{d}{K}-1} (\mathbf{x} \circ S_{\omega - rK} \overline{\mathbf{x}}) *_d \left(\widetilde{\mathbf{m}} \circ S_{rK - \omega} \widetilde{\mathbf{m}} \right) \in \mathbb{C}^{d \times 1}.$$

Taking one final Fourier transform now yields

$$F_d \left((Y_{K,d} - N_{K,d})^T F_K^T \right)_\omega = K \sum_{r=0}^{\frac{d}{K}-1} F_d (\mathbf{x} \circ S_{\omega - rK} \overline{\mathbf{x}}) \circ F_d \left(\widetilde{\mathbf{m}} \circ S_{rK - \omega} \widetilde{\mathbf{m}} \right), \quad (2.1.2)$$

by Lemma 1.3.2 and the linearity of the Fourier transform. \square

2.1.2 Sub-sampling in Frequency and Space

Let L be a positive integer which divides d . Let us assume that the measurements are collected at L equally spaced physical shifts of step-size $\frac{d}{L}$, so that the set of shifts is

$$\mathcal{L} = \frac{d}{L} [L]_0 = \left\{ 0, \frac{d}{L}, \frac{2d}{L}, \dots, d - \frac{d}{L} \right\}. \quad (2.1.3)$$

Definition. Given a matrix $A \in \mathbb{C}^{d \times d}$, and an integer L which divides d , we denote by $A_{d,L} \in \mathbb{C}^{d \times L}$ the submatrix of A whose rows are those of A , sub-sampled in step-size $\frac{d}{L}$.

We state a more generalized version of Lemma 2.1.1 and Lemma 1.3.5 below.

Lemma 2.1.2. *Suppose that the measurements in (1.3.9) are collected on a subset $\mathcal{K} \subseteq [d]_0$ of K equally spaced frequencies and a subset $\mathcal{L} \subseteq [d]_0$ of L equally spaced physical shifts. Then for any $\omega \in [K]_0$ and $\alpha \in [L]_0$,*

$$\begin{aligned} & \left(F_L (Y_{K,L} - N_{K,L})^T \left(F_K^T \right)_\omega \right)_\alpha \\ &= \frac{KL}{d^3} \sum_{r=0}^{\frac{d}{K}-1} \sum_{\ell=0}^{\frac{d}{L}-1} \left(F_d \left(\widehat{\mathbf{x}} \circ S_{\ell L - \alpha} \widehat{\mathbf{x}} \right) \right)_{\omega - rK} \left(F_d \left(\widehat{\mathbf{m}} \circ S_{\alpha - \ell L} \widehat{\mathbf{m}} \right) \right)_{\omega - rK}, \end{aligned} \quad (2.1.4)$$

where $(Y_{K,L} - N_{K,L}) \in \mathbb{C}^{K \times L}$ is the matrix of sub-sampled noiseless $K \cdot L$ measurements.

Proof. For fixed $\ell \in [d]_0$ and $\omega \in [K]_0$, we have computed (in the proof of Lemma 2.1.1)

$$\left(F_K \left(Z_{\frac{d}{K}} (\mathbf{y}_\ell - \eta_\ell) \right) \right)_\omega = K \sum_{r=0}^{\frac{d}{K}-1} \left((\mathbf{x} \circ S_{\omega - rK} \overline{\mathbf{x}}) *_d \left(\widetilde{\mathbf{m}} \circ S_{rK - \omega} \widetilde{\mathbf{m}} \right) \right)_\ell.$$

Let us fix $\omega \in [K]_0$, and look at the vector $\mathbf{p}_\omega \in \mathbb{C}^{L \times 1}$, defined componentwise via

$$(\mathbf{p}_\omega)_\ell := \left(F_K \left(Z_{\frac{d}{K}} \left(\mathbf{y}_{\ell \frac{d}{L}} - \eta_{\ell \frac{d}{L}} \right) \right) \right)_\omega \quad \forall \ell \in [L]_0. \quad (2.1.5)$$

Note that the rows of $(Y_{K,L} - N_{K,L}) \in \mathbb{C}^{K \times L}$ are those of $(Y_{K,d} - N_{K,d}) \in \mathbb{C}^{K \times d}$, subsampled in step-size of $\frac{d}{L}$. With this, one can see that

$$(\mathbf{p}_\omega)_\ell = \left((Y_{K,L} - N_{K,L})^T \left(F_K^T \right)_\omega \right)_\ell,$$

where $\left(F_K^T \right)_\omega \in \mathbb{C}^{K \times 1}$ is the ω^{th} column of F_K^T . Therefore,

$$\mathbf{p}_\omega = (Y_{K,L} - N_{K,L})^T \left(F_K^T \right)_\omega \in \mathbb{C}^{L \times 1} \quad \forall \omega \in [K]_0.$$

Now, observe that for any $\ell \in [L]_0$, we have

$$\begin{aligned} (\mathbf{p}_\omega)_\ell &= K \sum_{r=0}^{\frac{d}{K}-1} \left((\mathbf{x} \circ S_{\omega-rK} \bar{\mathbf{x}}) *_d \left(\tilde{\mathbf{m}} \circ S_{rK-\omega} \widetilde{\mathbf{m}} \right) \right)_{\ell \frac{d}{L}} \\ &= K \cdot \left(Z_{\frac{d}{L}} \left(\sum_{r=0}^{\frac{d}{K}-1} (\mathbf{x} \circ S_{\omega-rK} \bar{\mathbf{x}}) *_d \left(\tilde{\mathbf{m}} \circ S_{rK-\omega} \widetilde{\mathbf{m}} \right) \right) \right)_\ell. \end{aligned}$$

For any $\alpha \in [L]_0$, one has by Lemma 2.0.1 and Lemma 1.3.2

$$\begin{aligned} (F_L \mathbf{p}_\omega)_\alpha &= \frac{KL}{d} \sum_{r=0}^{\frac{d}{K}-1} \sum_{\ell=0}^{\frac{d}{L}-1} \left(F_d \left((\mathbf{x} \circ S_{\omega-rK} \bar{\mathbf{x}}) *_d \left(\tilde{\mathbf{m}} \circ S_{rK-\omega} \widetilde{\mathbf{m}} \right) \right) \right)_{\alpha-\ell L} \\ &= \frac{KL}{d} \sum_{r=0}^{\frac{d}{K}-1} \sum_{\ell=0}^{\frac{d}{L}-1} (F_d(\mathbf{x} \circ S_{\omega-rK} \bar{\mathbf{x}}))_{\alpha-\ell L} \left(F_d \left(\tilde{\mathbf{m}} \circ S_{rK-\omega} \widetilde{\mathbf{m}} \right) \right)_{\alpha-\ell L}. \end{aligned}$$

Using Lemma 2.0.2, we can write for any $\omega \in [K]_0$ and $\alpha \in [L]_0$,

$$\begin{aligned} & \left(F_L (Y_{K,L} - N_{K,L})^T \left(F_K^T \right)_\omega \right)_\alpha \\ &= \frac{KL}{d^3} \sum_{r=0}^{\frac{d}{K}-1} \sum_{\ell=0}^{\frac{d}{L}-1} \left(F_d \left(\widehat{\mathbf{x}} \circ S_{\ell L - \alpha} \widehat{\overline{\mathbf{x}}} \right) \right)_{\omega - rK} \left(F_d \left(\widehat{\mathbf{m}} \circ S_{\ell L - \alpha} \widehat{\overline{\mathbf{m}}} \right) \right)_{rK - \omega}. \end{aligned}$$

Finally, Lemma 1.3.1(7), applied to the last Fourier transform in the equality above, yields

$$\left(F_d \left(\widehat{\mathbf{m}} \circ S_{\ell L - \alpha} \widehat{\overline{\mathbf{m}}} \right) \right)_{rK - \omega} = \left(F_d \left(\widetilde{\widehat{\mathbf{m}}} \circ S_{\alpha - \ell L} \widetilde{\widehat{\overline{\mathbf{m}}}} \right) \right)_{\omega - rK} = \left(F_d \left(\widehat{\mathbf{m}} \circ S_{\alpha - \ell L} \widehat{\overline{\mathbf{m}}} \right) \right)_{\omega - rK}.$$

□

Lemma 1.3.5 can now be seen as a corollary of Lemma 2.1.2 above; in the special case where one collects data at all shifts $\ell \in [d]_0$ and all Fourier modes $\omega \in [d]_0$, i.e., when $K = L = d$, one has

$$\begin{aligned} \left(F_d (Y - N)^T \left(F_d^T \right)_\omega \right)_\alpha &= \frac{d \cdot d}{d^3} \sum_{r=0}^{\frac{d}{d}-1} \sum_{\ell=0}^{\frac{d}{d}-1} \left(F_d \left(\widehat{\mathbf{x}} \circ S_{\ell d - \alpha} \widehat{\overline{\mathbf{x}}} \right) \right)_{\omega - rd} \left(F_d \left(\widehat{\mathbf{m}} \circ S_{\alpha - \ell d} \widehat{\overline{\mathbf{m}}} \right) \right)_{\omega - rd} \\ &= \frac{1}{d} \left(F_d \left(\widehat{\mathbf{x}} \circ S_{-\alpha} \widehat{\overline{\mathbf{x}}} \right) \right)_\omega \left(F_d \left(\widehat{\mathbf{m}} \circ S_\alpha \widehat{\overline{\mathbf{m}}} \right) \right)_\omega, \end{aligned}$$

which is an equivalent result to that of Lemma 1.3.5.

2.1.3 Recovering Diagonals of $\widehat{\mathbf{x}\mathbf{x}}^*$

Let us assume that \mathbf{m} is band-limited with $\text{supp}(\widehat{\mathbf{m}}) = [\delta]_0$ for some $\delta \ll d$. Then Algorithm 1 below allows for the recovery of an estimate of $\widehat{\mathbf{x}}$ from spectrogram measurements via Wigner distribution deconvolution and angular synchronization.

Algorithm 1 WDD and Angular Synchronization for Band-limited Masks

Inputs

- 1: $Y_{d,L} \in \mathbb{C}^{d \times L}$: matrix of $d \cdot L$ noisy measurements of the form

$$(y_\ell)_k = \left| \sum_{n=0}^{d-1} x_n m_{n-\ell} e^{-\frac{2\pi i n k}{d}} \right|^2 + \eta_{k,\ell}, \quad (k, \ell) \in [d]_0 \times \frac{d}{L} [L]_0. \quad (2.1.6)$$

- 2: Band-limited mask (or window) $\mathbf{m} \in \mathbb{C}^{d \times 1}$, with $\text{supp}(\widehat{\mathbf{m}}) = [\delta]_0$.
- 3: Integer $\kappa \leq \delta$, so that $2\kappa - 1$ diagonals of $\widehat{\mathbf{x}}\widehat{\mathbf{x}}^*$ are estimated, and $L = \delta + \kappa - 1$.

Steps

- 1: Estimate the perturbed vectors $F_d(\widehat{\mathbf{x}} \circ S_\alpha \widehat{\mathbf{x}})$ (assuming no noise) according to

$$F_d(\widehat{\mathbf{x}} \circ S_{-\alpha} \widehat{\mathbf{x}}) \approx \frac{d^2 \left(F_d(Y_{d,L}) \left(F_L^T \right) \right)_\alpha}{L \cdot F_d(\widehat{\mathbf{m}} \circ S_\alpha \widehat{\mathbf{m}})} \quad \forall \alpha \in [\kappa]_0,$$

$$F_d(\widehat{\mathbf{x}} \circ S_{L-\alpha} \widehat{\mathbf{x}}) \approx \frac{d^2 \left(F_d(Y_{d,L}) \left(F_L^T \right) \right)_\alpha}{L \cdot F_d(\widehat{\mathbf{m}} \circ S_{\alpha-L} \widehat{\mathbf{m}})} \quad \forall \alpha \in [L]_0 \setminus [L - \kappa + 1]_0.$$

- 2: Invert the Fourier transforms above to recover estimates of the $(2\kappa - 1)$ vectors $\widehat{\mathbf{x}} \circ S_\alpha \widehat{\mathbf{x}}$.
- 3: Form the banded matrix $C_{2\kappa-1}(Y_{2\kappa-1})$ from the measurements in step 2.
- 4: Hermitianize the matrix above: $C_{2\kappa-1}(Y_{2\kappa-1}) \leftarrow \frac{1}{2}(C_{2\kappa-1}(Y_{2\kappa-1}) + C_{2\kappa-1}(Y_{2\kappa-1})^*)$.
- 5: Estimate $|\widehat{\mathbf{x}}|$ from the diagonal of $C_{2\kappa-1}(Y_{2\kappa-1})$.
- 6: Normalize $C_{2\kappa-1}(Y_{2\kappa-1})$ componentwise to form $\widetilde{Y}_{2\kappa-1}$.
- 7: Compute the leading eigenvector, \mathbf{u} , of $\widetilde{Y}_{2\kappa-1}$.

Output An estimate $\widehat{\mathbf{x}}_e$ (up to a global phase) to $\widehat{\mathbf{x}}$, given componentwise via:

$$(\widehat{\mathbf{x}}_e)_j := \sqrt{(C_{2\kappa-1}(Y_{2\kappa-1}))_{j,j}} \cdot u_j.$$

Lemma 2.1.3. Let $\mathbf{x} \in \mathbb{C}^{d \times 1}$ be arbitrary and $\mathbf{m} \in \mathbb{C}^{d \times 1}$ with $\text{supp}(\widehat{\mathbf{m}}) = [\delta]_0$. Assume $\frac{d}{L} \in \mathbb{N}$, and let $Y_{d,L} \in \mathbb{C}^{d \times L}$ contain $d \cdot L$ noisy autocorrelation measurements as in (2.1.6). Then for any $\alpha \in [L]_0$ and $\omega \in [d]_0$,

$$\left(F_L (Y_{d,L} - N_{d,L})^T \left(F_d^T \right)_\omega \right)_\alpha = \frac{L}{d^2} \sum_{\ell=0}^{\frac{d}{L}-1} \left(F_d \left(\widehat{\mathbf{x}} \circ S_{\ell L - \alpha} \overline{\widehat{\mathbf{x}}} \right) \right)_\omega \left(F_d \left(\widehat{\mathbf{m}} \circ S_{\alpha - \ell L} \overline{\widehat{\mathbf{m}}} \right) \right)_\omega. \quad (2.1.7)$$

Moreover, if $L = \delta + \kappa - 1$ for some $1 \leq \kappa \leq \delta$, then for all $\omega \in [d]_0$ the sum above reduces to exactly one term as follows:

$$\begin{aligned} & \frac{d^2}{L} \left(F_L (Y_{d,L} - N_{d,L})^T \left(F_d^T \right)_\omega \right)_\alpha \\ &= \begin{cases} \left(F_d \left(\widehat{\mathbf{x}} \circ S_{-\alpha} \overline{\widehat{\mathbf{x}}} \right) \right)_\omega \left(F_d \left(\widehat{\mathbf{m}} \circ S_\alpha \overline{\widehat{\mathbf{m}}} \right) \right)_\omega, & \text{if } \alpha \in [\kappa]_0, \\ \left(F_d \left(\widehat{\mathbf{x}} \circ S_{L-\alpha} \overline{\widehat{\mathbf{x}}} \right) \right)_\omega \left(F_d \left(\widehat{\mathbf{m}} \circ S_{\alpha-L} \overline{\widehat{\mathbf{m}}} \right) \right)_\omega, & \text{if } \alpha \in [L]_0 \setminus [\delta]_0. \end{cases} \end{aligned}$$

Proof. Equation (2.1.7) follows from equation (2.1.4) in Lemma 2.1.3 by setting $K = d$. It remains to show that if L is chosen so that $L = \delta - 1 + \kappa$ for some $1 \leq \kappa \leq \delta$ and α is chosen in $[L]_0 \setminus \{\kappa, \kappa + 1, \dots, L - \kappa\}$, then the sum reduces to a single term for all $\omega \in [d]_0$.

To that end, assume that $\text{supp}(\widehat{\mathbf{m}}) = [\delta]_0$ for some $\delta \ll d$ and set $L = \delta - 1 + \kappa$. Observe that $\widehat{\mathbf{m}} \circ S_{\alpha - \ell L} \overline{\widehat{\mathbf{m}}} = \mathbf{0}$ whenever the supports of $\widehat{\mathbf{m}}$ and $S_{\alpha - \ell L} \overline{\widehat{\mathbf{m}}}$ are disjoint. Note that

$$\text{supp}(\widehat{\mathbf{m}}) \cap \text{supp} \left(S_{\alpha - \ell L} \overline{\widehat{\mathbf{m}}} \right) \neq \emptyset \iff |\alpha - \ell L| \leq \delta - 1.$$

Now, since $L \leq 2\delta - 1$, then for any $\alpha \in [\kappa]_0$, $|\alpha - \ell L| \leq \delta - 1$ if and only if $\ell = 0$, and for any $\alpha \in \{L - \kappa + 1, \dots, L - 1\}$, $|\alpha - \ell L| \leq \delta - 1$ if and only if $\ell = 1$. \square

We are now ready to provide recovery guarantees for Algorithm 1.

Theorem 2.1.1. Let $\mathbf{x} \in \mathbb{C}^{d \times 1}$ be arbitrary and $\mathbf{m} \in \mathbb{C}^{d \times 1}$ with $\text{supp}(\widehat{\mathbf{m}}) = [\delta]_0$. Let $L = \delta + \kappa - 1$ for some $1 \leq \kappa \leq \delta$, and assume L divides d . Let $Y_{d,L} \in \mathbb{C}^{d \times L}$ contain $d \cdot L$ noisy autocorrelation measurements as in (2.1.6). Define

$$S_\epsilon := \left\{ n : |\widehat{x}_n| < \epsilon^{-\frac{1}{4}} \cdot \|N_{d,L}\|_F^{\frac{1}{4}} \right\}, \quad (2.1.8)$$

and let $\mu > 0$ denote the mask-dependent constant

$$\mu := \min_{\substack{|p| \leq \kappa - 1 \\ q \in [d]_0}} \left| F_d \left(\widehat{\mathbf{m}} \circ S_p \overline{\widehat{\mathbf{m}}} \right)_q \right|. \quad (2.1.9)$$

Then Algorithm 1 outputs an estimate $\widehat{\mathbf{x}}_e$ to $\widehat{\mathbf{x}}$ with

$$\min_{\phi \in [0, 2\pi]} \left\| \widehat{\mathbf{x}} - e^{i\phi} \widehat{\mathbf{x}}_e \right\|_2 \leq C' \|\widehat{\mathbf{x}}\|_\infty \cdot \frac{d^2}{\kappa^2} \cdot \sqrt{\frac{\epsilon d^4}{\kappa L \mu^2} \|N_{d,L}\|_F + |S_\epsilon|} + C'' \left(\frac{d^5}{L} \right)^{\frac{1}{4}} \sqrt{\frac{\|N_{d,L}\|_F}{\mu}}, \quad (2.1.10)$$

for some constants $C', C'' \in \mathbb{R}$. If $\epsilon = \frac{\|N_{d,L}\|_F}{\min |\widehat{\mathbf{x}}|^4}$, then

$$\min_{\phi \in [0, 2\pi]} \left\| \widehat{\mathbf{x}} - e^{i\phi} \widehat{\mathbf{x}}_e \right\|_2 \leq C' \frac{d^4 \|\widehat{\mathbf{x}}\|_\infty \|N_{d,L}\|_F}{L^{\frac{1}{2}} \mu \kappa^{\frac{5}{2}} \cdot \min |\widehat{\mathbf{x}}|^2} + C'' \frac{d^{\frac{5}{4}} \|N_{d,L}\|_F^{\frac{1}{2}}}{L^{\frac{1}{4}} \mu^{\frac{1}{2}}}. \quad (2.1.11)$$

Proof. Let \mathbf{x} , \mathbf{m} , and the measurements be as in Theorem 2.1.1. By Lemma 2.1.3,

$$F_d \left(\widehat{\mathbf{x}} \circ S_{-\alpha} \overline{\widehat{\mathbf{x}}} \right) = \frac{d^2 \left(F_d(Y_{d,L} - N_{d,L}) \left(F_L^T \right) \right)_\alpha}{F_d \left(\widehat{\mathbf{m}} \circ S_\alpha \overline{\widehat{\mathbf{m}}} \right)} \quad \forall \alpha \in [\kappa]_0,$$

$$F_d \left(\widehat{\mathbf{x}} \circ S_{L-\alpha} \overline{\widehat{\mathbf{x}}} \right) = \frac{d^2 \left(F_d(Y_{d,L} - N_{d,L}) \left(F_L^T \right) \right)_\alpha}{F_d \left(\widehat{\mathbf{m}} \circ S_{\alpha-L} \overline{\widehat{\mathbf{m}}} \right)} \quad \forall \alpha \in [L]_0 \setminus [L - \kappa + 1]_0,$$

where the division is componentwise. Thus, the $(2\kappa - 1)$ diagonals of the rank-one matrix $\widehat{\mathbf{x}}\widehat{\mathbf{x}}^*$ can be computed as

$$\begin{aligned}\widehat{\mathbf{x}} \circ S_{-\alpha}\widehat{\mathbf{x}} &= \frac{d^2}{L}F_d^{-1} \left(\frac{\left(F_d(Y_{d,L} - N_{d,L}) \left(F_L^T \right) \right)_\alpha}{F_d(\widehat{\mathbf{m}} \circ S_\alpha \widehat{\mathbf{m}})} \right) \quad \forall \alpha \in [\kappa]_0, \\ \widehat{\mathbf{x}} \circ S_{L-\alpha}\widehat{\mathbf{x}} &= \frac{d^2}{L}F_d^{-1} \left(\frac{\left(F_d(Y_{d,L} - N_{d,L}) \left(F_L^T \right) \right)_\alpha}{F_d(\widehat{\mathbf{m}} \circ S_{\alpha-L}\widehat{\mathbf{m}})} \right) \quad \forall \alpha \in [L]_0 \setminus [L - \kappa + 1]_0.\end{aligned}$$

Distributing the inverse Fourier transform yields

$$\widehat{\mathbf{x}} \circ S_{-\alpha}\widehat{\mathbf{x}} + \frac{d^2}{L}F_d^{-1} \left(\frac{\left(F_d N_{d,L} \left(F_L^T \right) \right)_\alpha}{F_d(\widehat{\mathbf{m}} \circ S_\alpha \widehat{\mathbf{m}})} \right) = \frac{d^2}{L}F_d^{-1} \left(\frac{\left(F_d Y_{d,L} \left(F_L^T \right) \right)_\alpha}{F_d(\widehat{\mathbf{m}} \circ S_\alpha \widehat{\mathbf{m}})} \right)$$

for all $\alpha \in [\kappa]_0$, and

$$\widehat{\mathbf{x}} \circ S_{L-\alpha}\widehat{\mathbf{x}} + \frac{d^2}{L}F_d^{-1} \left(\frac{\left(F_d N_{d,L} \left(F_L^T \right) \right)_\alpha}{F_d(\widehat{\mathbf{m}} \circ S_{\alpha-L}\widehat{\mathbf{m}})} \right) = \frac{d^2}{L}F_d^{-1} \left(\frac{\left(F_d Y_{d,L} \left(F_L^T \right) \right)_\alpha}{F_d(\widehat{\mathbf{m}} \circ S_{\alpha-L}\widehat{\mathbf{m}})} \right)$$

for all $\alpha \in [L]_0 \setminus [L - \kappa + 1]_0$. One can thus learn $(2\kappa - 1)$ diagonals of $\widehat{\mathbf{x}}\widehat{\mathbf{x}}^*$ exactly assuming the noise is known and the mask \mathbf{m} is chosen so that μ (as in (2.1.9)) is positive. In practice, however, $N_{d,L}$ is entirely unknown, save for possibly an estimate on its norm.

Let us denote by $X_{2\kappa-1} \in \mathbb{C}^{d \times (2\kappa-1)}$ the matrix with columns

$$\widehat{\mathbf{x}} \circ S_\sigma \widehat{\mathbf{x}}, \quad |\sigma| \leq \kappa - 1,$$

ordered by increasing σ . Also, denote by $N_{2\kappa-1} \in \mathbb{C}^{d \times (2\kappa-1)}$ the matrix with ordered

columns

$$\frac{d^2}{L} F_d^{-1} \left(\frac{\left(F_d N_{d,L} \left(F_L^T \right) \right)_\alpha}{F_d \left(\widehat{\mathbf{m}} \circ S_\alpha \widehat{\mathbf{m}} \right)} \right), \quad \alpha \in \{\kappa - 1, \kappa - 2, \dots, 0\},$$

and

$$\frac{d^2}{L} F_d^{-1} \left(\frac{\left(F_d N_{d,L} \left(F_L^T \right) \right)_\alpha}{F_d \left(\widehat{\mathbf{m}} \circ S_{\alpha-L} \widehat{\mathbf{m}} \right)} \right), \quad \alpha \in \{2\kappa - 2, 2\kappa - 3, \dots, k\}.$$

Similarly, denote by $Y_{2\kappa-1} \in \mathbb{C}^{d \times (2\kappa-1)}$ the matrix with ordered columns

$$\frac{d^2}{L} F_d^{-1} \left(\frac{\left(F_d Y_{d,L} \left(F_L^T \right) \right)_\alpha}{F_d \left(\widehat{\mathbf{m}} \circ S_\alpha \widehat{\mathbf{m}} \right)} \right), \quad \alpha \in \{\kappa - 1, \kappa - 2, \dots, 0\},$$

and

$$\frac{d^2}{L} F_d^{-1} \left(\frac{\left(F_d Y_{d,L} \left(F_L^T \right) \right)_\alpha}{F_d \left(\widehat{\mathbf{m}} \circ S_{\alpha-L} \widehat{\mathbf{m}} \right)} \right), \quad \alpha \in \{2\kappa - 2, 2\kappa - 3, \dots, k\}.$$

Then

$$Y_{2\kappa-1} = X_{2\kappa-1} + N_{2\kappa-1}. \quad (2.1.12)$$

Using $\|F_d\|_2 = \sqrt{d}$ and $\|F_d^{-1}\|_2 = \frac{1}{\sqrt{d}}$, we compute the following bound on the Frobenius norm of $N_{2\kappa-1}$:

$$\begin{aligned} \|Y_{2\kappa-1} - X_{2\kappa-1}\|_F^2 &= \|N_{2\kappa-1}\|_F^2 \\ &\leq \frac{d^4}{L^2} \cdot \left(\frac{1}{\sqrt{d}} \right)^2 \frac{\|F_d N_{d,L} F_L^T\|_F^2}{\mu^2} \\ &= \frac{d^3}{L^2 \mu^2} \cdot L \cdot d \|N_{d,L}\|_F^2 \\ &= \frac{d^4}{L \mu^2} \|N_{d,L}\|_F^2, \end{aligned}$$

where μ is as in (2.1.9). Thus,

$$\|N_{2\kappa-1}\|_F \leq \frac{d^2}{\sqrt{L}\mu} \|N_{d,L}\|_F. \quad (2.1.13)$$

Now, one can write (2.1.12) into a circulant form using the operator $C_{2\kappa-1}$ defined in (2.0.1):

$$C_{2\kappa-1}(X_{2\kappa-1}) = C_{2\kappa-1}(Y_{2\kappa-1}) - C_{2\kappa-1}(N_{2\kappa-1}).$$

Finally, let $\tilde{X}_{2\kappa-1}$ and $\tilde{Y}_{2\kappa-1}$ be the (componentwise) normalized versions of the matrices $C_{2\kappa-1}(X_{2\kappa-1})$ and $C_{2\kappa-1}(Y_{2\kappa-1})$, respectively:

$$\tilde{X}_{2\kappa-1} := C_{2\kappa-1}(\text{sgn}(X_{2\kappa-1})),$$

$$\tilde{Y}_{2\kappa-1} := C_{2\kappa-1}(\text{sgn}(Y_{2\kappa-1})).$$

Let S_ϵ be as in (2.1.8). For any $j, k \in S_\epsilon^c$, we bound $\left| \left(\tilde{X}_{2\kappa-1} \right)_{j,k} - \left(\tilde{Y}_{2\kappa-1} \right)_{j,k} \right|$ as follows:

$$\begin{aligned} & \left| \left(\tilde{X}_{2\kappa-1} \right)_{j,k} - \text{sgn} \left(\frac{(C_{2\kappa-1}(Y_{2\kappa-1}))_{j,k}}{|(C_{2\kappa-1}(X_{2\kappa-1}))_{j,k}|} \right) \right| \\ & \leq \left| \left(\tilde{X}_{2\kappa-1} \right)_{j,k} - \frac{(C_{2\kappa-1}(Y_{2\kappa-1}))_{j,k}}{|(C_{2\kappa-1}(X_{2\kappa-1}))_{j,k}|} \right| \\ & \quad + \left| \frac{(C_{2\kappa-1}(Y_{2\kappa-1}))_{j,k}}{|(C_{2\kappa-1}(X_{2\kappa-1}))_{j,k}|} - \text{sgn} \left(\frac{(C_{2\kappa-1}(Y_{2\kappa-1}))_{j,k}}{|(C_{2\kappa-1}(X_{2\kappa-1}))_{j,k}|} \right) \right| \\ & \leq 2 \left| \left(\tilde{X}_{2\kappa-1} \right)_{j,k} - \frac{(C_{2\kappa-1}(Y_{2\kappa-1}))_{j,k}}{|(C_{2\kappa-1}(X_{2\kappa-1}))_{j,k}|} \right| \end{aligned}$$

$$\begin{aligned}
&= 2 \frac{\left| (C_{2\kappa-1} (N_{2\kappa-1}))_{j,k} \right|}{\left| (C_{2\kappa-1} (X_{2\kappa-1}))_{j,k} \right|} \\
&\leq 2 \sqrt{\epsilon \|N_{d,L}\|_F^{-1}} \cdot \left| (C_{2\kappa-1} (N_{2\kappa-1}))_{j,k} \right|.
\end{aligned}$$

The last inequality holds since $j, k \in S_\epsilon^c$, whence

$$\frac{1}{|\hat{x}_k \hat{x}_j|} > \epsilon^{-\frac{1}{2}} \|N_{d,L}\|_F^{\frac{1}{2}}.$$

We can now calculate

$$\begin{aligned}
\left\| \tilde{Y}_{2\kappa-1} - \tilde{X}_{2\kappa-1} \right\|_F^2 &\leq \sum_{j,k \in S_\epsilon^c} \frac{4\epsilon}{\|N_{d,L}\|_F} \left| (C_{2\kappa-1} (N_{2\kappa-1}))_{j,k} \right|^2 \\
&\quad + \sum_{j \text{ or } k \in S_\epsilon} \left| \left(\tilde{X}_{2\kappa-1} \right)_{j,k} - \left(\tilde{Y}_{2\kappa-1} \right)_{j,k} \right|^2 \\
&\leq \frac{4\epsilon}{\|N_{d,L}\|_F} \|N_{2\kappa-1}\|_F^2 + \sum_{j \in S_\epsilon} 4(4\kappa - 3) \\
&\leq \frac{4\epsilon d^4}{L\mu^2} \|N_{d,L}\|_F + 4(4\kappa - 3) \cdot |S_\epsilon|,
\end{aligned}$$

where the last inequality follows from (2.1.13). Thus, there exists a constant $C' \in \mathbb{R}$ such that

$$\left\| \tilde{Y}_{2\kappa-1} - \tilde{X}_{2\kappa-1} \right\|_F^2 \leq C' \left(\frac{\epsilon d^4}{L\mu^2} \|N_{d,L}\|_F + \kappa |S_\epsilon| \right).$$

Since $\left\| \tilde{X}_{2\kappa-1} \right\|_F = \sqrt{(2\kappa - 1)d}$, we can write

$$\left\| \tilde{Y}_{2\kappa-1} - \tilde{X}_{2\kappa-1} \right\|_F \leq C \sqrt{d^{-1} \left(\frac{\epsilon d^4}{\kappa L \mu^2} \|N_{d,L}\|_F + |S_\epsilon| \right)} \cdot \left\| \tilde{X}_{2\kappa-1} \right\|_F$$

for some universal constant C . Now, by Corollary 2 of [36], we have

$$\min_{\theta \in [0, 2\pi]} \left\| \frac{\widehat{\mathbf{x}}}{|\widehat{\mathbf{x}}|} - e^{i\theta} \operatorname{sgn}(\mathbf{u}) \right\|_2 \leq C' \sqrt{d^{-1} \left(\frac{\epsilon d^4}{\kappa L \mu^2} \|N_{d,L}\|_F + |S_\epsilon| \right)} \cdot \frac{d^{\frac{5}{2}}}{\kappa^2}, \quad (2.1.14)$$

where $\frac{\widehat{\mathbf{x}}}{|\widehat{\mathbf{x}}|}$ is the vector of true phases of $\widehat{\mathbf{x}}$, and \mathbf{u} is the top eigenvector of $\widetilde{Y}_{2\kappa-1}$.

Let $\widehat{\mathbf{x}}_e$ be the estimate of $\widehat{\mathbf{x}}$ produced by Algorithm 1, so that

$$(\widehat{\mathbf{x}}_e)_j = \sqrt{(C_{2\kappa-1} (Y_{2\kappa-1}))_{j,j}} \cdot \operatorname{sgn}(\mathbf{u})_j \quad \forall j \in [d]_0.$$

We compute

$$\begin{aligned} \min_{\phi \in [0, 2\pi]} \left\| \widehat{\mathbf{x}} - e^{i\phi} \widehat{\mathbf{x}}_e \right\|_2 &= \min_{\phi \in [0, 2\pi]} \left\| |\widehat{\mathbf{x}}| \circ \frac{\widehat{\mathbf{x}}}{|\widehat{\mathbf{x}}|} - |\widehat{\mathbf{x}}_e| \circ e^{i\phi} \frac{\widehat{\mathbf{x}}_e}{|\widehat{\mathbf{x}}_e|} \right\|_2 \\ &\leq \min_{\phi \in [0, 2\pi]} \left\| |\widehat{\mathbf{x}}| \circ \frac{\widehat{\mathbf{x}}}{|\widehat{\mathbf{x}}|} - |\widehat{\mathbf{x}}| \circ e^{i\phi} \frac{\widehat{\mathbf{x}}_e}{|\widehat{\mathbf{x}}_e|} \right\|_2 + \left\| |\widehat{\mathbf{x}}| \circ e^{i\phi} \frac{\widehat{\mathbf{x}}_e}{|\widehat{\mathbf{x}}_e|} - |\widehat{\mathbf{x}}_e| \circ e^{i\phi} \frac{\widehat{\mathbf{x}}_e}{|\widehat{\mathbf{x}}_e|} \right\|_2, \end{aligned}$$

where the second term is independent of ϕ . We thus have

$$\min_{\phi \in [0, 2\pi]} \left\| \widehat{\mathbf{x}} - e^{i\phi} \widehat{\mathbf{x}}_e \right\|_2 \leq \|\widehat{\mathbf{x}}\|_\infty \left(\min_{\phi \in [0, 2\pi]} \left\| \frac{\widehat{\mathbf{x}}}{|\widehat{\mathbf{x}}|} - e^{i\phi} \frac{\widehat{\mathbf{x}}_e}{|\widehat{\mathbf{x}}_e|} \right\|_2 \right) + C'' \sqrt{\sqrt{d} \cdot \frac{d^2}{\sqrt{L}\mu} \|N_{d,L}\|_F}$$

for some absolute constant $C'' > 0$. Here the bound on the second term follows from Lemma 3 of [37] and the Cauchy-Schwartz inequality. Combining the bound above with (2.1.14) yields

$$\begin{aligned} \min_{\phi \in [0, 2\pi]} \left\| \widehat{\mathbf{x}} - e^{i\phi} \widehat{\mathbf{x}}_e \right\|_2 &\leq C' \frac{\|\widehat{\mathbf{x}}\|_\infty}{\sqrt{d}} \sqrt{\frac{\epsilon d^4}{\kappa L \mu^2} \|N_{d,L}\|_F + |S_\epsilon|} \cdot \frac{d^{\frac{5}{2}}}{\kappa^2} + C'' \sqrt{\frac{d^{\frac{5}{2}}}{\sqrt{L}\mu} \|N_{d,L}\|_F} \\ &= C' \|\widehat{\mathbf{x}}\|_\infty \frac{d^2}{\kappa^2} \sqrt{\frac{\epsilon d^4}{\kappa L \mu^2} \|N_{d,L}\|_F + |S_\epsilon|} + C'' \left(\frac{d^5}{L} \right)^{\frac{1}{4}} \sqrt{\frac{\|N_{d,L}\|_F}{\mu}}. \end{aligned}$$

Note that if $\epsilon = \frac{\|N_{d,L}\|_F}{\min|\widehat{\mathbf{x}}|^4}$, then $S_\epsilon = \emptyset$, and thus

$$\min_{\phi \in [0, 2\pi]} \left\| \widehat{\mathbf{x}} - e^{i\phi} \widehat{\mathbf{x}}_e \right\|_2 \leq C' \frac{d^4 \|\widehat{\mathbf{x}}\|_\infty \|N_{d,L}\|_F}{L^{\frac{1}{2}} \mu \kappa^{\frac{5}{2}} \cdot \min|\widehat{\mathbf{x}}|^2} + C'' \frac{d^{\frac{5}{4}} \|N_{d,L}\|_F^{\frac{1}{2}}}{L^{\frac{1}{4}} \mu^{\frac{1}{2}}}.$$

□

In order to guarantee that the constant μ is nonzero, we state the following lemma.

Lemma 2.1.4. *Let $\mathbf{m} \in \mathbb{C}^{d \times 1}$ be band-limited to $[\delta]_0$, so that its Fourier transform is*

$$\widehat{\mathbf{m}} = \left(a_0 e^{i\theta_0}, \dots, a_{\delta-1} e^{i\theta_{\delta-1}}, 0, \dots, 0 \right)^T$$

for some real numbers $a_0, \dots, a_{\delta-1}$. Let

$$\mu := \min_{\substack{|p| \leq \kappa - 1 \\ q \in [d]_0}} \left| F_d \left(\widehat{\mathbf{m}} \circ S_p \overline{\widehat{\mathbf{m}}} \right)_q \right|,$$

where $1 \leq \kappa \leq \delta$. If

$$|a_0| > (\delta - 1) |a_1| \tag{2.1.15}$$

and

$$|a_1| \geq |a_2| \geq \dots \geq |a_{\delta-1}| > 0, \tag{2.1.16}$$

then $\mu > 0$.

Proof. For $0 \leq p \leq \kappa - 1$, we have

$$\left(\widehat{\mathbf{m}} \circ S_p \overline{\widehat{\mathbf{m}}}\right)_n = \begin{cases} a_n a_{n+p} e^{i(\theta_n - \theta_{n+p})}, & \text{if } n \in [\delta - p]_0, \\ 0, & \text{otherwise,} \end{cases}$$

and for $-\kappa + 1 \leq p < 0$,

$$\left(\widehat{\mathbf{m}} \circ S_p \overline{\widehat{\mathbf{m}}}\right)_n = \begin{cases} a_{n-|p|} a_n e^{i(\theta_n - \theta_{n-|p|})}, & \text{if } n \in \{|p|, |p| + 1, \dots, \delta - 1\}, \\ 0, & \text{otherwise.} \end{cases}$$

Therefore for any $q \in [d]_0$,

$$F_d \left(\widehat{\mathbf{m}} \circ S_p \overline{\widehat{\mathbf{m}}}\right)_q = \sum_{n=0}^{\delta-1-|p|} a_n a_{|p|+n} e^{i\phi_{n,p,q}},$$

where $\phi_{n,p,q}$ is some real number depending only on n, p , and q . Using the assumptions (2.1.15) and (2.1.16) we see that

$$\left| \sum_{n=1}^{\delta-1-|p|} a_n a_{|p|+n} e^{i\phi_{n,p,q}} \right| \leq (\delta - 1) |a_1| |a_{1+|p|}| < |a_0| |a_{|p|}|. \quad (2.1.17)$$

With this,

$$\begin{aligned} \left| F_d \left(\widehat{\mathbf{m}} \circ S_p \overline{\widehat{\mathbf{m}}}\right)_q \right| &= \left| \sum_{n=0}^{\delta-1-|p|} a_n a_{|p|+n} e^{i\phi_{n,p,q}} \right| \\ &= \left| a_0 a_{|p|} e^{i\phi_{0,p,q}} + \sum_{n=1}^{\delta-1-|p|} a_n a_{|p|+n} e^{i\phi_{n,p,q}} \right| \end{aligned}$$

$$\begin{aligned}
&\geq \left| \left| a_0 a_{|p|} e^{i\phi_{0,p,q}} \right| - \left| \sum_{n=1}^{\delta-1-|p|} a_n a_{|p|+n} e^{i\phi_{n,p,q}} \right| \right| \\
&= \left| \left| a_0 a_{|p|} \right| - \left| \sum_{n=1}^{\delta-1-|p|} a_n a_{|p|+n} e^{i\phi_{n,p,q}} \right| \right| > 0,
\end{aligned}$$

where the last inequality follows by (2.1.17). This completes the proof. \square

The interested reader may read Proposition 2 on page 63 of [48] for a connection between μ and the condition number of the measurement system.

2.1.3.1 A Special Case of Theorem 2.1.1

Let us consider the special case of Theorem 2.1.1, where $\delta = 2$ so that $\text{supp}(\widehat{\mathbf{m}}) = \{0, 1\}$, $\kappa = \delta = 2$ so that $L = 3$. We may design $\mathbf{m} \in \mathbb{C}^{d \times 1}$ so that

$$\widehat{\mathbf{m}} = (ae^{i\psi}, be^{i\phi}, 0, \dots, 0)^T$$

for some nonzero $a, b \in \mathbb{R}$, with $|a| > |b|$. For this choice of mask, we have for any $\omega \in [d]_0$:

$$\begin{aligned}
\left(F_d(\widehat{\mathbf{m}} \circ \widehat{\mathbf{m}}) \right)_\omega &= \left(F_d(a^2, b^2, 0, \dots, 0)^T \right)_\omega = a^2 + b^2 e^{-\frac{2\pi i \omega}{d}} \neq 0, \\
\left(F_d(\widehat{\mathbf{m}} \circ S_1 \widehat{\mathbf{m}}) \right)_\omega &= \left(F_d(abe^{i(\psi-\phi)}, 0, \dots, 0)^T \right)_\omega = abe^{i(\psi-\phi)} \neq 0, \\
\left(F_d(\widehat{\mathbf{m}} \circ S_{-1} \widehat{\mathbf{m}}) \right)_\omega &= \left(F_d(0, abe^{i(\phi-\psi)}, 0, \dots, 0)^T \right)_\omega = abe^{i(\phi-\psi)} e^{-\frac{2\pi i \omega}{d}} \neq 0.
\end{aligned}$$

The mask-dependent constant μ is

$$\mu := \min_{\omega \in [d]_0} \left\{ |ab|, \left| a^2 + b^2 e^{-\frac{2\pi i \omega}{d}} \right| \right\} > 0.$$

We have

$$\widehat{\mathbf{x}} \circ S_{-p} \overline{\widehat{\mathbf{x}}} + \frac{d^2}{3} F_d^{-1} \left(\frac{\left(F_d N_{d,3} F_3^T \right)_p}{F_d \left(\widehat{\mathbf{m}} \circ S_p \widehat{\mathbf{m}} \right)} \right) = \frac{d^2}{3} F_d^{-1} \left(\frac{\left(F_d Y_{d,3} F_3^T \right)_p}{F_d \left(\widehat{\mathbf{m}} \circ S_p \widehat{\mathbf{m}} \right)} \right), \quad p \in \{-1, 0, 1\}.$$

Let us denote by $X_3 \in \mathbb{C}^{d \times 3}$ the matrix with columns $\widehat{\mathbf{x}} \circ S_{-1} \overline{\widehat{\mathbf{x}}}$, $\widehat{\mathbf{x}} \circ \overline{\widehat{\mathbf{x}}}$, and $\widehat{\mathbf{x}} \circ S_1 \overline{\widehat{\mathbf{x}}}$, so that

$$X_3 = \begin{bmatrix} \widehat{x}_0 \overline{\widehat{x}}_{d-1} & |\widehat{x}_0|^2 & \widehat{x}_0 \overline{\widehat{x}}_1 \\ \widehat{x}_1 \overline{\widehat{x}}_0 & |\widehat{x}_1|^2 & \widehat{x}_1 \overline{\widehat{x}}_2 \\ \vdots & \vdots & \vdots \\ \widehat{x}_{d-1} \overline{\widehat{x}}_{d-2} & |\widehat{x}_{d-1}|^2 & \widehat{x}_{d-1} \overline{\widehat{x}}_0 \end{bmatrix},$$

and by $Y_3, N_3 \in \mathbb{C}^{d \times 3}$ the matrices

$$Y_3 = \frac{d^2}{3} F_d^{-1} ([\psi_1 | \psi_0 | \psi_{-1}]), \quad N_3 = \frac{d^2}{3} F_d^{-1} ([\phi_1 | \phi_0 | \phi_{-1}]),$$

whose columns are given by

$$\psi_p := \frac{\left(F_d Y_{d,3} F_3^T \right)_p}{F_d \left(\widehat{\mathbf{m}} \circ S_p \widehat{\mathbf{m}} \right)}, \quad \phi_p := \frac{\left(F_d N_{d,3} F_3^T \right)_p}{F_d \left(\widehat{\mathbf{m}} \circ S_p \widehat{\mathbf{m}} \right)}.$$

We may write

$$C_3(X_3) = C_3(Y_3) - C_3(N_3),$$

where

$$C_3(X_3) = \begin{bmatrix} |\widehat{x}_0|^2 & \widehat{x}_0\widehat{x}_1 & \cdots & 0 & \widehat{x}_0\widehat{x}_{d-1} \\ \widehat{x}_1\widehat{x}_0 & |\widehat{x}_1|^2 & \widehat{x}_1\widehat{x}_2 & & 0 \\ \vdots & \ddots & \ddots & \ddots & \vdots \\ 0 & & \widehat{x}_{d-2}\widehat{x}_{d-3} & |\widehat{x}_{d-2}|^2 & \widehat{x}_{d-2}\widehat{x}_{d-1} \\ \widehat{x}_{d-1}\widehat{x}_0 & 0 & \cdots & \widehat{x}_{d-1}\widehat{x}_{d-2} & |\widehat{x}_{d-1}|^2 \end{bmatrix}$$

is a banded version of the rank-one matrix $\widehat{\mathbf{x}}\widehat{\mathbf{x}}^* \in \mathbb{C}^{d \times d}$. Finally, let \widetilde{X}_3 , \widetilde{Y}_3 , and \widetilde{N}_3 be the (componentwise) normalized versions of $C_3(X_3)$, $C_3(Y_3)$, and $C_3(N_3)$, respectively, so that if $\widehat{\mathbf{x}} = (|\widehat{x}_0|e^{i\alpha_0}, \dots, |\widehat{x}_{d-1}|e^{i\alpha_{d-1}})$, then

$$\widetilde{X}_3 = \begin{bmatrix} 1 & e^{i(\alpha_0-\alpha_1)} & \cdots & 0 & e^{i(\alpha_0-\alpha_{d-1})} \\ e^{i(\alpha_1-\alpha_0)} & 1 & e^{i(\alpha_1-\alpha_2)} & & 0 \\ \vdots & \ddots & \ddots & \ddots & \vdots \\ 0 & & e^{i(\alpha_{d-2}-\alpha_{d-3})} & 1 & e^{i(\alpha_{d-2}-\alpha_{d-1})} \\ e^{i(\alpha_{d-1}-\alpha_0)} & 0 & \cdots & e^{i(\alpha_{d-1}-\alpha_{d-2})} & 1 \end{bmatrix}.$$

We have

$$\widetilde{Y}_3 = \widetilde{X}_3 + \widetilde{N}_3.$$

As before, define the set

$$S_\epsilon := \left\{ n : |\widehat{x}_n| < \epsilon^{-\frac{1}{4}} \cdot \|N_{d,3}\|_F^{\frac{1}{4}} \right\},$$

and let $\widehat{\mathbf{x}}_e$ be the estimate of $\widehat{\mathbf{x}}$ produced by Algorithm 1. Then

$$\min_{\phi \in [0, 2\pi]} \left\| \widehat{\mathbf{x}} - e^{i\phi} \widehat{\mathbf{x}}_e \right\|_2 \leq C' \|\widehat{\mathbf{x}}\|_\infty \frac{d^2}{2^2} \sqrt{\frac{\epsilon d^4}{3\mu^2} \|N_{d,3}\|_F + |S_\epsilon|} + C'' d^{\frac{5}{4}} \sqrt{\frac{\|N_{d,3}\|_F}{\sqrt{3}\mu}}.$$

Additionally, if $\epsilon = \frac{\|N_{d,3}\|_F}{\min|\widehat{\mathbf{x}}|^4}$, then $S_\epsilon = \emptyset$ and

$$\min_{\phi \in [0, 2\pi]} \left\| \widehat{\mathbf{x}} - e^{i\phi} \widehat{\mathbf{x}}_e \right\|_2 \leq C' \frac{d^4 \|\widehat{\mathbf{x}}\|_\infty \|N_{d,3}\|_F}{\mu \min|\widehat{\mathbf{x}}|^2} + C'' \frac{d^{\frac{5}{4}} \|N_{d,3}\|_F^{\frac{1}{2}}}{\mu^{\frac{1}{2}}}.$$

2.1.4 Other Support Conditions

We have considered above the case where the mask $\mathbf{m} \in \mathbb{C}^{d \times 1}$ is band-limited so that $\text{supp}(\widehat{\mathbf{m}}) = [\delta]_0$ with $\delta \ll d$, and $\mathbf{x} \in \mathbb{C}^{d \times 1}$ is arbitrary. Let us now consider other cases on the supports of $\mathbf{x}, \widehat{\mathbf{x}}, \mathbf{m}$, and/or $\widehat{\mathbf{m}}$.

Lemma 2.1.5. *Let $\mathbf{x} \in \mathbb{C}^{d \times 1}$ be arbitrary and $\mathbf{m} \in \mathbb{C}^{d \times 1}$ with $\text{supp}(\mathbf{m}) = [\rho]_0$. Assume*

$\frac{d}{K} \in \mathbb{N}$, and let $Y_{K,d} \in \mathbb{R}^{K \times d}$ contain noisy autocorrelation measurements of the form

$$(\mathbf{y}_\ell)_k = \left| \sum_{n=0}^{d-1} x_n m_{n-\ell} e^{-\frac{2\pi i n k}{d}} \right|^2 + \eta_{k,\ell}, \quad (k, \ell) \in \frac{d}{K} [K]_0 \times [d]_0.$$

Then for any $\alpha \in [d]_0$ and $\omega \in [K]_0$,

$$\left(F_d (Y_{K,d} - N_{K,d})^T \left(F_K^T \right)_\omega \right)_\alpha = \frac{K}{d^2} \sum_{r=0}^{\frac{d}{K}-1} \left(F_d \left(\widehat{\mathbf{x}} \circ S_{-\alpha} \widehat{\mathbf{x}} \right) \right)_{\omega-rK} \left(F_d \left(\widehat{\mathbf{m}} \circ S_\alpha \widehat{\mathbf{m}} \right) \right)_{\omega-rK} \quad (2.1.18)$$

$$\begin{aligned}
&= K \sum_{r=0}^{\frac{d}{K}-1} (F_d(\mathbf{x} \circ S_{\omega-rK}\bar{\mathbf{x}}))_{\alpha} (F_d(\mathbf{m} \circ S_{\omega-rK}\bar{\mathbf{m}}))_{-\alpha}.
\end{aligned} \tag{2.1.19}$$

Moreover, if $K = \rho - 1 + \kappa$ for some $1 \leq \kappa \leq \rho$, and if $\omega \in [K]_0 \setminus \{\kappa, \kappa + 1, \dots, K - \kappa\}$, then for all $\alpha \in [d]_0$, the sum above collapses to only one term as follows:

$$\begin{aligned}
&\left(F_d(Y_{K,d} - N_{K,d})^T \left(F_K^T \right)_{\omega} \right)_{\alpha} \\
&= \begin{cases} K (F_d(\mathbf{x} \circ S_{\omega}\bar{\mathbf{x}}))_{\alpha} (F_d(\mathbf{m} \circ S_{\omega}\bar{\mathbf{m}}))_{-\alpha}, & \text{if } \omega \in [\kappa]_0, \\ K (F_d(\mathbf{x} \circ S_{\omega-K}\bar{\mathbf{x}}))_{\alpha} (F_d(\mathbf{m} \circ S_{\omega-K}\bar{\mathbf{m}}))_{-\alpha}, & \text{if } \omega \in [K]_0 \setminus [K - \kappa + 1]_0. \end{cases}
\end{aligned}$$

Proof. The equality in (2.1.18) follows from Lemma 2.1.2 with $L = d$, while (2.1.19) holds by by Lemma 2.0.2:

$$\begin{aligned}
\left(F_d(\widehat{\mathbf{x}} \circ S_{-\alpha}\widehat{\bar{\mathbf{x}}}) \right)_{\omega-rK} &= d \cdot e^{\frac{-2\pi i \alpha(\omega-rK)}{d}} (F_d(\mathbf{x} \circ S_{\omega-rK}\bar{\mathbf{x}}))_{\alpha}, \\
\left(F_d(\widehat{\mathbf{m}} \circ S_{\alpha}\widehat{\bar{\mathbf{m}}}) \right)_{\omega-rK} &= d \cdot e^{\frac{+2\pi i \alpha(\omega-rK)}{d}} (F_d(\mathbf{m} \circ S_{\omega-rK}\bar{\mathbf{m}}))_{-\alpha}.
\end{aligned}$$

It remains to show that if K is chosen so that $K = \rho - 1 + \kappa$ for some $1 \leq \kappa \leq \rho$ and ω is chosen from $[K]_0 \setminus \{\kappa, \kappa + 1, \dots, K - \kappa\}$, then the sum reduces to a single term for all $\alpha \in [d]_0$.

Assume that $\text{supp}(\mathbf{m}) = [\rho]_0$ for some $\rho \ll d$ and set $K = \rho - 1 + \kappa$. Observe that $\mathbf{m} \circ S_{\omega-rK}\bar{\mathbf{m}} = \mathbf{0}$ whenever the supports of \mathbf{m} and $S_{\omega-rK}\bar{\mathbf{m}}$ are disjoint. Now,

$$\text{supp}(\mathbf{m}) \cap \text{supp}(S_{\omega-rK}\bar{\mathbf{m}}) \neq \emptyset \iff |\omega - rK| \leq \rho - 1.$$

Note that since $K \leq 2\rho - 1$, for any $\omega \in [\kappa]_0$, $|\omega - rK| \leq \rho - 1$ if and only if $r = 0$, and for any $\omega \in \{K - \kappa + 1, \dots, K - 1\}$, $|\omega - rK| \leq \rho - 1$ if and only if $r = 1$. \square

We have so far considered conditions on the supports of the mask \mathbf{m} or its Fourier transform $\widehat{\mathbf{m}}$. Next, we consider the effect of imposing support conditions on $\widehat{\mathbf{x}}$.

Lemma 2.1.6. *Let $\mathbf{x} \in \mathbb{C}^{d \times 1}$ be arbitrary with $\text{supp}(\widehat{\mathbf{x}}) = [\gamma]_0$ and $\mathbf{m} \in \mathbb{C}^{d \times 1}$ with $\text{supp}(\mathbf{m}) = [\rho]_0$. Assume L and K divide d , and let $Y_{K,L} \in \mathbb{R}^{K \times L}$ contain noisy auto-correlation measurements of the form*

$$(\mathbf{y}_\ell)_k = \left| \sum_{n=0}^{d-1} x_n m_{n-\ell} e^{-\frac{2\pi i n k}{d}} \right|^2 + \eta_{k,\ell}, \quad (k, \ell) \in \frac{d}{K} [K]_0 \times \frac{d}{L} [L]_0.$$

Then for any $\alpha \in [L]_0$ and $\omega \in [K]_0$,

$$\begin{aligned} & \left(F_L (Y_{K,L} - N_{K,L})^T \left(F_K^T \right)_\omega \right)_\alpha \\ &= \frac{KL}{d^3} \sum_{r=0}^{\frac{d}{K}-1} \sum_{\ell=0}^{\frac{d}{L}-1} \left(F_d \left(\widehat{\mathbf{x}} \circ S_{\ell L - \alpha} \widehat{\mathbf{x}} \right) \right)_{\omega - rK} \left(F_d \left(\widehat{\mathbf{m}} \circ S_{\alpha - \ell L} \widehat{\mathbf{m}} \right) \right)_{\omega - rK} \\ &= \frac{KL}{d^2} \sum_{r=0}^{\frac{d}{K}-1} \sum_{\ell=0}^{\frac{d}{L}-1} e^{\frac{2\pi i}{d}(\omega - rK)(\alpha - \ell L)} \left(F_d \left(\widehat{\mathbf{x}} \circ S_{\ell L - \alpha} \widehat{\mathbf{x}} \right) \right)_{\omega - rK} \left(F_d \left(\mathbf{m} \circ S_{\omega - rK} \overline{\mathbf{m}} \right) \right)_{\ell L - \alpha}. \end{aligned}$$

Moreover, if $K = \rho - 1 + \kappa$ for some $1 \leq \kappa \leq \rho$ and $L = \gamma - 1 + \xi$ for some $1 \leq \xi \leq \gamma$, then for all $\omega \in [K]_0 \setminus \{\kappa, \kappa + 1, \dots, K - \kappa\}$ and $\alpha \in [L]_0 \setminus \{\xi, \xi + 1, \dots, L - \xi\}$, the sum above collapses to only one term, so that $\left(F_L (Y_{K,L} - N_{K,L})^T \left(F_K^T \right)_\omega \right)_\alpha$ is equal to

1. $\frac{KL}{d^3} \left(F_d \left(\widehat{\mathbf{x}} \circ S_{-\alpha} \widehat{\mathbf{x}} \right) \right)_\omega \left(F_d \left(\widehat{\mathbf{m}} \circ S_\alpha \widehat{\mathbf{m}} \right) \right)_\omega$ if $\omega \in [\kappa]_0$ and $\alpha \in [\xi]_0$, or
2. $\frac{KL}{d^3} \left(F_d \left(\widehat{\mathbf{x}} \circ S_{L-\alpha} \widehat{\mathbf{x}} \right) \right)_\omega \left(F_d \left(\widehat{\mathbf{m}} \circ S_{\alpha-L} \widehat{\mathbf{m}} \right) \right)_\omega$ if $\alpha \in \{L - \xi + 1, \dots, L - 1\}$ and $\omega \in [\kappa]_0$, or

3. $\frac{KL}{d^3} \left(F_d \left(\widehat{\mathbf{x}} \circ S_{-\alpha} \widehat{\mathbf{x}} \right) \right)_{\omega-K} \left(F_d \left(\widehat{\mathbf{m}} \circ S_{\alpha} \widehat{\mathbf{m}} \right) \right)_{\omega-K}$ if $\omega \in \{K - \kappa + 1, \dots, K - 1\}$ and $\alpha \in [\xi]_0$, or
4. $\frac{KL}{d^3} \left(F_d \left(\widehat{\mathbf{x}} \circ S_{L-\alpha} \widehat{\mathbf{x}} \right) \right)_{\omega-K} \left(F_d \left(\widehat{\mathbf{m}} \circ S_{\alpha-L} \widehat{\mathbf{m}} \right) \right)_{\omega-K}$ if $\omega \in \{K - \kappa + 1, \dots, K - 1\}$ and $\alpha \in \{L - \xi + 1, \dots, L - 1\}$.

Proof. The equivalence of the two double sums in the lemma above is an application of Lemma 2.0.2. Let's consider the second double sum; using the argument from Lemma 2.1.5, we observe the following cases:

1. If $\omega \in [\kappa]_0$ and $\alpha \in [\xi]_0$, the sum reduces to $r = 0$ and $\ell = 0$.
2. If $\omega \in [\kappa]_0$ and $\alpha \in \{L - \xi + 1, \dots, L - 1\}$, the sum reduces to $r = 0$ and $\ell = 1$.
3. If $\omega \in \{K - \kappa + 1, \dots, K - 1\}$ and $\alpha \in [\xi]_0$, the sum reduces to $r = 1$ and $\ell = 0$.
4. If $\omega \in \{K - \kappa + 1, \dots, K - 1\}$ and $\alpha \in \{L - \xi + 1, \dots, L - 1\}$, the sum reduces to $r = 1$ and $\ell = 1$.

□

If we think of $\widehat{\mathbf{x}} \circ S_j \widehat{\mathbf{x}}$, $|j| \leq \xi - 1$, as columns of a matrix $\widetilde{X}_{2\xi-1} \in \mathbb{C}^{d \times (2\xi-1)}$, then the theorem above allows us to recover estimates of the first κ and last $\kappa - 1$ entries of each of the columns of $F_d \left(\widetilde{X}_{2\xi-1} \right) \in \mathbb{C}^{d \times (2\xi-1)}$.

2.1.4.1 A Special Case of Lemma 2.1.6.

We present below an algorithm which allows for the recovery of a band-limited signal \mathbf{x} through measurements with a compactly supported mask \mathbf{m} . Specifically, if $\text{supp}(\widehat{\mathbf{x}}) = [\gamma]_0$ and $\text{supp}(\mathbf{m}) = \rho$, then $\widehat{\mathbf{x}}$ may be recovered from $(2\rho - 1) \cdot (2\gamma - 1)$ measurements as prescribed in Algorithm 2.

Algorithm 2 Aliased WDD and Angular Synchronization for Band-limited \mathbf{x}

Inputs

1: $Y_{K,L} \in \mathbb{R}^{K \times L}$: matrix of KL noisy measurements of the form

$$(\mathbf{y}\ell)_k = \left| \sum_{n=0}^{d-1} x_n m_{n-\ell} e^{-\frac{2\pi i n k}{d}} \right|^2 + \eta_{k,\ell}, \quad (k, \ell) \in \frac{d}{K} [K]_0 \times \frac{d}{L} [L]_0. \quad (2.1.20)$$

2: Spatially-limited mask (or window) $\mathbf{m} \in \mathbb{C}^{d \times 1}$.

3: Integers γ and ρ , support sizes of $\widehat{\mathbf{x}}$ and \mathbf{m} , respectively, so that $L = 2\gamma - 1$, $K = 2\rho - 1$.

Steps

1: Estimate $\left(F_d \left(\widehat{\mathbf{x}} \circ S_\sigma \widehat{\widehat{\mathbf{x}}} \right) \right)_\beta$ (assuming no noise) for $|\sigma| \leq \gamma - 1$ and $|\beta| \leq \rho - 1$ as:

- if $\omega \in [\rho]_0$ and $\alpha \in [\gamma]_0$, then

$$\left(F_d \left(\widehat{\mathbf{x}} \circ S_{-\alpha} \widehat{\widehat{\mathbf{x}}} \right) \right)_\omega \approx \frac{d^3}{KL} \frac{\left(F_L Y_{K,L}^T \left(F_K^T \right)_\omega \right)_\alpha}{\left(F_d \left(\widehat{\mathbf{m}} \circ S_\alpha \widehat{\widehat{\mathbf{m}}} \right) \right)_\omega};$$

- if $\omega \in [\rho]_0$ and $\alpha \in \{\gamma, \dots, 2\gamma - 2\}$, then

$$\left(F_d \left(\widehat{\mathbf{x}} \circ S_{L-\alpha} \widehat{\widehat{\mathbf{x}}} \right) \right)_\omega \approx \frac{d^3}{KL} \frac{\left(F_L Y_{K,L}^T \left(F_K^T \right)_\omega \right)_\alpha}{\left(F_d \left(\widehat{\mathbf{m}} \circ S_{\alpha-L} \widehat{\widehat{\mathbf{m}}} \right) \right)_\omega};$$

- if $\omega \in \{\rho, \dots, 2\rho - 2\}$ and $\alpha \in [\gamma]_0$, then

$$\left(F_d \left(\widehat{\mathbf{x}} \circ S_{-\alpha} \widehat{\widehat{\mathbf{x}}} \right) \right)_{\omega-K} \approx \frac{d^3}{KL} \frac{\left(F_L Y_{K,L}^T \left(F_K^T \right)_\omega \right)_\alpha}{\left(F_d \left(\widehat{\mathbf{m}} \circ S_\alpha \widehat{\widehat{\mathbf{m}}} \right) \right)_{\omega-K}};$$

- if $\omega \in \{\rho, \dots, 2\rho - 2\}$ and $\alpha \in \{\gamma, \dots, 2\gamma - 2\}$, then

$$\left(F_d \left(\widehat{\mathbf{x}} \circ S_{L-\alpha} \widehat{\widehat{\mathbf{x}}} \right) \right)_{\omega-K} \approx \frac{d^3}{KL} \frac{\left(F_L Y_{K,L}^T \left(F_K^T \right)_\omega \right)_\alpha}{\left(F_d \left(\widehat{\mathbf{m}} \circ S_{\alpha-L} \widehat{\widehat{\mathbf{m}}} \right) \right)_{\omega-K}}.$$

Algorithm 2 Continued

- 2: Organize the estimates of $\left(F_d\left(\widehat{\mathbf{x}} \circ S_\sigma \overline{\widehat{\mathbf{x}}}\right)\right)_\beta$ in a matrix $V \in \mathbb{C}^{(2\rho-1) \times (2\gamma-1)}$.
- 3: Compute W^+V as an estimate to $A \in \mathbb{C}^{\gamma \times (2\gamma-1)}$, where

$$W_{j,k} = e^{-\frac{2\pi i(j-\rho+1)k}{d}}, \quad (j, k) \in [2\rho-1]_0 \times [\gamma]_0,$$

$$W^+ = (W^*W)^{-1}W^* \in \mathbb{C}^{\gamma \times (2\rho-1)},$$

$$A = \begin{bmatrix} 0 & \cdots & 0 & |\widehat{x}_0|^2 & \widehat{x}_0\overline{\widehat{x}_1} & \cdots & \widehat{x}_0\overline{\widehat{x}_{\gamma-1}} \\ 0 & \cdots & \widehat{x}_1\overline{\widehat{x}_0} & |\widehat{x}_1|^2 & \widehat{x}_1\overline{\widehat{x}_2} & \cdots & 0 \\ \vdots & \vdots & \vdots & \vdots & \vdots & \vdots & \vdots \\ 0 & \cdots & \widehat{x}_{\gamma-2}\overline{\widehat{x}_{\gamma-3}} & |\widehat{x}_{\gamma-2}|^2 & \widehat{x}_{\gamma-2}\overline{\widehat{x}_{\gamma-1}} & \cdots & 0 \\ \widehat{x}_{\gamma-1}\overline{\widehat{x}_0} & \cdots & \widehat{x}_{\gamma-1}\overline{\widehat{x}_{\gamma-2}} & |\widehat{x}_{\gamma-1}|^2 & 0 & \cdots & 0 \end{bmatrix}. \quad (2.1.21)$$

- 4: From W^+V , form an estimate $G \in \mathbb{C}^{\gamma \times \gamma}$ to the rank-one matrix

$$\widehat{\mathbf{x}}|_{[\gamma]_0} \widehat{\mathbf{x}}^*|_{[\gamma]_0} = \begin{bmatrix} |\widehat{x}_0|^2 & \widehat{x}_0\overline{\widehat{x}_1} & \widehat{x}_0\overline{\widehat{x}_2} & \cdots & \widehat{x}_0\overline{\widehat{x}_{\gamma-1}} \\ \widehat{x}_1\overline{\widehat{x}_0} & |\widehat{x}_1|^2 & \widehat{x}_1\overline{\widehat{x}_2} & \cdots & \widehat{x}_1\overline{\widehat{x}_{\gamma-1}} \\ \vdots & \vdots & \ddots & \vdots & \vdots \\ \widehat{x}_{\gamma-1}\overline{\widehat{x}_0} & \widehat{x}_{\gamma-1}\overline{\widehat{x}_1} & \widehat{x}_{\gamma-1}\overline{\widehat{x}_2} & \cdots & |\widehat{x}_{\gamma-1}|^2 \end{bmatrix}.$$

- 5: Hermitianize the matrix G above: $G \leftarrow \frac{1}{2}(G + G^*)$.
- 6: Compute λ_1 , the largest magnitude eigenvalue of G , and \mathbf{v}_1 , its associated eigenvector.

Output An estimate $\widehat{\mathbf{x}}_e$ (up to a global phase) to $\widehat{\mathbf{x}}$, given componentwise via

$$(\widehat{\mathbf{x}}_e)_j = \begin{cases} \sqrt{|\lambda_1|} (\mathbf{v}_1)_j, & \text{if } j \in [\gamma]_0, \\ 0, & \text{otherwise.} \end{cases}$$

We are now ready to provide recovery guarantees for Algorithm 2.

Theorem 2.1.2. *Let $\mathbf{x} \in \mathbb{C}^{d \times 1}$ be band-limited so that $\text{supp}(\widehat{\mathbf{x}}) = [\gamma]_0$ and $\mathbf{m} \in \mathbb{C}^{d \times 1}$ with $\text{supp}(\mathbf{m}) = [\rho]_0$. Let $L = 2\gamma - 1$ and $K = 2\rho - 1$, and assume $\rho \geq \gamma$ and $\frac{d}{L}, \frac{d}{K} \in \mathbb{N}$. Let $Y_{K,L} \in \mathbb{C}^{K \times L}$ contain KL noisy autocorrelation measurements as in (2.1.20), with $\|N_{K,L}\|_F \leq \beta \|\widehat{\mathbf{x}}\|_2^2$ for some $\beta \geq 0$. Let $\mu > 0$ denote the mask-dependent constant*

$$\mu := \min_{\substack{|p| \leq \gamma-1 \\ |q| \leq \rho-1}} \left| F_d \left(\widehat{\mathbf{m}} \circ S_p \overline{\widehat{\mathbf{m}}} \right)_q \right|. \quad (2.1.22)$$

Then Algorithm 2 outputs an estimate $\widehat{\mathbf{x}}_e$ to $\widehat{\mathbf{x}}$ with

$$\min_{\phi \in [0, 2\pi]} \left\| e^{i\phi} \widehat{\mathbf{x}} - \widehat{\mathbf{x}}_e \right\|_2 \leq \frac{(1 + 2\sqrt{2}) \beta}{\sigma_{\min}(W)} \frac{d^3}{\sqrt{KL}\mu} \|\widehat{\mathbf{x}}\|_2, \quad (2.1.23)$$

where W is the partial DFT matrix described in (2.1.21).

Proof. Let us consider the special case of Lemma 2.1.6 where L and K are chosen as

$$L := 2\gamma - 1, \quad K := 2\rho - 1,$$

where γ and ρ are the support sizes of $\widehat{\mathbf{x}}$ and \mathbf{m} , respectively. Then we have the following:

1. if $\omega \in [\rho]_0$ and $\alpha \in [\gamma]_0$, then

$$\left(F_d \left(\widehat{\mathbf{x}} \circ S_{-\alpha} \overline{\widehat{\mathbf{x}}} \right) \right)_\omega + \frac{d^3}{KL} \frac{\left(F_L N_{K,L}^T \left(F_K^T \right)_\omega \right)_\alpha}{\left(F_d \left(\widehat{\mathbf{m}} \circ S_\alpha \overline{\widehat{\mathbf{m}}} \right) \right)_\omega} = \frac{d^3}{KL} \frac{\left(F_L Y_{K,L}^T \left(F_K^T \right)_\omega \right)_\alpha}{\left(F_d \left(\widehat{\mathbf{m}} \circ S_\alpha \overline{\widehat{\mathbf{m}}} \right) \right)_\omega},$$

2. if $\omega \in [\rho]_0$ and $\alpha \in \{\gamma, \dots, 2\gamma - 2\}$, then

$$\left(F_d\left(\widehat{\mathbf{x}} \circ S_{L-\alpha}\widehat{\mathbf{x}}\right)\right)_\omega + \frac{d^3}{KL} \frac{\left(F_L N_{K,L}^T \left(F_K^T\right)_\omega\right)_\alpha}{\left(F_d\left(\widehat{\mathbf{m}} \circ S_{\alpha-L}\widehat{\mathbf{m}}\right)\right)_\omega} = \frac{d^3}{KL} \frac{\left(F_L Y_{K,L}^T \left(F_K^T\right)_\omega\right)_\alpha}{\left(F_d\left(\widehat{\mathbf{m}} \circ S_{\alpha-L}\widehat{\mathbf{m}}\right)\right)_\omega};$$

3. if $\omega \in \{\rho, \dots, 2\rho - 2\}$ and $\alpha \in [\gamma]_0$, then

$$\left(F_d\left(\widehat{\mathbf{x}} \circ S_{-\alpha}\widehat{\mathbf{x}}\right)\right)_{\omega-K} + \frac{d^3}{KL} \frac{\left(F_L N_{K,L}^T \left(F_K^T\right)_\omega\right)_\alpha}{\left(F_d\left(\widehat{\mathbf{m}} \circ S_\alpha\widehat{\mathbf{m}}\right)\right)_{\omega-K}} = \frac{d^3}{KL} \frac{\left(F_L Y_{K,L}^T \left(F_K^T\right)_\omega\right)_\alpha}{\left(F_d\left(\widehat{\mathbf{m}} \circ S_\alpha\widehat{\mathbf{m}}\right)\right)_{\omega-K}};$$

4. if $\omega \in \{\rho, \dots, 2\rho - 2\}$ and $\alpha \in \{\gamma, \dots, 2\gamma - 2\}$, then

$$\left(F_d\left(\widehat{\mathbf{x}} \circ S_{L-\alpha}\widehat{\mathbf{x}}\right)\right)_{\omega-K} + \frac{d^3}{KL} \frac{\left(F_L N_{K,L}^T \left(F_K^T\right)_\omega\right)_\alpha}{\left(F_d\left(\widehat{\mathbf{m}} \circ S_{\alpha-L}\widehat{\mathbf{m}}\right)\right)_{\omega-K}} = \frac{d^3}{KL} \frac{\left(F_L Y_{K,L}^T \left(F_K^T\right)_\omega\right)_\alpha}{\left(F_d\left(\widehat{\mathbf{m}} \circ S_{\alpha-L}\widehat{\mathbf{m}}\right)\right)_{\omega-K}}.$$

Let us represent the four cases above with a matrix equation

$$T + U = V,$$

where $T, U, V \in \mathbb{C}^{(2\rho-1) \times (2\gamma-1)}$ have entries

$$\left(F_d\left(\widehat{\mathbf{x}} \circ S_{-\alpha}\widehat{\mathbf{x}}\right)\right)_\omega, \frac{d^3}{KL} \frac{\left(F_L N_{K,L}^T \left(F_K^T\right)_\omega\right)_\alpha}{\left(F_d\left(\widehat{\mathbf{m}} \circ S_\alpha\widehat{\mathbf{m}}\right)\right)_\omega}, \frac{d^3}{KL} \frac{\left(F_L Y_{K,L}^T \left(F_K^T\right)_\omega\right)_\alpha}{\left(F_d\left(\widehat{\mathbf{m}} \circ S_\alpha\widehat{\mathbf{m}}\right)\right)_\omega},$$

respectively, for properly chosen α and ω . Let μ be as in (2.1.22). We compute the following bound:

$$\|V - T\|_F^2 = \|U\|_F^2$$

$$\begin{aligned}
&\leq \frac{d^6}{K^2 L^2} \cdot \frac{\|F_L N_{K,L} F_K^T\|_F^2}{\mu^2} \\
&= \frac{d^6}{K^2 L^2 \mu^2} \cdot L \cdot K \|N_{K,L}\|_F^2 \\
&= \frac{d^6}{KL\mu^2} \|N_{K,L}\|_F^2,
\end{aligned}$$

so that

$$\|U\|_F \leq \frac{d^3}{\sqrt{KL}\mu} \|N_{K,L}\|_F. \quad (2.1.24)$$

In short, we are able to estimate

$$\left(F_d \left(\widehat{\mathbf{x}} \circ S_\sigma \overline{\widehat{\mathbf{x}}} \right) \right)_\phi$$

for all $|\sigma| \leq \gamma - 1$ and $|\phi| \leq \rho - 1$. Observe furthermore that for all such ϕ and σ ,

$$\begin{aligned}
\left(F_d \left(\widehat{\mathbf{x}} \circ S_\sigma \overline{\widehat{\mathbf{x}}} \right) \right)_\phi &= \sum_{n=0}^{\gamma-1} e^{-\frac{2\pi i \phi n}{d}} \widehat{x}_n \overline{\widehat{x}_{n+\sigma}} \\
&=: \mathbf{v}^\phi \mathbf{a}_\sigma
\end{aligned}$$

where \mathbf{v}^ϕ is the ϕ^{th} row of the matrix $W \in \mathbb{C}^{(2\rho-1) \times \gamma}$ and \mathbf{a}_σ is the σ^{th} column of the matrix $A \in \mathbb{C}^{\gamma \times (2\gamma-1)}$ as in (2.1.21).

One can organize the $(2\rho - 1) \cdot (2\gamma - 1)$ values of $\left(F_d \left(\widehat{\mathbf{x}} \circ S_\sigma \overline{\widehat{\mathbf{x}}} \right) \right)_\phi$ in the matrix $T \in \mathbb{C}^{(2\rho-1) \times (2\gamma-1)}$ so that

$$T_{(2\rho-1) \times (2\gamma-1)} = W_{(2\rho-1) \times \gamma} A_{\gamma \times (2\gamma-1)}.$$

Since the measurements are contaminated with noise, we have

$$T + U = WA + U = V,$$

so that

$$W^+V = A + W^+U,$$

where

$$W^+ = (W^*W)^{-1} W^* \in \mathbb{C}^{\gamma \times (2\rho-1)}$$

is the pseudoinverse of W . This matrix exists since $\rho \geq \gamma$ and since W is full-rank (being the transpose of a Vandermonde matrix). We have

$$\begin{aligned} \|W^+V - A\|_F &= \|W^+U\|_F \\ &\leq \|W^+\|_2 \|U\|_F \\ &\leq \frac{1}{\sigma_{\min}(W)} \frac{d^3}{\sqrt{KL\mu}} \|N_{K,L}\|_F, \end{aligned}$$

where the last inequality follows from (2.1.24).

Once an estimate of the matrix $A \in \mathbb{C}^{\gamma \times (2\gamma-1)}$ is computed as W^+V , one can form an estimate $G \in \mathbb{C}^{\gamma \times \gamma}$ of the rank-one matrix

$$\widehat{\mathbf{x}}|_{[\gamma]_0} \widehat{\mathbf{x}}^*|_{[\gamma]_0} = \begin{bmatrix} |\widehat{x}_0|^2 & \widehat{x}_0 \widehat{x}_1^* & \widehat{x}_0 \widehat{x}_2^* & \cdots & \widehat{x}_0 \widehat{x}_{\gamma-1}^* \\ \widehat{x}_1 \widehat{x}_0^* & |\widehat{x}_1|^2 & \widehat{x}_1 \widehat{x}_2^* & \cdots & \widehat{x}_1 \widehat{x}_{\gamma-1}^* \\ \vdots & \vdots & \ddots & \vdots & \vdots \\ \widehat{x}_{\gamma-1} \widehat{x}_0^* & \widehat{x}_{\gamma-1} \widehat{x}_1^* & \widehat{x}_{\gamma-1} \widehat{x}_2^* & \cdots & |\widehat{x}_{\gamma-1}|^2 \end{bmatrix},$$

where $\widehat{\mathbf{x}}|_{[\gamma]_0} = (\widehat{x}_0, \dots, \widehat{x}_{\gamma-1})^T \in \mathbb{C}^{\gamma \times 1}$. We have

$$\begin{aligned} \left\| G - \widehat{\mathbf{x}}|_{[\gamma]_0} \widehat{\mathbf{x}}^*|_{[\gamma]_0} \right\|_F &\leq \|A - W^+V\|_F \\ &\leq \frac{1}{\sigma_{\min}(W)} \frac{d^3}{\sqrt{KL\mu}} \|N_{K,L}\|_F. \end{aligned}$$

Given that $\|N_{K,L}\|_F \leq \beta \|\widehat{\mathbf{x}}\|_2^2$ for some $\beta \geq 0$, we obtain

$$\left\| G - \widehat{\mathbf{x}}|_{[\gamma]_0} \widehat{\mathbf{x}}^*|_{[\gamma]_0} \right\|_F \leq \frac{\beta}{\sigma_{\min}(W)} \frac{d^3}{\sqrt{KL\mu}} \|\widehat{\mathbf{x}}\|_2^2.$$

Finally, by Lemma 8 of [36], if λ_i is the i^{th} largest magnitude eigenvalue of G and \mathbf{v}_i an associated eigenvector, such that the \mathbf{v}_i form an orthonormal eigenbasis, then

$$\begin{aligned} \min_{\theta \in [0, 2\pi]} \left\| e^{i\theta} \widehat{\mathbf{x}} - \widehat{\mathbf{x}}_e \right\|_2 &= \min_{\theta \in [0, 2\pi]} \left\| e^{i\theta} \widehat{\mathbf{x}}|_{[\gamma]_0} - \sqrt{|\lambda_1|} \mathbf{v}_1 \right\|_2 \\ &\leq \frac{(1 + 2\sqrt{2}) \beta}{\sigma_{\min}(W)} \frac{d^3}{\sqrt{KL\mu}} \|\widehat{\mathbf{x}}\|_2. \end{aligned}$$

□

Remark 2.1.1. *While there are literary works on the condition numbers of Vandermonde matrices (see for example [2]), the formulations therein do not apply to the matrix W above.*

Before exploring the proposed algorithms numerically, we note that the recovery guarantees (upper bounds) provided in this chapter suffer from a dependence on powers of the signal dimension, d . A natural question arises then, concerning the lower Lipschitz bounds for phase retrieval from locally supported measurements. This is the topic of Chapter 3. As we will see, the dependence on powers of d is not entirely out of the ordinary.

2.2 Numerical Results

Numerical experiments demonstrating the robustness and efficiency of the proposed framework, as well as comparisons to existing phase retrieval algorithms are now presented. These results were generated using the open source *BlockPR* Matlab software package (freely available at [34]) on a laptop computer with an Intel[®] Core[™]M-5Y10c (5th generation, dual core) processor, 8GB RAM, and running GNU/Linux (Ubuntu 16.04 x86_64) and Matlab R2018a. Each data point in the execution time and robustness plots was obtained by averaging results from 100 trials.

Unless otherwise stated, we use i.i.d. zero-mean complex Gaussian random test signals with measurement errors modeled using a (real) i.i.d. Gaussian noise model. In particular, applied measurement noise and reconstruction error are both reported in decibels (dB) in terms of signal-to-noise ratios (SNRs), with

$$\text{SNR (dB)} = 10 \log_{10} \left(\frac{\sum_1^D |\langle \mathbf{x}, \mathbf{m}_{\mathbf{k},\ell} \rangle|^4}{D\sigma^2} \right), \quad \text{Error (dB)} = 10 \log_{10} \left(\frac{\min_{\theta} \|e^{i\theta} \mathbf{x}_e - \mathbf{x}\|_2^2}{\|\mathbf{x}\|_2^2} \right),$$

where $\mathbf{m}_{\mathbf{k},\ell} = \overline{W_k S_{-\ell} \mathbf{m}}$ is one of D shifted and modulated versions of the mask \mathbf{m} , and $\mathbf{x}, \mathbf{x}_e, \sigma^2$ and $D = KL$ denote the true signal, recovered signal, (Gaussian) noise variance, and number of measurements respectively.

For completeness, we also present selected results comparing the proposed formulation against other well established phase retrieval algorithms such as *PhaseLift* [16] (implemented as a trace-regularized least-squares problem using the first order convex optimization package TFOCS [9, 8], *Hybrid Input-Output/Error Reduction (HIO+ER)* alternating projection algorithm [7, 23], and *Wirtinger Flow* [13]. We note that more accurate results using *PhaseLift* may be obtained using other solvers and software packages (such as CVX [26, 25]), albeit at

prohibitively expensive computational costs. For the HIO+ER algorithm, the following two projections were utilized: (i) projection onto the measured magnitudes, and (ii) projection onto the span of the measurement vectors $\{\mathbf{m}_{k,\ell}\} = \{\overline{W_k S_{-\ell} \mathbf{m}}\}$. The initial guess was set to be the all-zero vector, although use of a random starting guess did not change the qualitative nature of the results. Furthermore, as implemented in popular practice (see, for example, [23]) every few (25) HIO iterations were followed by a small number of (5) ER iterations, with the maximum number of HIO+ER iterations limited to 600 – this choice of iteration count ensures convergence of the algorithm (see Figure 2.2.1) while comparing favorably with the computational cost (see Figure 2.2.5) of the proposed method.

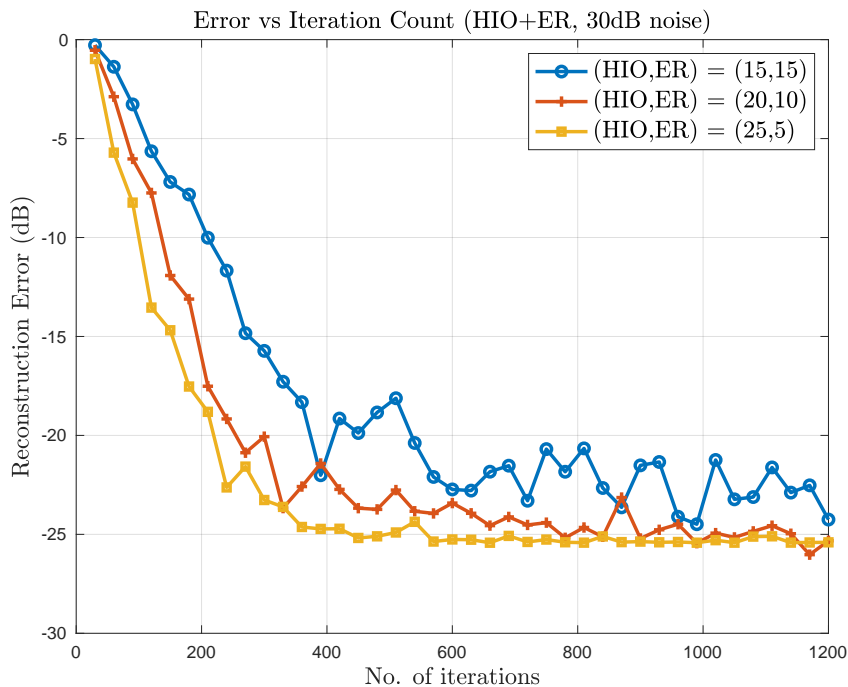


Figure 2.2.1: Selection of HIO+ER iteration parameters. $(\text{HIO}, \text{ER}) = (x, y)$ indicates that every set of x iterations of the HIO algorithm was followed by a set of y iterations of the ER algorithm.

2.2.1 Empirical Validation of Theorem 2.1.1 (Algorithm 1)

Recall from Algorithm 1 that this measurement construction involves the use of band-limited masks. Numerical experiments were performed with the following three types of masks:

$$\widehat{m}_k = \begin{cases} a_{\mathcal{N}} e^{2\pi i \theta_{\mathcal{U}}}, & \text{if } k \in [\delta]_0, \\ 0, & \text{otherwise,} \end{cases} \quad a_{\mathcal{N}} \sim \mathcal{N}(0, 1), \quad \theta_{\mathcal{U}} \sim \mathcal{U}(0, 1), \quad (\text{random mask}) \quad (2.2.1)$$

where $\mathcal{N}(0, 1)$ and $\mathcal{U}(0, 1)$ denote i.i.d. standard Gaussian and uniform (in the interval $[0, 1]$) random distributions respectively;

$$\widehat{m}_k = \begin{cases} \frac{e^{-k/a}}{\sqrt[4]{2\delta-1}}, & \text{if } k \in [\delta]_0, \\ 0, & \text{otherwise,} \end{cases} \quad a = \max(4, (\delta - 1)/2), \quad (\text{exponential mask}) \quad (2.2.2)$$

and

$$\widehat{m}_k = \begin{cases} 1 + \left(\frac{k}{\delta-1}\right) (\delta - 1), & \text{if } k \in [\delta]_0, \\ 0, & \text{otherwise.} \end{cases} \quad (\text{linear mask}) \quad (2.2.3)$$

The exponential mask in (2.2.2) is related to the deterministic masks first introduced and constructed in [36]. The corresponding values of the mask-dependent constant μ (see Lemma 2.1.4) for these three masks were 3.085×10^{-1} , 6.149×10^{-2} , and 2.585×10^1 respectively. The qualitative and quantitative performance of all three masks were similar.

We begin by examining the improvement in accuracy offered by adding an inexpensive post-processing step to Algorithm 1. More specifically, the recovered solution \mathbf{x}_e is post-processed using 60 iterations of the HIO+ER algorithm (in two blocks; each block consisting of 25 iterations of HIO followed by 5 iterations of ER). In addition, an eigenvector-based

magnitude estimation procedure described in §6.1 of [36] may be utilized in place of the diagonal element based estimates in Step 5 of Algorithm 1. Numerical results showing the utility of these procedures is shown in Figure 2.2.2, which plots the reconstruction error in recovering a test signal ($d = 255$) using 15 shifts and a random mask band-limited to $\delta = 8$ at several noise levels. The figure shows that the combination of these two procedures improves reconstruction accuracy (at a negligible increase in computational cost), and will therefore be utilized in the numerical results which follow.¹

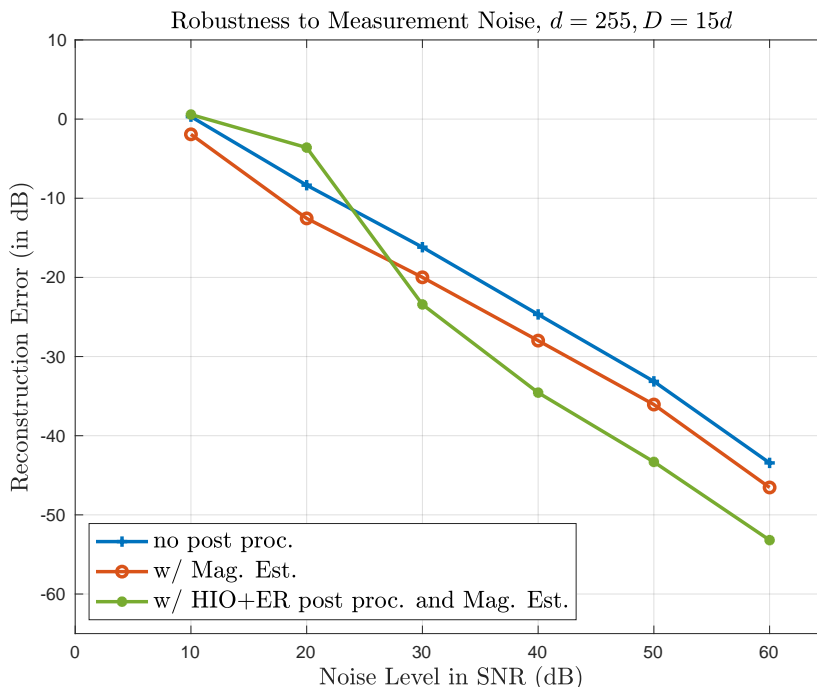


Figure 2.2.2: Reconstruction accuracy with and without HIO+ER (60 iterations) post-processing, improved magnitude estimation.

Next, we examine the importance of the number of shifts L in relation to reconstruction accuracy. We expect that reconstructions using larger L (which entails using more measurements, each corresponding to greater overlap between successive masked regions of the specimen) would offer improved accuracy. This is indeed confirmed by Figure 2.2.3 where

¹Where appropriate, results using no post-processing will also be included.

the reconstruction accuracy (at various noise levels) for several different values of L is plotted. We note that each value of L corresponds to a slightly different value of d to ensure L divides d . In this case, $\delta = 16$ was chosen, along with random masks and the post-processing procedure described earlier. As expected, reconstruction accuracy improves for larger L , with about a 10dB performance spread. A suitable value of L can be chosen depending on whether the proposed method is used as a reconstruction procedure, or as an initializer for another algorithm.

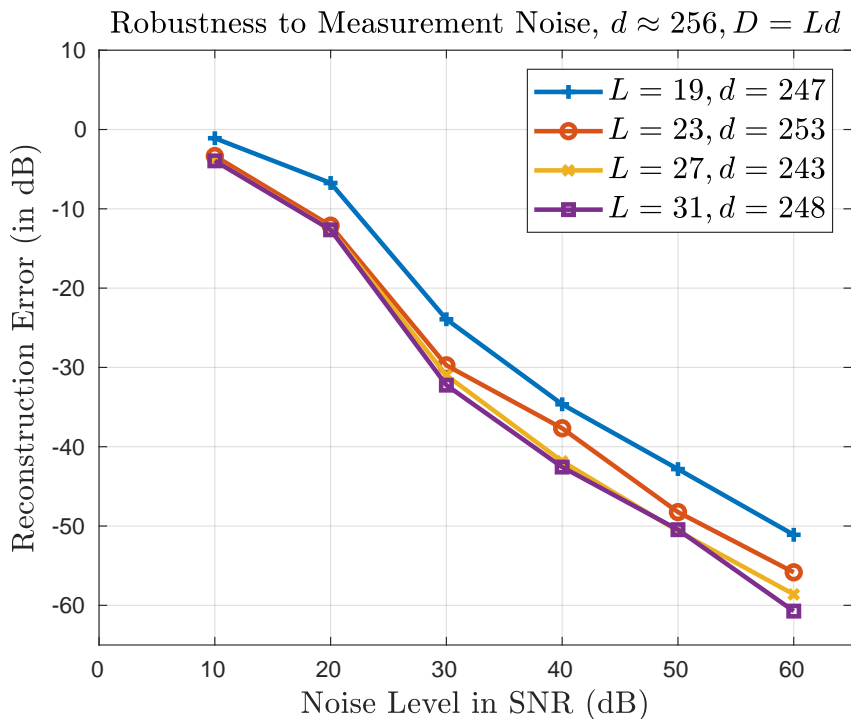


Figure 2.2.3: Reconstruction accuracy vs. number of shifts L .

In Figure 2.2.4, we compare the performance of the proposed method to other popular phase retrieval methods. Reconstruction errors for recovering a $d = 60$ -length signal using a random mask with $\delta = 8$ and $L = 15$ shifts are plotted for different levels of added noise.

We see that the proposed method (both with and without post-processing) compares well with the popular *HIO+ER* algorithm. The noise performance is also almost as good as the significantly more expensive SDP-based *PhaseLift* algorithm. We note that the Wirtinger Flow method is sensitive to the choice of parameters and iteration counts. We use fewer total iterations (50 at 10dB noise) at higher noise levels and more iterations (6500 at 60dB) as the noise level decreases to ensure convergence of the algorithm to the level of noise. We are not aware of any methodical procedure for setting the various algorithmic parameters when utilizing the (local) measurement constructions considered in this paper. We also note that none of the competing methods shown in the plot have recovery guarantees for this class of (local, spectrogram-type) measurements.

Finally, Figure 2.2.5 plots the corresponding execution time for the competing algorithms as a function of the problem size d . In this case, random masks were chosen with $\delta = \lceil 1.25 \log_2 d \rceil$ along with $L = \delta + \lceil \delta/2 \rceil - 1$ shifts. The figure confirms the essentially FFT-time computational cost of Algorithm 1; furthermore, it also confirms that the post-processing procedure introduced in Figure 2.2.2 does not increase the computational cost drastically. More specifically, the proposed method provides best-in-class computational efficiency, is about a factor of 2 – 5 faster than the *HIO+ER* and *Wirtinger Flow* methods, and several orders faster than the SDP *PhaseLift*.

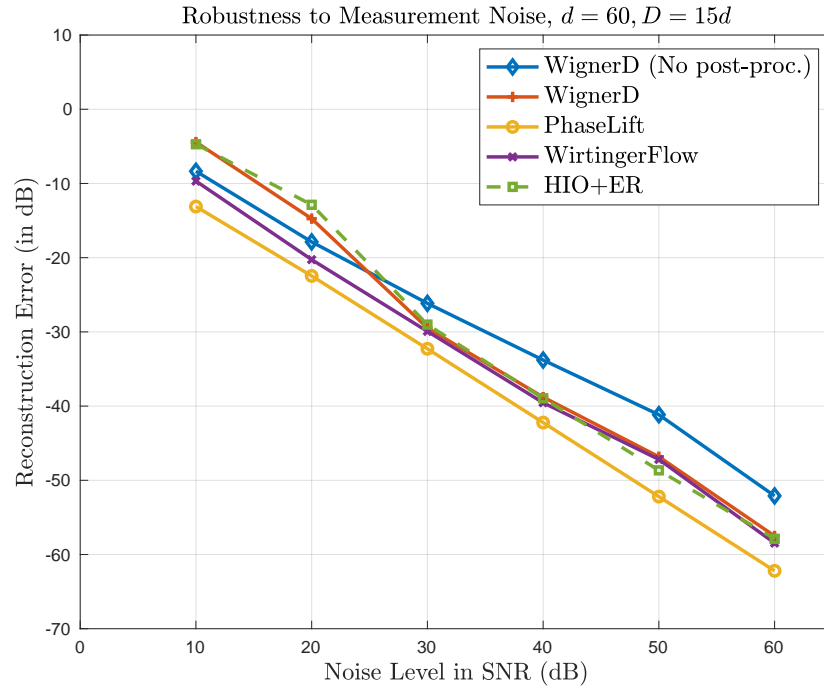


Figure 2.2.4: Reconstruction accuracy vs. added noise.

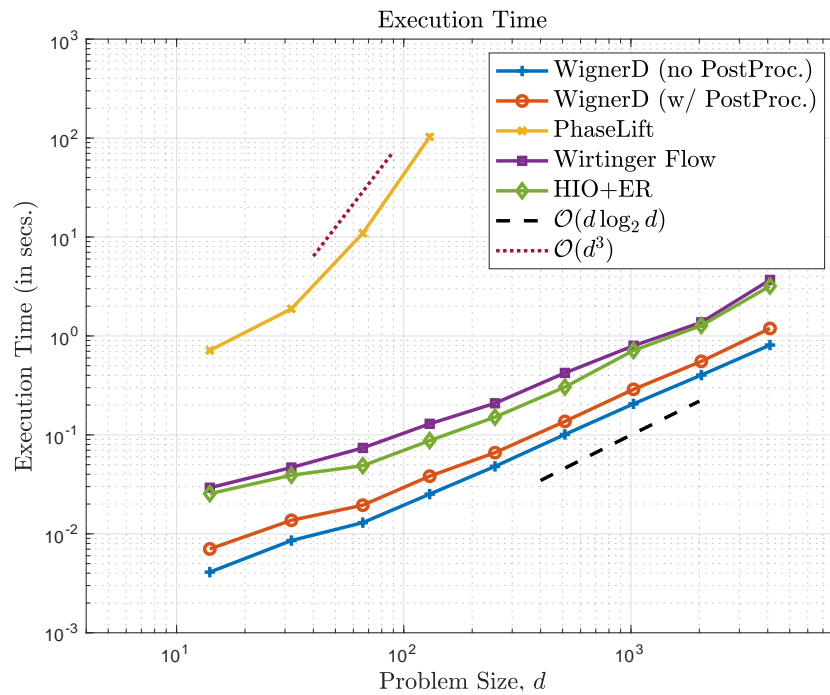


Figure 2.2.5: Execution time vs. signal size d .

2.2.2 Empirical Validation of Lemma 2.1.5

We next provide numerical results validating Lemma 2.1.5. Recall that this measurement construction requires that $\text{supp}(\mathbf{m}) = [\rho]_0$; i.e., support restrictions are imposed in the physical (space) domain. As with Section 2.2.1, experiments were conducted with various masks – all yielding comparable qualitative and quantitative results. The figures below use the exponential mask construction first introduced in [36]

$$m_k = \begin{cases} \frac{e^{-k/a}}{\sqrt[4]{2^{\rho-1}}}, & \text{if } k \in [\rho]_0, \\ 0, & \text{otherwise,} \end{cases} \quad a = \max(4, (\rho - 1)/2), \quad (2.2.4)$$

thereby allowing us to directly compare the performance of the proposed method with the algorithm introduced in [36]. We begin with Figure 2.2.6 which plots the reconstruction error in recovering a test signal ($d = 257$) using the masks in (2.2.4) with $\rho = 10$ and $K = 19$ (yielding a total of $19d$ measurements). Results with and without the post-processing procedure detailed in Section 2.2.1 are provided, along with results from [36] with and without the same post-processing procedure.

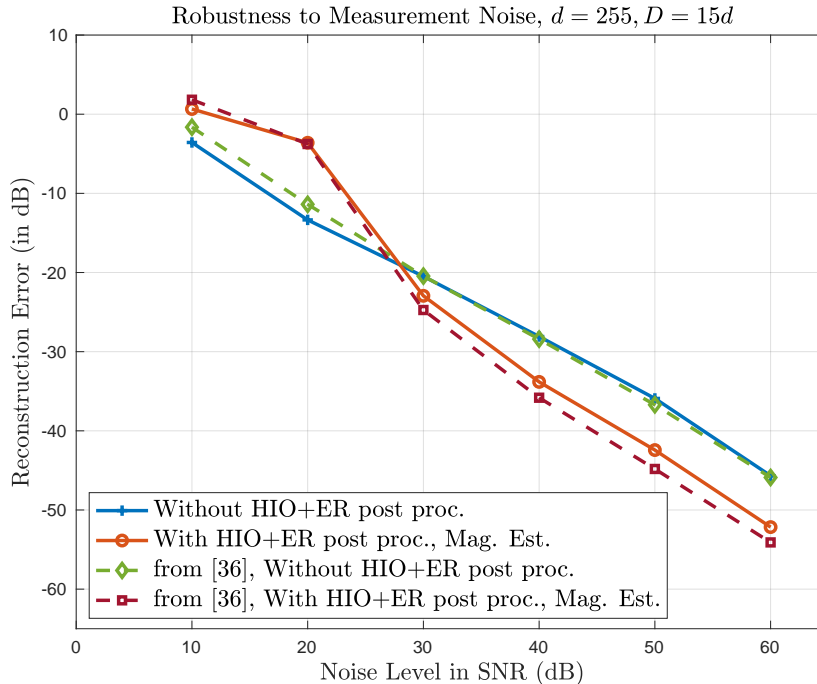


Figure 2.2.6: Reconstruction accuracy with and without HIO+ER (60 iterations) post-processing, improved magnitude estimation, and comparison with results from [36].

As can be seen in the figure, the post-processing procedure yields a small improvement of about 5dB in the reconstruction error, especially at low noise levels. We also observe that the proposed method compares well with those from [36]. Although the results from [36] are comparable, they are less flexible; for example, they do not allow for physical domain shifts (L) greater than 1 as was possible in Section 2.2.1.

Next, we investigate the reconstruction accuracy as a function of K , the number of Fourier modes. Figure 2.2.7 plots reconstruction error in recovering a test signal for $K = 13, 15, 17$ and 19 respectively. The test signal size (approximately $d = 256$) varies slightly in each case to satisfy the divisibility conditions (d divides K) while the support of the exponential mask, ρ , was chosen to be 10. As expected, the plot shows that reconstruction accuracy improves over a wide range of added noise levels when K increases; i.e., when more measurements are acquired.

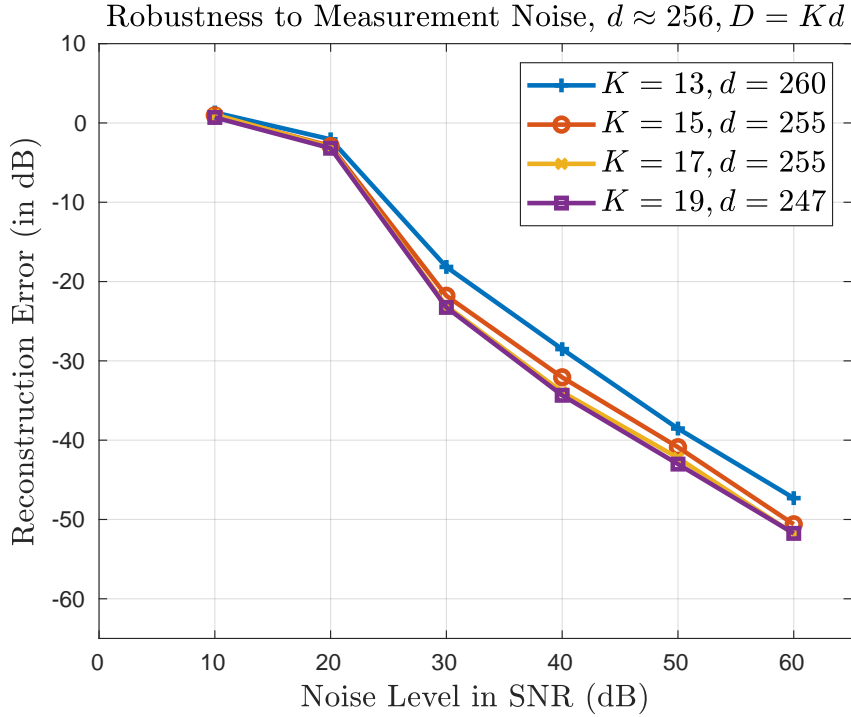


Figure 2.2.7: Reconstruction accuracy vs. number of Fourier modes K .

For completeness, we include noise robustness (Figure 2.2.8) and execution time (Figure 2.2.9) plots comparing the performance of the proposed method to the *HIO+ER*, *PhaseLift*, and *Wirtinger Flow* algorithms. From Figure 2.2.8, we see that the proposed method (both with and without post-processing) compares well with the *HIO+ER* implementation across a wide range of SNRs. We also see, as with Figure 2.2.9 in Section 2.2.1, the essentially FFT-time computational cost of the method as well as the best-in-class computational efficiency when compared to other competing algorithms.

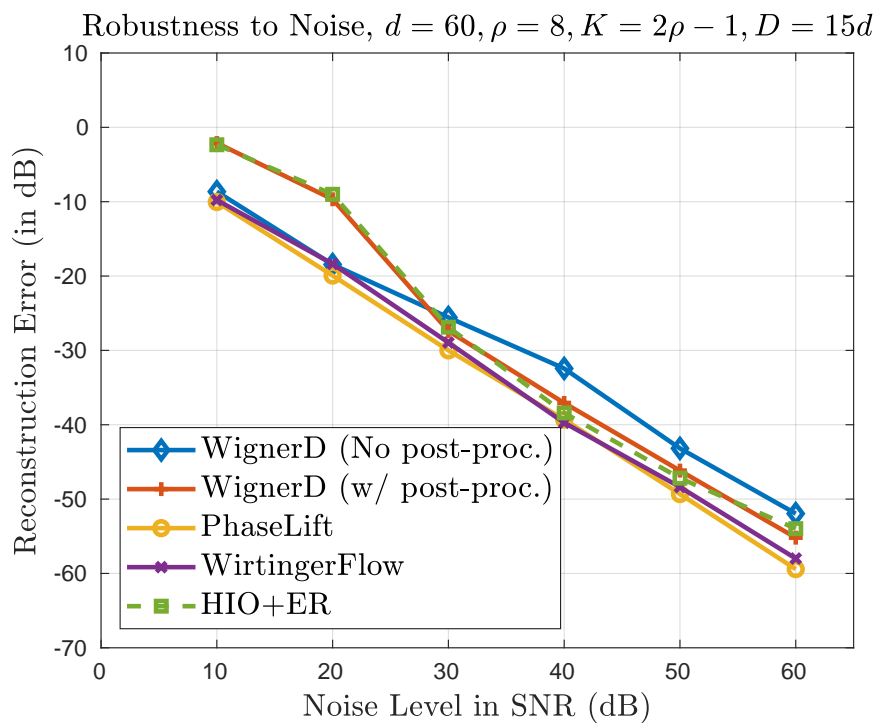


Figure 2.2.8: Reconstruction accuracy vs. added noise.

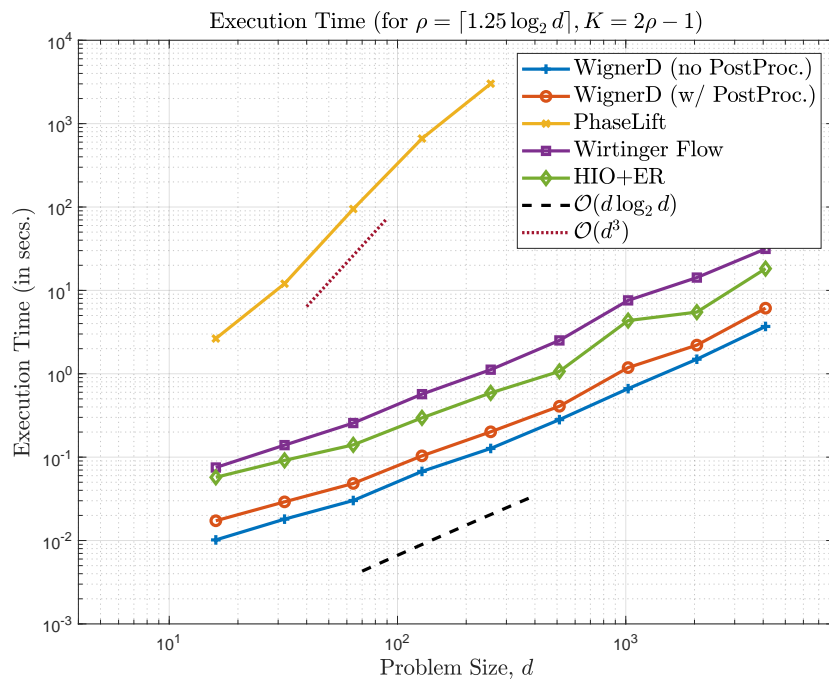


Figure 2.2.9: Execution time versus signal size d .

2.2.3 Empirical Validation of Theorem 2.1.2 (Algorithm 2)

We provide preliminary numerical results validating Algorithm 2, with comparisons to the *HIO+ER* algorithm. Consider the signal parameters: $d = 190, \rho = 48, \gamma = 10, K = 2\rho - 1, L = 2\gamma - 1, D = KL$. Algorithm 2 has an execution time of 0.033 seconds. When adding the post-processing method from Section 2.2.1, the execution time increases to 0.589 seconds. Both of these methods are considerably faster than *HIO+ER*, which reconstructs signals in 2.635 seconds. Note that in Step 3 of Algorithm 2, we utilize the Tikhonov regularization $A = (W^*W + \sigma^2 I)^{-1}W^*V$, where σ^2 is chosen using the L-curve method.

Finally, in Figure 2.2.10 we compare Algorithm 2 to *HIO+ER*. When post-processed with 60 iterations of *HIO+ER*, Algorithm 2 compares well with the *HIO+ER* implementation (600 iterations) across a wide range of SNRs, while being significantly faster in reconstruction.

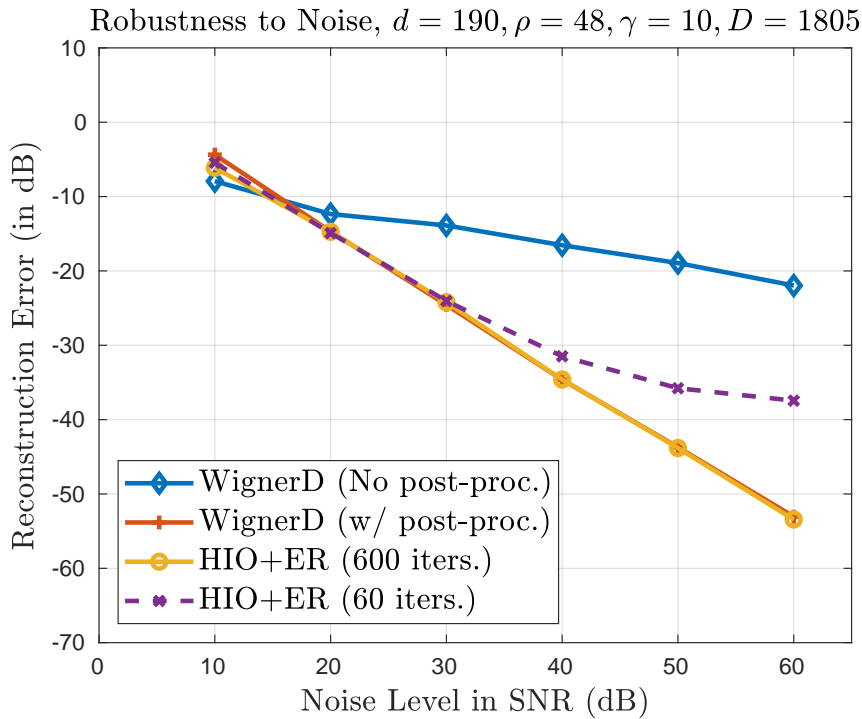


Figure 2.2.10: Reconstruction accuracy vs. added noise.

Chapter 3

Lower Lipschitz Bounds for Phase Retrieval from Locally Supported Measurements

The work in this chapter first appeared in [35].

As demonstrated in Chapter 2, noise robustness guarantees are desirable for any reliable phase retrieval algorithm. Much of the work in this field is dedicated to the design of algorithms that are simultaneously efficient and robust. As in many other areas of harmonic analysis, a natural question arises: what is the worst-case noise robustness of any phase retrieval algorithm? As it stands this question is too general, as algorithms vary widely based on the measurement model and the assumptions on the specimen of interest. In this chapter, we narrow down the question above to the following setting: what is the worst-case noise robustness of any phase retrieval algorithm which aims to reconstruct all nonvanishing vectors $\mathbf{x} \in \mathbb{C}^d$ (up to a single global phase multiple) from the magnitudes of an arbitrary collection of local correlation measurements?

Examples of such measurements include both spectrogram measurements of \mathbf{x} using locally supported windows and masked Fourier transform intensity measurements of \mathbf{x} using band-limited masks. As a result, the robustness results considered herein apply to a wide

range of both ptychographic and Fourier ptychographic imaging scenarios. In particular, the main results imply that the accurate recovery of high-resolution images of extremely large samples using highly localized probes is likely to require an extremely large number of measurements in order to be robust to worst-case measurement noise, independent of the recovery algorithm employed. As a result, recent pushes to achieve high-speed and high-resolution ptychographic imaging of integrated circuits for process verification and failure analysis will likely need to carefully balance probe design (e.g., their effective time-frequency support) against the total number of measurements acquired in order for their imaging techniques to be stable to measurement noise, no matter what reconstruction algorithms are applied.

3.1 Introduction and Statement of Results

We consider the robustness of the *finite-dimensional phase retrieval problem* in which one attempts to recover a signal $\mathbf{x} := (x_1, \dots, x_d)^T \in \mathbb{C}^d$ from one of two nonlinear measurement maps $\alpha, \beta : \mathbb{C}^d \rightarrow \mathbb{R}^N$ given by

$$\alpha(\mathbf{x}) = \{|\langle \mathbf{x}, \mathbf{f}_{\mathbf{k}} \rangle|\}_{\mathbf{k}=1}^N \text{ and } \beta(\mathbf{x}) = \{|\langle \mathbf{x}, \mathbf{f}_{\mathbf{k}} \rangle|^2\}_{\mathbf{k}=1}^N,$$

where the vectors $\{\mathbf{f}_{\mathbf{1}}, \dots, \mathbf{f}_{\mathbf{N}}\} \subset \mathbb{C}^d$ form a frame (i.e., a spanning set) of \mathbb{C}^d . We will focus on a special class of frame vectors $\mathbf{f}_{\mathbf{k}}$ which have *localized support* (i.e., all of whose nonzero entries are contained in an interval of length at most $\delta \ll d$). Such frames are commonly encountered in applications like ptychographic imaging.

Since, as previously stated, phase retrieval is only possible up to a global phase, consider the equivalence relation $\mathbf{x} \sim \mathbf{x}'$, if $\mathbf{x} = e^{i\theta} \mathbf{x}'$ for some $\theta \in \mathbb{R}$. Following the work of Balan et

al. [3, 5], we will consider two commonly used metrics on \mathbb{C}^d / \sim : the natural metric

$$D_2(\mathbf{x}, \mathbf{x}') := \min_{\theta \in \mathbb{R}} \|\mathbf{x} - e^{i\theta} \mathbf{x}'\|_2,$$

and the matrix-norm induced metric

$$d_1(\mathbf{x}, \mathbf{x}') := \|\mathbf{x}\mathbf{x}^* - \mathbf{x}'\mathbf{x}'^*\|_1 := \sum_k \sigma_k(\mathbf{x}\mathbf{x}^* - \mathbf{x}'\mathbf{x}'^*),$$

where $\sigma_k(\mathbf{x}\mathbf{x}^* - \mathbf{x}'\mathbf{x}'^*)$ is the k -th singular value of the (at most rank-two) matrix $\mathbf{x}\mathbf{x}^* - \mathbf{x}'\mathbf{x}'^*$. In [5], Balan et al. showed that if α and β are injective on \mathbb{C}^d / \sim , then β is bi-Lipschitz with respect to d_1 , and α is bi-Lipschitz with respect to D_2 , where in both cases \mathbb{R}^N is equipped with the Euclidean norm.

Motivated by applications such as (Fourier) ptychography [52, 60] and related numerical methods [37, 36], we will study frames which are constructed as the shifts of a family of locally supported measurement vectors. Specifically, we assume that $\{\mathbf{m}_1, \mathbf{m}_2, \dots, \mathbf{m}_K\}$ is a family of measurement masks in \mathbb{C}^d such that for all $1 \leq k \leq K$ the nonzero entries of \mathbf{m}_k are contained in the set $[\delta] := \{1, \dots, \delta\}$ for some $\delta \leq \frac{d}{4}$ (although all of our results remain valid if the support of our masks are contained in any interval of length δ). Letting L be an integer which divides d , such that $a := \frac{d}{L} < \delta$, we consider nonlinear phaseless measurement maps $Y, Z : \mathbb{C}^d \rightarrow \mathbb{R}^{K \times L}$ defined by their coordinate functions

$$Y_{k,\ell}(\mathbf{x}) := |\langle S_{\ell a} \mathbf{m}_k, \mathbf{x} \rangle|^2 \tag{3.1.1}$$

and

$$Z_{k,\ell}(\mathbf{x}) := |\langle S_{\ell a} \mathbf{m}_k, \mathbf{x} \rangle| \tag{3.1.2}$$

for $1 \leq k \leq K$ and $1 \leq \ell \leq L$. Here S_ℓ is the circular shift operator on \mathbb{C}^d defined for all $\ell \in \mathbb{Z}$ by

$$(S_\ell \mathbf{x})_n := x_{(n+\ell-1) \bmod d+1}.$$

(The $+1$ is needed because we are indexing our vectors from one.) For notational convenience, we will assume that d is even, although our results remain valid, with similar proofs, when d is odd.

The purpose of this work is to provide lower bounds on the Lipschitz constants of any maps, A and B , which reconstruct \mathbf{x} from Y and Z , respectively. With such lower bounds in hand, one would be better equipped to, e.g., judge the optimality of theoretical noisy reconstruction guarantees for phase retrieval algorithms which utilize locally supported measurements (see, e.g., [37, 36]). Unfortunately, Y and Z are not injective on all of \mathbb{C}^d / \sim . For example, if two vectors $\mathbf{x}^\pm \in \mathbb{C}^d$ are defined by

$$x_n^\pm := \begin{cases} 1, & 1 \leq n \leq \frac{d}{2} - \delta \\ 0, & \frac{d}{2} - \delta < n \leq \frac{d}{2} \\ \pm 1, & \frac{d}{2} < n \leq d - \delta \\ 0, & d - \delta < n \leq d \end{cases}, \quad (3.1.3)$$

then $\mathbf{x}^+ \not\sim \mathbf{x}^-$, but $Y(\mathbf{x}^+) = Y(\mathbf{x}^-)$ and $Z(\mathbf{x}^+) = Z(\mathbf{x}^-)$. (If d were odd, we could add an extra entry of 1 to \mathbf{x}^\pm .) However, it can be shown [37] that Y and Z are injective when restricted to the subset of \mathbb{C}^d such that $x_n \neq 0$ for all $1 \leq n \leq d$, for certain choices of masks in the case where $L = d$. Given this, we will consider the maps Y and Z restricted to the

subset

$$\mathcal{C}_{p,q} = \{\mathbf{x} \in \mathbb{C}^d / \sim \text{ such that } p \leq |x_n| \leq q \text{ for all } 1 \leq n \leq d\},$$

for some fixed $0 < p \leq q$, and provide lower bounds on the Lipschitz constants of A and B which grow linearly with respect to the ratio $\frac{q}{p}$.

3.1.1 Related Work and Implications

Our local measurement maps (3.1.1) and (3.1.2) are closely related to several practical measurement models that have been explored in the phase retrieval literature including, for example, short-time Fourier transform (STFT) magnitude measurements (see, e.g., [10, 38, 47, 53]). In particular, suppose that our STFT magnitude measurements are generated by a compactly supported window $\mathbf{w} \in \mathbb{C}^d$ whose n^{th} -entry w_n is nonzero only if $n \in [\delta]$. In this setting, we can use one locally supported mask $\mathbf{m}_{\mathbf{k}}$ to represent each measured frequency $\omega_k \in \Omega \subset [d] := \{1, \dots, d\}$ by letting $\mathbf{m}_{\mathbf{k}} := W_{\omega_k} \mathbf{w}$ for each frequency index k , where W_{ω_k} is the modulation operator defined on \mathbb{C}^d by

$$(W_{\omega_k} \mathbf{w})_n := e^{\frac{2\pi i(n-1)(\omega_k-1)}{d}} w_n.$$

In this case, we have

$$|\langle S_{\ell a} \mathbf{m}_{\mathbf{k}}, \mathbf{x} \rangle| = \left| \left\langle \mathbf{x}, S_{\ell a} W_{\omega_k} \mathbf{w} \right\rangle \right| = \left| \left\langle \mathbf{x}, e^{\frac{2\pi i \ell a (\omega_k - 1)}{d}} W_{\omega_k} S_{\ell a} \mathbf{w} \right\rangle \right| = \left| \left\langle \mathbf{x}, W_{\omega_k} S_{\ell a} \mathbf{w} \right\rangle \right|$$

for all k and ℓ . Therefore, one can see that the main results below yield lower Lipschitz bounds for any such STFT magnitude measurements in terms of the total number of shifts L , the number of measured frequencies K , and the window \mathbf{w} 's support size δ .

Another common model considered in the phase retrieval literature concerns masked Fourier measurements of the form

$$|F \text{Diag}(\mathbf{w}_{\mathbf{k}}) \mathbf{x}|^2, \quad (3.1.4)$$

where F is the $d \times d$ discrete Fourier transform matrix whose entries are defined by

$$F_{j,k} := e^{-\frac{2\pi i(j-1)(k-1)}{d}},$$

and $\{\mathbf{w}_{\mathbf{1}}, \dots, \mathbf{w}_{\mathbf{K}}\} \subset \mathbb{C}^d$ is a family of measurement vectors (see, e.g., [6, 14, 15, 28]). In this setting one can ask what effect, if any, requiring each $\mathbf{w}_{\mathbf{k}}$ to be band-limited (i.e., to have support size $\delta \ll d$ in the Fourier basis) might have on the stability of these measurements. Furthermore, one might also consider sub-sampling each of the masked Fourier measurements in frequency instead of acquiring measurements for all d frequencies. (This may even be a necessity due to, for example, detector limitations.) We will show that our results may also be applied to these types of measurements as a special case.

Suppose for example that each measurement vector $\mathbf{w}_{\mathbf{k}}$ has $(\widehat{\mathbf{w}_{\mathbf{k}}})_n := (F\mathbf{w}_{\mathbf{k}})_n = 0$ for all $n \notin \{1\} \cup \{d - \delta + 2, \dots, d\}$.¹ For a vector $\mathbf{u} \in \mathbb{C}^d$, let $\tilde{\mathbf{u}} \in \mathbb{C}^d$ be the vector obtained by reflecting the entries of \mathbf{u} about its first entry so that

$$\tilde{u}_n := u_{(1-n) \bmod d+1}.$$

In this case, we see that the measurements (3.1.4) are given by the measurement map (3.1.1)

¹Note that this particular support interval (modulo d) is not particularly special. The same arguments below can be extended to apply to any interval of support of size $\leq \delta$ in a straightforward fashion.

applied to $\widehat{\mathbf{x}}$ with the locally supported measurement masks $\mathbf{m}_{\mathbf{k}} := \frac{1}{d} \widetilde{\widetilde{\mathbf{w}_{\mathbf{k}}}}$. Indeed,

$$\begin{aligned}
|\langle S_{\ell a} \mathbf{m}_{\mathbf{k}}, \widehat{\mathbf{x}} \rangle| &= \frac{1}{d} \left| \left\langle \widehat{\mathbf{x}}, S_{\ell a} \widetilde{\widetilde{\mathbf{w}_{\mathbf{k}}}} \right\rangle \right| = \frac{1}{d} \left| \sum_{n=1}^d \widehat{x}_n \left(S_{\ell a} \widetilde{\widetilde{\mathbf{w}_{\mathbf{k}}}} \right)_n \right| \\
&= \frac{1}{d} \left| \sum_{n=1}^d \widehat{x}_n (\widehat{\mathbf{w}_{\mathbf{k}}})_{(1-\ell a-n) \bmod d+1} \right| \\
&= \frac{1}{d} \left| (\widehat{\mathbf{w}_{\mathbf{k}}} * \widehat{\mathbf{x}})_{-\ell a \bmod d+1} \right|, \tag{3.1.5}
\end{aligned}$$

where $\mathbf{x} * \mathbf{y} \in \mathbb{C}^d$ is the circular convolution of $\mathbf{x}, \mathbf{y} \in \mathbb{C}^d$, defined componentwise by

$$(\mathbf{x} * \mathbf{y})_m = \sum_{n=1}^d x_n y_{(m-n) \bmod d+1}.$$

Continuing from (3.1.5), we see by the Convolution Theorem

$$|\langle S_{\ell a} \mathbf{m}_{\mathbf{k}}, \widehat{\mathbf{x}} \rangle| = \left| F(\mathbf{w}_{\mathbf{k}} \circ \mathbf{x})_{(-\ell a \bmod d)+1} \right| = \left| F(\text{Diag}(\mathbf{w}_{\mathbf{k}}) \mathbf{x})_{(-\ell a \bmod d)+1} \right|,$$

where \circ represents the Hadamard (componentwise) product.

As a result, we see that recovering a vector \mathbf{x} from masked Fourier measurements of the form (3.1.4) with band-limited measurement vectors $\mathbf{w}_{\mathbf{k}}$ is equivalent to recovering $\widehat{\mathbf{x}}$ from measurements (3.1.1) with locally supported measurement masks $\mathbf{m}_{\mathbf{k}}$. Therefore, the main results below also yield lower Lipschitz bounds for any such masked Fourier magnitude measurements in terms of the total number of frequencies L collected per measurement vector, the total number K of measurement vectors used, and the maximum Fourier support size δ of each band-limited measurement vector.

3.1.2 Main Results

The main results of this paper are the following two theorems which provide lower bounds for the Lipschitz constants of any maps A and B for which $A(Y(\mathbf{x})) = \mathbf{x}$ and $B(Z(\mathbf{x})) = \mathbf{x}$ for all $\mathbf{x} \in \mathcal{C}_{p,q}$.

Theorem 3.1.1. *Let $0 < p \leq q$, and consider the map Z restricted to the subset $\mathcal{C}_{p,q} \subset \mathbb{C}^d / \sim$. Assume that $\delta \leq \frac{d}{4}$ and that $d = aL$ for some integer $1 \leq a < \delta$. Then if B is any Lipschitz map (with respect to D_2) such that $B(Z(\mathbf{x})) = \mathbf{x}$ for all $\mathbf{x} \in \mathcal{C}_{p,q}$, we have that*

$$C_B \geq C \frac{q\sqrt{da}}{p\sqrt{K}\|\mathbf{m}\|_\infty \delta^{3/2}} = C \frac{qd}{p\sqrt{KL}\|\mathbf{m}\|_\infty \delta^{3/2}}, \quad (3.1.6)$$

where C_B is the Lipschitz constant of B , $\|\mathbf{m}\|_\infty := \max_{1 \leq k \leq K} \|\mathbf{m}_k\|_\infty$, and C is a universal constant.

Theorem 3.1.2. *Let $0 < p \leq q$, and consider the map Y restricted to the subset $\mathcal{C}_{p,q} \subset \mathbb{C}^d / \sim$. Assume that $\delta \leq \frac{d}{4}$ and that $d = aL$ for some integer $1 \leq a < \delta$. Then if A is any Lipschitz map (with respect to d_1) such that $A(Y(\mathbf{x})) = \mathbf{x}$ for all $\mathbf{x} \in \mathcal{C}_{p,q}$, we have that*

$$C_A \geq C \frac{qd\sqrt{a}}{p\sqrt{K}\|\mathbf{m}\|_\infty^2 \delta^{5/2}} = C \frac{qd^{3/2}}{p\sqrt{KL}\|\mathbf{m}\|_\infty^2 \delta^{5/2}}, \quad (3.1.7)$$

where C_A is the Lipschitz constant of A , $\|\mathbf{m}\|_\infty := \max_{1 \leq k \leq K} \|\mathbf{m}_k\|_\infty$, and C is a universal constant.

Ideally, we would like a stable phase retrieval algorithm to have $C_A = \mathcal{O}(1)$ (or $C_B = \mathcal{O}(1)$) while using only $KL = \mathcal{O}(d)$ total measurements. Unfortunately, Theorems 3.1.1 and 3.1.2 demonstrate that this is impossible when δ , the support size of the masks, is very small. At best, a phase retrieval algorithm that uses only $KL = \mathcal{O}(d)$ local

correlation measurements can have global Lipschitz constants that are of size $\mathcal{O}\left(\frac{d}{\delta^{5/2}}\right)$ in the case of Y -measurements, and $\mathcal{O}\left(\frac{\sqrt{d}}{\delta^{3/2}}\right)$ in the case of Z -measurements. This implies that extremely large samples \mathbf{x} (i.e., with d large) cannot be stably recovered from measurements which are noisy and extremely localized (i.e., with δ small) in the worst case using only $\mathcal{O}(d)$ total measurements. To contextualize this in an application setting, one may consider recent research initiatives aimed at achieving the ability to rapidly obtain detailed images of relatively large circuit boards [33]. One approach to solving this problem involves using ptychographic imaging and taking STFT magnitude measurements of the circuit board using a probe (i.e., an STFT window function) with a comparably small effective support size δ . In this context, Theorem 3.1.2 implies that the probe's effective support size should not be taken to be too small unless additional measurements are taken in order to help ensure stability to noise.

As we shall see, the proofs of both Theorems 3.1.1 and 3.1.2 will depend on signals modeled along the lines of (3.1.3) whose support sets are composed of two disjoint components separated from one another by at least δ zeroes. In [37] it was noted that phase retrieval of such signals using locally supported masks $\mathbf{m}_{\mathbf{k}}$ of the type proposed herein was impossible, and that recovery of signals with more than δ consecutive small entries appeared to be unstable. Interestingly enough, subsequent work in the infinite-dimensional setting has independently identified such disjointly supported signals as being the principal cause of instability in phase retrieval problems using continuous Gabor measurements as well because they lead to measurements which are supported on disjoint subsets of the time-frequency plane [1, 27]. Similarly, we will use (essentially) disjointly supported signals similar to those in (3.1.3) to provide lower bounds on the Lipschitz constants of our maps A and B using the fact that they (i) are relatively far apart with respect to the D_2 and d_1 metrics defined

above and (ii) produce measurements with respect to our maps Y and Z which are (nearly) identical.

3.2 The Proofs of Theorem 3.1.1 and Theorem 3.1.2

We are now prepared to prove our main results.

Proof of Theorem 3.1.1. First observe that for any $\mathbf{x}, \mathbf{x}' \in \mathcal{C}_{p,q}$,

$$D_2(\mathbf{x}, \mathbf{x}') = D_2(B(Z(\mathbf{x})), B(Z(\mathbf{x}')))) \leq C_B \|Z(\mathbf{x}) - Z(\mathbf{x}')\|_2.$$

Therefore,

$$C_B \geq \sup \frac{D_2(\mathbf{x}, \mathbf{x}')}{\|Z(\mathbf{x}) - Z(\mathbf{x}')\|_2}, \quad (3.2.1)$$

where the supremum is taken over all $\mathbf{x} \not\sim \mathbf{x}' \in \mathcal{C}_{p,q}$. Define \mathbf{x}^+ and $\mathbf{x}^- \in \mathbb{C}^d$ by

$$x_n^\pm := \begin{cases} q, & 1 \leq n \leq \frac{d}{2} - \delta, \\ p, & \frac{d}{2} - \delta < n \leq \frac{d}{2}, \\ \pm q, & \frac{d}{2} < n \leq d - \delta, \\ p, & d - \delta < n \leq d. \end{cases}$$

Note that $D_2(\mathbf{x}^+, \mathbf{x}^-) \geq q\sqrt{d}$ since $d < \frac{d}{4}$ and for all $\theta \in \mathbb{R}$,

$$\begin{aligned} \|\mathbf{x}^+ - e^{i\theta} \mathbf{x}^-\|_2^2 &\geq \sum_{n=1}^{d/2-\delta} |(1 - e^{i\theta})q|^2 + \sum_{n=d/2+1}^{d-\delta} |(1 + e^{i\theta})q|^2 \\ &= \left(\frac{d}{2} - \delta\right) q^2 |1 - e^{i\theta}|^2 + \left(\frac{d}{2} - \delta\right) q^2 |1 + e^{i\theta}|^2 \end{aligned}$$

$$\geq \frac{d}{4}q^2 \left(|1 - e^{i\theta}|^2 + |1 + e^{i\theta}|^2 \right) = dq^2,$$

since $|1 - e^{i\theta}|^2 + |1 + e^{i\theta}|^2 = 4$ for all θ . Let $Z^\pm := Z(\mathbf{x}^\pm)$. We will show that

$$\|Z^+ - Z^-\|_2 \leq C\sqrt{K}p\|\mathbf{m}\|_\infty \frac{\delta^{3/2}}{\sqrt{a}}. \quad (3.2.2)$$

Since $B(Z^\pm) = \mathbf{x}^\pm$, combining this with (3.2.1) will complete the proof.

Observe that for all k , the support of $S_{\ell a} \mathbf{m}_k$ is contained in $[1 + \ell a, \delta + \ell a]$. Therefore, $Z_{k,\ell}^+ = Z_{k,\ell}^-$ except when $1 + \ell a \leq \frac{d}{2} < \delta + \ell a$ or $1 + \ell a \leq d - \delta < \delta + \ell a$ since if the support of $S_{\ell a} \mathbf{m}_k$ does not intersect $(\frac{d}{2}, d - \delta]$, we have that $\langle S_{\ell a} \mathbf{m}_k, \mathbf{x}^+ \rangle = \langle S_{\ell a} \mathbf{m}_k, \mathbf{x}^- \rangle$, and if the support of $S_{\ell a} \mathbf{m}_k$ is contained in $(\frac{d}{2}, d - \delta]$, then $\langle S_{\ell a} \mathbf{m}_k, \mathbf{x}^+ \rangle = -\langle S_{\ell a} \mathbf{m}_k, \mathbf{x}^- \rangle$. We will restrict attention to the case where $1 + \ell a \leq d - \delta < \delta + \ell a$. The case where $1 + \ell a \leq \frac{d}{2} < \delta + \ell a$ is similar.

For fixed ℓ such that $1 + \ell a \leq d - \delta < \delta + \ell a$, let

$$j := \ell a + 2\delta - d$$

so that the last j nonzero entries of $S_{\ell a} \mathbf{m}_k$ are located in positions greater than $d - \delta$ and the first $\delta - j$ nonzero entries are located in positions less than or equal to $d - \delta$. (Note that $1 \leq j \leq \delta - 1$.) Then,

$$\langle S_{\ell a} \mathbf{m}_k, \mathbf{x}^- \rangle = -q \sum_{n=1}^{\delta-j} (\mathbf{m}_k)_n + p \sum_{n=\delta-j+1}^{\delta} (\mathbf{m}_k)_n = -\langle S_{\ell a} \mathbf{m}_k, \mathbf{x}^+ \rangle + 2p \sum_{n=\delta-j+1}^{\delta} (\mathbf{m}_k)_n.$$

Therefore,

$$|Z_{k,\ell}^- - Z_{k,\ell}^+| \leq 2jp\|\mathbf{m}\|_\infty. \quad (3.2.3)$$

Since $1 \leq j \leq \delta - 1$, summing over the set of ℓ such that $1 + \ell a \leq d - \delta < \delta + \ell a$, corresponds to summing over $j = a, 2a, \dots, \lfloor \frac{\delta-1}{a} \rfloor a$ if a divides $d - 2\delta$, or summing over $j = j_0, j_0 + a, j_0 + 2a, \dots, j_0 + \lfloor \frac{\delta-j_0-1}{a} \rfloor a$ for some $0 < j_0 < a$ otherwise. Therefore, in either case

$$\|Z^+ - Z^-\|_2^2 \leq C \|\mathbf{m}\|_\infty^2 p^2 \sum_{k=1}^K \sum_{t=1}^{\lfloor \delta/a \rfloor + 1} |at|^2 \leq CKa^2 \|\mathbf{m}\|_\infty^2 p^2 \left(\frac{\delta}{a}\right)^3 = CKp^2 \|\mathbf{m}\|_\infty^2 \frac{\delta^3}{a}, \quad (3.2.4)$$

which proves (3.2.2) and completes the proof. \square

Proof of Theorem 3.1.2. Similarly to the proof of Theorem 3.1.1,

$$C_A \geq \sup \frac{d_1(\mathbf{x}, \mathbf{x}')}{\|Y(\mathbf{x}) - Y(\mathbf{x}')\|_2}, \quad (3.2.5)$$

where the supremum is again taken over all $\mathbf{x} \not\sim \mathbf{x}' \in \mathcal{C}_{p,q}$. Let \mathbf{x}^\pm be in as in the proof of Theorem 3.1.1, and let $Y^\pm := Y(\mathbf{x}^\pm)$. By the same reasoning as in the previous proof, $Y_{k,\ell}^+ = Y_{k,\ell}^-$, unless $1 + \ell a \leq \frac{d}{2} < \delta + \ell a$ or $1 + \ell a \leq d - \delta < \delta + \ell a$. We will again restrict attention to the case where $1 + \ell a \leq d - \delta < \delta + \ell a$. Let ℓ be such that $1 + \ell a \leq d - \delta < d + \ell a$, and again let $j := \ell a + 2\delta - d$.

Since for all k and ℓ , we have

$$|Z_{k,\ell}^\pm| \leq q \|\mathbf{m}\|_\infty \delta,$$

we see

$$|Y_{k,\ell}^+ - Y_{k,\ell}^-|_2 = |(Z_{k,\ell}^+)^2 - (Z_{k,\ell}^-)^2| = |Z_{k,\ell}^+ + Z_{k,\ell}^-| |Z_{k,\ell}^+ - Z_{k,\ell}^-| \leq 4 \|\mathbf{m}\|_\infty^2 q \delta p j,$$

by (3.2.3). Therefore, by the same reasoning as in (3.2.4),

$$\begin{aligned}
\|Y^+ - Y^-\|_2^2 &\leq C\|\mathbf{m}\|_\infty^4 q^2 \delta^2 p^2 \sum_{k=1}^K \sum_{t=1}^{[\delta/a]+1} |ta|^2 \\
&\leq CK\|\mathbf{m}\|_\infty^4 q^2 \delta^2 p^2 a^2 \left(\frac{\delta}{a}\right)^3 \\
&= CK\|\mathbf{m}\|_\infty^4 q^2 p^2 \frac{\delta^5}{a}.
\end{aligned}$$

Thus, the proof will follow from (3.2.5) once we show $d_1(\mathbf{x}^+, \mathbf{x}^-) \geq Cdq^2$.

For $n, m \in \mathbb{N}$, let $\mathbf{0}_{n \times m}$ and $\mathbf{1}_{n \times m}$ denote the $n \times m$ matrices of all zeros and of all ones respectively. With this notation we see that

$$\mathbf{x}^\pm = (q\mathbf{1}_{1 \times \eta}, p\mathbf{1}_{1 \times \delta}, \pm q\mathbf{1}_{1 \times \eta}, p\mathbf{1}_{1 \times \delta})^T,$$

and

$$\mathbf{x}^\pm \mathbf{x}^{\pm*} = \begin{pmatrix} q^2 \mathbf{1}_{\eta \times \eta} & qp \mathbf{1}_{\eta \times \delta} & \pm q^2 \mathbf{1}_{\eta \times \eta} & qp \mathbf{1}_{\eta \times \delta} \\ qp \mathbf{1}_{\delta \times \eta} & p^2 \mathbf{1}_{\delta \times \delta} & \pm qp \mathbf{1}_{\delta \times \eta} & p^2 \mathbf{1}_{\delta \times \delta} \\ \pm q^2 \mathbf{1}_{\eta \times \eta} & \pm qp \mathbf{1}_{\eta \times \delta} & q^2 \mathbf{1}_{\eta \times \eta} & \pm qp \mathbf{1}_{\eta \times \delta} \\ qp \mathbf{1}_{\delta \times \eta} & p^2 \mathbf{1}_{\delta \times \delta} & \pm qp \mathbf{1}_{\delta \times \eta} & p^2 \mathbf{1}_{\delta \times \delta} \end{pmatrix},$$

where $\eta := \frac{d}{2} - \delta$. Therefore,

$$\mathbf{x}^+ \mathbf{x}^{+*} - \mathbf{x}^- \mathbf{x}^{-*} = 2q \begin{pmatrix} \mathbf{0}_{\eta \times \eta} & \mathbf{0}_{\eta \times \delta} & q\mathbf{1}_{\eta \times \eta} & \mathbf{0}_{\eta \times \delta} \\ \mathbf{0}_{\delta \times \eta} & \mathbf{0}_{\delta \times \delta} & p\mathbf{1}_{\delta \times \eta} & \mathbf{0}_{\delta \times \delta} \\ q\mathbf{1}_{\eta \times \eta} & p\mathbf{1}_{\eta \times \delta} & \mathbf{0}_{\eta \times \eta} & p\mathbf{1}_{\eta \times \delta} \\ \mathbf{0}_{\delta \times \eta} & \mathbf{0}_{\delta \times \delta} & p\mathbf{1}_{\delta \times \eta} & \mathbf{0}_{\delta \times \delta} \end{pmatrix}.$$

We will show that the matrix

$$M := \begin{pmatrix} \mathbf{0}_{\eta \times \eta} & \mathbf{0}_{\eta \times \delta} & q\mathbf{1}_{\eta \times \eta} & \mathbf{0}_{\eta \times \delta} \\ \mathbf{0}_{\delta \times \eta} & \mathbf{0}_{\delta \times \delta} & p\mathbf{1}_{\delta \times \eta} & \mathbf{0}_{\delta \times \delta} \\ q\mathbf{1}_{\eta \times \eta} & p\mathbf{1}_{\eta \times \delta} & \mathbf{0}_{\eta \times \eta} & p\mathbf{1}_{\eta \times \delta} \\ \mathbf{0}_{\delta \times \eta} & \mathbf{0}_{\delta \times \delta} & p\mathbf{1}_{\delta \times \eta} & \mathbf{0}_{\delta \times \delta} \end{pmatrix} \in \mathbb{R}^{d \times d}$$

has two nonzero singular values given by

$$\sigma_1 = \sigma_2 = \sqrt{\eta^2 q^2 + 2\eta\delta p^2}. \quad (3.2.6)$$

This will imply $d_1(\mathbf{x}^+, \mathbf{x}^-) = 4q\sqrt{\eta^2 q^2 + 2\eta\delta p^2} \geq Cdq^2$ as desired.

Using the fact that $\mathbf{1}_{m \times n}\mathbf{1}_{n \times k} = n\mathbf{1}_{m \times k}$, we see that

$$\begin{aligned} M^T M &= \begin{pmatrix} q\mathbf{1}_{\eta \times \eta}q\mathbf{1}_{\eta \times \eta} & q\mathbf{1}_{\eta \times \eta}p\mathbf{1}_{\eta \times \delta} & \mathbf{0}_{\eta \times \eta} & q\mathbf{1}_{\eta \times \eta}p\mathbf{1}_{\eta \times \delta} \\ p\mathbf{1}_{\delta \times \eta}q\mathbf{1}_{\eta \times \eta} & p\mathbf{1}_{\delta \times \eta}p\mathbf{1}_{\eta \times \delta} & \mathbf{0}_{\delta \times \eta} & p\mathbf{1}_{\delta \times \eta}p\mathbf{1}_{\eta \times \delta} \\ \mathbf{0}_{\eta \times \eta} & \mathbf{0}_{\eta \times \delta} & q\mathbf{1}_{\eta \times \eta}q\mathbf{1}_{\eta \times \eta} + 2p\mathbf{1}_{\eta \times \delta}p\mathbf{1}_{\delta \times \eta} & \mathbf{0}_{\eta \times \delta} \\ p\mathbf{1}_{\delta \times \eta}q\mathbf{1}_{\eta \times \eta} & p\mathbf{1}_{\delta \times \eta}p\mathbf{1}_{\eta \times \delta} & \mathbf{0}_{\delta \times \eta} & p\mathbf{1}_{\delta \times \eta}p\mathbf{1}_{\eta \times \delta} \end{pmatrix} \\ &= \begin{pmatrix} \eta q^2 \mathbf{1}_{\eta \times \eta} & \eta q p \mathbf{1}_{\eta \times \delta} & \mathbf{0}_{\eta \times \eta} & \eta q p \mathbf{1}_{\eta \times \delta} \\ \eta q p \mathbf{1}_{\delta \times \eta} & \eta p^2 \mathbf{1}_{\delta \times \delta} & \mathbf{0}_{\delta \times \eta} & \eta p^2 \mathbf{1}_{\delta \times \delta} \\ \mathbf{0}_{\eta \times \eta} & \mathbf{0}_{\eta \times \delta} & \eta q^2 \mathbf{1}_{\eta \times \eta} + 2\delta p^2 \mathbf{1}_{\eta \times \eta} & \mathbf{0}_{\eta \times \delta} \\ \eta q p \mathbf{1}_{\delta \times \eta} & \eta p^2 \mathbf{1}_{\delta \times \delta} & \mathbf{0}_{\delta \times \eta} & \eta p^2 \mathbf{1}_{\delta \times \delta} \end{pmatrix}. \end{aligned}$$

Therefore, $M^T M$ has rank at most two because the second block of rows is equal to the fourth block of rows, which in turn is a multiple of the first block of rows. (Each block can of course have at most one linearly independent row.) We may check that two linearly

independent eigenvectors are given by

$$(\mathbf{0}_{1 \times \eta}, \mathbf{0}_{1 \times \delta}, \mathbf{1}_{1 \times \eta}, \mathbf{0}_{1 \times \delta})^T$$

and

$$(q\mathbf{1}_{1 \times \eta}, p\mathbf{1}_{1 \times \delta}, \mathbf{0}_{1 \times \eta}, p\mathbf{1}_{1 \times \delta})^T,$$

each with eigenvalue $\eta(\eta q^2 + 2\delta p^2)$. This proves (3.2.6) and therefore completes the proof. \square

3.3 Examples: Lower Bounds for Specific Measurement Masks

In this section, we will see that the estimates of Theorems 3.1.1 and 3.1.2 can be improved for specific choices of well-conditioned measurement masks.

3.3.1 Windowed Fourier Measurement Masks

In this subsection, we consider a family of masks $\{\mathbf{m}_{\mathbf{k}}\}_{k=1}^{2\delta-1}$, defined by

$$(\mathbf{m}_{\mathbf{k}})_n := \begin{cases} \frac{e^{-n/b}}{(2\delta-1)^{1/4}} e^{2\pi i(k-1)(n-1)/(2\delta-1)}, & \text{if } 1 \leq n \leq \delta, \\ 0, & \text{if } \delta < n \leq d, \end{cases} \quad (3.3.1)$$

for some fixed parameter $b > 4$. Masks of this form are closely related to those used in ptychographic imaging (see, for example, [37], Section 1.3 and the references provided therein).

In [37] it was shown that, with this choice of masks, the map Y , restricted to the subset of \mathbb{C}^d where $x_n \neq 0$ for all $1 \leq n \leq d$, can be inverted by an algorithm which is both efficient

and numerically stable in the case where $L = d$.

Corollary 3.3.1. *Let $0 < p \leq q$, and consider the map Z restricted to the subset $\mathcal{C}_{p,q} \subset \mathbb{C}^d / \sim$. Assume that $\delta \leq \frac{d}{4}$ and that $d = aL$ for some integer $a < \delta$. Then if $\{\mathbf{m}_{\mathbf{k}}\}_{k=1}^{2\delta-1}$ is the family of masks given by (3.3.1) and B is any Lipschitz map (with respect to d_1) such $B(Z(\mathbf{x})) = \mathbf{x}$ for all $\mathbf{x} \in \mathcal{C}_{p,q}$, then*

$$C_B \geq CK_b \frac{q\sqrt{da}}{p(2\delta-1)^{1/4}\delta^{1/2}} = CK_b \frac{qd}{p\sqrt{L}(2\delta-1)^{1/4}\delta^{1/2}}, \quad (3.3.2)$$

where $K_b := e^{1/b} - 1$, C_B is the Lipschitz constant of B , and C is a universal constant.

Corollary 3.3.2. *Let $0 < p \leq q$, and consider the map Y restricted to the subset $\mathcal{C}_{p,q} \subset \mathbb{C}^d / \sim$. Assume that $\delta \leq \frac{d}{4}$ and that $d = aL$ for some integer $a < \delta$. Then if $\{\mathbf{m}_{\mathbf{k}}\}_{k=1}^{2\delta-1}$ is the family of masks given by (3.3.1) and A is any Lipschitz map (with respect to d_1) such $A(Y(\mathbf{x})) = \mathbf{x}$, for all $\mathbf{x} \in \mathcal{C}_{p,q}$, then*

$$C_A \geq CK_b^2 \frac{qd\sqrt{a}}{p\sqrt{\delta}} = CK_b^2 \frac{qd^{3/2}}{p\sqrt{L}\sqrt{\delta}}, \quad (3.3.3)$$

where $K_b := e^{1/b} - 1$, C_A is the Lipschitz constant of A , and C is a universal constant.

Remark 3.3.1. *For this choice of masks, $K = 2\delta - 1$ and $\|\mathbf{m}\|_\infty = e^{-1/b}(2\delta - 1)^{-1/4}$. Therefore, the constants obtained in Corollaries 3.3.1 and 3.3.2 have the same asymptotic behavior with respect to a and d , but are larger with respect to δ than those obtained by directly applying Theorems 3.1.1 and 3.1.2 to this choice of masks.*

Remark 3.3.2. *Similar lower bounds can be derived for any choice of masks along the lines of (3.3.1) whose nonzero entries have magnitudes that form a truncated geometric progression.*

Proof of Corollary 3.3.1. Let \mathbf{x}^\pm and Z^\pm be as in the proofs of Theorems 3.1.1 and 3.1.2. As before, note that $Z_{k,\ell}^+ = Z_{k,\ell}^-$ except when either $1 + \ell a \leq \frac{d}{2} < \delta + \ell a$ or $1 + \ell a \leq d - \delta < \delta + \ell a$. We will again restrict attention to the case where $1 + \ell a \leq d - \delta < \delta + \ell a$.

Fix ℓ such that $1 + \ell a \leq d - \delta < \delta + \ell a$, and as in the proof of the preceding theorems, let $j := \ell a + 2\delta - d$ so that the last j nonzero entries of $S_{\ell a} \mathbf{m}_\mathbf{k}$ are located in positions greater than $d - \delta$ and the first $\delta - j$ nonzero entries are located in positions less than or equal to $d - \delta$. We have seen that

$$Z_{k,\ell}^\pm = \left| \pm q \sum_{n=1}^{\delta-j} (\mathbf{m}_\mathbf{k})_n + p \sum_{n=\delta-j+1}^{\delta} (\mathbf{m}_\mathbf{k})_n \right|.$$

Therefore,

$$|Z_{k,\ell}^- - Z_{k,\ell}^+| \leq 2p \left| \sum_{n=\delta-j+1}^{\delta} (\mathbf{m}_\mathbf{k})_n \right| \leq 2p \sum_{n=\delta-j+1}^{\delta} |(\mathbf{m}_\mathbf{k})_n|. \quad (3.3.4)$$

To estimate the above sum, we note that $|(\mathbf{m}_\mathbf{k})_n| = (2\delta - 1)^{-1/4} s^n$, where $s := e^{-1/b}$. Since $0 < s < 1$,

$$\sum_{n=\delta-j+1}^{\delta} |(\mathbf{m}_\mathbf{k})_n| \leq (2\delta - 1)^{-1/4} \sum_{n=1}^{\delta} s^n \leq (2\delta - 1)^{-1/4} \frac{s}{1-s}.$$

For each $1 \leq k \leq 2\delta - 1$, there are at most $\frac{\delta}{a}$ choices of ℓ such that $1 + \ell a \leq d - \delta < \delta + \ell a$.

Therefore,

$$\begin{aligned} \|Z^+ - Z^-\|_2^2 &\leq C(2\delta - 1) \frac{\delta}{a} p^2 (2\delta - 1)^{-1/2} \left(\frac{s}{1-s} \right)^2 \\ &= C(2\delta - 1)^{1/2} \frac{\delta}{a} p^2 \left(\frac{e^{-1/b}}{1 - e^{-1/b}} \right)^2 \\ &= C(2\delta - 1)^{1/2} \frac{\delta}{a} p^2 \left(\frac{1}{e^{1/b} - 1} \right)^2. \end{aligned}$$

Recalling that $D_2(\mathbf{x}^+, \mathbf{x}^-) \geq q\sqrt{d}$ as shown in the proof of Theorem 3.1.1 and applying (3.2.1) completes the proof. \square

Proof of Corollary 3.3.2. Let \mathbf{x}^\pm and Y^\pm be as in the proofs of Theorems 3.1.1 and 3.1.2. Note that for all k, ℓ ,

$$|Z_{k,\ell}^\pm| \leq q \sum_{n=1}^{\delta} |(\mathbf{m}_{\mathbf{k}})_n| \leq q(2\delta - 1)^{-1/4} \sum_{n=1}^{\delta} s^n \leq q(2\delta - 1)^{-1/4} \frac{s}{1-s}, \quad (3.3.5)$$

where $s = e^{-1/b}$ as in the proof of Corollary 3.3.2. We again note that $Y_{k,\ell}^+ = Y_{k,\ell}^-$ except when either $1 + \ell a \leq \frac{d}{2} < \delta + \ell a$ or $1 + \ell a \leq d - \delta < \delta + \ell a$ and again restrict attention to the case where $1 + \ell a \leq d - \delta < \delta + \ell a$. Combining (3.3.4) and (3.3.5) gives

$$\begin{aligned} |Y_{k,\ell}^+ - Y_{k,\ell}^-| &= |Z_{k,\ell}^+ + Z_{k,\ell}^-| |Z_{k,\ell}^+ - Z_{k,\ell}^-| \\ &\leq Cqp(2\delta - 1)^{-1/2} \left(\frac{s}{1-s} \right)^2. \end{aligned}$$

For each $1 \leq k \leq 2\delta - 1$, there are at most $\frac{\delta}{a}$ choices of ℓ such that $1 + \ell a \leq d - \delta < \delta + \ell a$.

Therefore,

$$\begin{aligned} \|Y^+ - Y^-\|_2^2 &\leq C(2\delta - 1) \frac{\delta}{a} q^2 p^2 (2\delta - 1)^{-1} \left(\frac{s}{1-s} \right)^4 \\ &\leq C \frac{\delta}{a} q^2 p^2 \left(\frac{e^{-1/b}}{1 - e^{-1/b}} \right)^4 \\ &= C \frac{\delta}{a} q^2 p^2 \left(\frac{1}{e^{1/b} - 1} \right)^4. \end{aligned}$$

Recalling $d_1(\mathbf{x}^+, \mathbf{x}^-) \geq Cdq^2$, as shown in the proof of Theorem 3.1.1, completes the proof. \square

3.3.2 Two-Shot Measurement Masks

Consider the family of masks $\{\mathbf{m}_{\mathbf{k}}\}_{k=1}^{2\delta-1}$ defined by

$$\begin{aligned}\mathbf{m}_1 &:= \mathbf{e}_1 \\ \mathbf{m}_{2j} &:= \mathbf{e}_1 + \mathbf{e}_{j+1} \\ \mathbf{m}_{2j+1} &:= \mathbf{e}_1 + i\mathbf{e}_{j+1}\end{aligned}\tag{3.3.6}$$

for $1 \leq j \leq \delta - 1$, where $\{\mathbf{e}_1, \dots, \mathbf{e}_d\}$ is the standard orthonormal basis for \mathbb{R}^d . In [36] it was shown that, with this choice of masks, the map Y is injective on the subset of \mathbb{C}^d where all entries are nonzero and can be inverted through a well-conditioned algorithm in the case $L = d$.

Corollary 3.3.3. *Fix $0 < p \leq q$, and consider the map Z restricted to the subset $\mathcal{C}_{p,q} \subset \mathbb{C}^d / \sim$. Assume that $\delta \leq \frac{d}{4}$ and that $d = aL$ for some integer $a < \delta$. Then if $\{\mathbf{m}_{\mathbf{k}}\}_{k=1}^{2\delta-1}$ is the family of masks defined by (3.3.6) and B is any Lipschitz map (with respect to D_2) such that $B(Z(\mathbf{x})) = \mathbf{x}$ for all $\mathbf{x} \in \mathcal{C}_{p,q}$, then*

$$C_B \geq C \frac{q\sqrt{da}}{p\delta} = C \frac{qd}{\sqrt{L}p\delta},$$

where C_B is the Lipschitz constant of B and C is a universal constant.

Corollary 3.3.4. *Let $0 < p \leq q$, and consider the map Y restricted to the subset $\mathcal{C}_{p,q} \subset \mathbb{C}^d / \sim$. Assume that $\delta \leq \frac{d}{4}$ and that $d = aL$ for some integer $a < \delta$. Then if $\{\mathbf{m}_{\mathbf{k}}\}_{k=1}^{2\delta-1}$ is the family of masks defined by (3.3.6) and A is any Lipschitz map (with respect to d_1) such that $A(Y(\mathbf{x})) = \mathbf{x}$ for all $\mathbf{x} \in \mathcal{C}_{p,q}$, then*

$$C_A \geq C \frac{qd\sqrt{a}}{p\delta} = C \frac{qd^{3/2}}{\sqrt{L}p\delta},$$

where C_A is the Lipschitz constant of A and C is a universal constant.

Remark 3.3.3. Note that for this choice of masks $K = 2\delta - 1$. Therefore, the constants obtained in Corollaries 3.3.3 and 3.3.4 exhibit the same asymptotic behavior with respect to d and are asymptotically larger with respect to δ than those obtained by applying Theorems 3.1.1 and 3.1.2 to this choice of masks.

Proof of Corollary 3.3.3. Let \mathbf{x}^\pm be as in the proof of Theorems 3.1.1 and 3.1.2. Note that for all $1 \leq n \leq d$, $|x_n^+| = |x_n^-|$. Therefore, it is clear that for all ℓ ,

$$|\langle S_{\ell a} \mathbf{m}_1, \mathbf{x}^+ \rangle| = |x_{\ell a+1}^+| = |x_{\ell a+1}^-| = |\langle S_{\ell a} \mathbf{m}_1, \mathbf{x}^- \rangle|,$$

and

$$\begin{aligned} |\langle S_{\ell a} \mathbf{m}_{2j+1}, \mathbf{x}^+ \rangle| &= |x_{\ell a+1}^+ + ix_{\ell a+j+1}^+| \\ &= |x_{\ell a+1}^- + ix_{\ell a+j+1}^-| \\ &= |\langle S_{\ell a} \mathbf{m}_{2j+1}, \mathbf{x}^- \rangle| \end{aligned}$$

since the real and imaginary parts of $\langle S_{\ell a} \mathbf{m}_{2j+1}, \mathbf{x}^+ \rangle$ and $\langle S_{\ell a} \mathbf{m}_{2j+1}, \mathbf{x}^- \rangle$ have the same absolute values. Therefore, to estimate $\|Z^+ - Z^-\|_2$ we only need to consider the terms $Z_{2j,\ell}^+ - Z_{2j,\ell}^-$. Furthermore, it is clear that $Z_{2j,\ell}^+$ will equal $Z_{2j,\ell}^-$, unless ℓ is chosen in such a way that either $\ell a + 1 \leq \frac{d}{2} < \ell a + j + 1$ or $\ell a + 1 \leq d - \delta < \ell a + j + 1$. In either of these cases,

$$|Z_{2j,\ell}^+ - Z_{2j,\ell}^-| = 2p. \quad (3.3.7)$$

Therefore, we will be able to compute $\|Z^+ - Z^-\|_2$ once we estimate the number of ℓ such that $la + 1 \leq \frac{d}{2} < la + j + 1$ or $la + 1 \leq d - \delta < la + j + 1$, which we will do in the following lemma.

Lemma 3.3.1. *For fixed j , the number of ℓ such that $la + 1 \leq \frac{d}{2} < la + j + 1$ is less than or equal to $\frac{j}{a}$. Likewise, the number of ℓ such that $la + 1 \leq d - \delta < la + j + 1$ is less than or equal to $\frac{j}{a}$.*

Proof. If $la + 1 \leq \frac{d}{2} < la + j + 1$, then $\frac{d}{2} - j \leq la \leq \frac{d}{2} - 1$, and any set of j consecutive integers can contain at most $\frac{j}{a}$ multiples of a . Likewise, if $la + 1 \leq d - \delta < la + j + 1$, then $d - \delta - j \leq la \leq d - \delta - 1$. □

Combining (3.3.7) and Lemma 3.3.1 gives

$$\|Z^+ - Z^-\|_2^2 \leq \sum_{j=1}^{\delta} \frac{2j}{a} (2p)^2 \leq C \frac{p^2 \delta^2}{a} = C \frac{Lp^2 \delta^2}{d}.$$

Therefore, recalling the fact that $D_2(\mathbf{x}^+, \mathbf{x}^-) \geq \sqrt{dq}$, as shown in the proof of Theorem 3.1.1, the proof follows from (3.2.1). □

Proof of Corollary 3.3.4. Since each $\mathbf{m}_{\mathbf{k}}$ has at most two nonzero entries, $|Z_{k,\ell}^+ + Z_{k,\ell}^-| \leq 4q$ for all k and ℓ . Therefore, by (3.3.7) each nonzero entry of $Y^+ - Y^-$ satisfies

$$|Y_{k,\ell}^+ - Y_{k,\ell}^-| \leq |Z_{k,\ell}^+ + Z_{k,\ell}^-| |Z_{k,\ell}^+ - Z_{k,\ell}^-| \leq Cqp.$$

Furthermore, similarly to the proof of Corollary 3.3.3, $Y_{k,\ell}^+ - Y_{k,\ell}^-$ is nonzero if and only if

$k = 2j$ for some $1 \leq j \leq \delta - 1$ and $\ell a + 1 \leq \frac{d}{2} < \ell a + j + 1$ or $\ell a + 1 \leq d - \delta < \ell a + j + 1$.

Therefore, by Lemma 3.3.1,

$$\|Y^+ - Y^-\|_2^2 \leq C \sum_{j=1}^{\delta} \frac{2j}{a} (pq)^2 \leq C \frac{q^2 p^2 \delta^2}{a} = C \frac{Lq^2 p^2 \delta^2}{d}.$$

Finally, recalling from the proof of Theorem 3.1.2 that $d_1(\mathbf{x}^+, \mathbf{x}^-) \geq Cdq^2$, the result follows from (3.2.5). □

3.4 Discussion and Future Work

We believe that this initial work opens up several interesting corridors for further research. First and perhaps most obvious among these is the development of algorithms together with optimal STFT windows, etc., that have Lipschitz upper bounds which match these lower bounds to the extent possible (keeping in mind, of course, that the lower bounds developed here may be gross underestimates). Existing algorithms for local correlation measurements such as [37, 36] yield upper bounds for the measurements Y considered above (3.1.1) with respect to the D_2 -metric, a metric with respect to which an inverse of Y will not generally be Lipschitz [5]. As a result, the upper bounds they provide are not quite appropriate to compare to the lower bounds considered here. Nonetheless, the Lipschitz lower bounds developed here do seem to at least heuristically justify the necessity of, e.g., the d -dependence present in those existing worst-case upper bounds.

Another interesting avenue of research would be to explore the extension of the related infinite-dimensional results developed by Alaifari et al. [1, 27] to the finite-dimensional discrete setting. The resulting theory would potentially provide more fine-grained insights

into the recovery of samples \mathbf{x} from discrete STFT magnitude measurements, and could also possibly be extended to results concerning general local correlation measurement maps of the type we consider here in a way that would allow for the relaxation of the support assumptions currently made on the masks $\{\mathbf{m}_1, \mathbf{m}_2, \dots, \mathbf{m}_K\}$. Finally, one could also consider local Lipschitz and Hölder lower bounds as opposed to global lower bounds. Though perhaps more difficult to analyze, such lower bounds may be more likely to correspond to achievable upper bounds.

Chapter 4

Recovery of Compactly Supported

Functions from Spectrogram

Measurements via Lifting

The work in this chapter first appeared in [44].

In Section 1.3.2, we discussed an existing Wigner distribution deconvolution method for phase retrieval. The model, which assumed continuous ptychographic measurements of the form

$$b(\ell, \omega) = \left| \int_{-\infty}^{\infty} f(t) g(t - \ell) e^{-2\pi i \omega t} dt \right|^2,$$

was based on decoupling the unknown signal f from the known mask g . This was done through two consecutive applications of the continuous Fourier transform to the measurements. This formulation, however, says nothing about parameter selection, i.e., for which values of physical shifts and Fourier modes is recovery possible. While the aliased WDD formulation in Chapter 2 provides the means for parameter selection, it does not assume a continuous model.

In this chapter, we attempt to bridge the gap between continuous phase retrieval and parameter selection. Thus, a novel phase retrieval method, motivated by ptychographic imaging, is proposed for the approximate recovery of a compactly supported specimen function

$f : \mathbb{R} \rightarrow \mathbb{C}$ from its continuous short-time Fourier transform (STFT) spectrogram measurements. The method, partially inspired by the *PhaseLift* algorithm, is based on a lifted formulation of the infinite dimensional problem, which is then later truncated for the sake of computation. Numerical experiments demonstrate the promise of the proposed approach.

4.1 Introduction

Motivated by ptychographic imaging in the 1-D setting, consider a compactly supported specimen, $f : \mathbb{R} \rightarrow \mathbb{C}$, being scanned by a focused illuminating beam $g : \mathbb{R} \rightarrow \mathbb{C}$ which translates across f in fixed overlapping shifts $\ell_1, \dots, \ell_K \in \mathbb{R}$. At each such shift of the beam (or, equivalently, the specimen) a phaseless diffraction image is then sampled in bulk by a detector. Due to the underlying physics the collected measurements are modeled as sampled STFT magnitude measurements of f of the form

$$b_{k,j} := \left| \int_{-\infty}^{\infty} f(t) g(t - \ell_k) e^{-2\pi i \omega_j t} dt \right|^2 \quad (4.1.1)$$

for a finite set of KN shift and frequency pairs $(\ell_k, \omega_j) \in \{\ell_1, \dots, \ell_K\} \times \{\omega_1, \dots, \omega_N\}$. Our objective is to approximate f (up to a global phase) using these $b_{k,j}$ measurements.

As discussed in the Introduction, there has been a good deal of work on signal recovery from phaseless STFT measurements in the last few of years in the *discrete setting*, where f and g are modeled as vectors ab initio, and then recovered from discrete STFT magnitude measurements. In this setting many related recovery techniques have been considered including iterative methods along the lines of Griffin and Lim [46, 56] and alternating projections [43], graph theoretic methods for Gabor frames based on polarization [53, 47], and

semi-definite relaxation-based methods [38], among others [20, 10, 37, 36].

Herein we will instead consider the approximate recovery of f (as a compactly supported function) from samples of its continuous STFT magnitude measurements $b_{k,j}$ as per (4.1.1). Besides perhaps better matching the continuous models considered in some applications such as ptychography, and allowing one to more naturally consider approaches that utilize, e.g., irregular sampling, we also take recent work on phase retrieval in infinite dimensional Hilbert spaces [57, 12, 1] as motivation for exploring numerical methods to solve this problem.

In particular, the recent work of Daubechies and her collaborators implies that the stability of such continuous phase retrieval problems is generally less well behaved than their discrete counterparts [12, 1]. Specifically, [1] characterizes a class of functions for which infinite dimensional phase retrieval (up to a single global phase) from Gabor measurements is unstable, and then proposes the reconstruction of these worst-case functions up to several local phase multiples as a stable alternative. We take this initial work on stable infinite dimensional phase retrieval from Gabor measurements as a further motivation to explore new fast numerical techniques for the robust recovery of compactly supported functions from their continuous spectrogram measurements.

4.1.1 The Problem Statement and Specifications

Given a vector of stacked spectrogram samples from (4.1.1),

$$\mathbf{b} = \left(b_{1,1}, \dots, b_{1,N}, b_{2,1}, \dots, b_{K,N} \right)^T \in [0, \infty)^{NK}, \quad (4.1.2)$$

our goal is to approximately recover a piecewise smooth and compactly supported function $f : \mathbb{R} \rightarrow \mathbb{C}$. Of course f can only be recovered up to certain ambiguities (such as up to a

global phase, etc.) which depend not only on f , but also the window function g (see, e.g., [1]). Without loss of generality, we will assume that the support of f is contained in $[-1, 1]$. Given our motivation from ptychographic imaging we will, herein at least, primarily consider the unshifted beam function g to also be (approximately) compactly supported within a smaller subset $[-a, a] \subset [-1, 1]$. Furthermore, we will also assume that g is smooth enough that its Fourier transform decays relatively rapidly in frequency space compared to \widehat{f} . Examples of such g include both suitably scaled Gaussians, as well as compactly supported C^∞ bump functions [39].

4.1.2 The Proposed Numerical Approach

The proposed method aims to recover samples from the Fourier transform of f at frequencies in $\Omega = \{\omega_1, \dots, \omega_N\}$, giving $\mathbf{f} \in \mathbb{C}^N$ with $f_j = \widehat{f}(\omega_j)$, from which \widehat{f} can then be approximately recovered via standard sampling theorems (see, e.g., [55]). The inverse Fourier transform of this approximation of \widehat{f} then provides our approximation of f .

Recovery of the samples from \widehat{f} , $\mathbf{f} \in \mathbb{C}^N$, is performed in two steps using techniques from [37, 36] adapted to this continuous setting: first, a truncated lifted linear system is inverted in order to learn a portion of the rank-one matrix $\mathbf{f}\mathbf{f}^*$ from a finite set of STFT spectrogram samples, then, an eigenvector based angular synchronization method is used in order to recover \mathbf{f} from the portion of $\mathbf{f}\mathbf{f}^*$ computed in the first step. Note that this truncated lifted linear system is both banded and Toeplitz, with band size determined by the decay of \widehat{g} . If g is effectively band-limited to $[-\delta, \delta]$ the proposed lifting-based algorithm can be implemented to run in $\mathcal{O}(\delta N(\log N + \delta^2))$ -time, which is essentially FFT-time in N for small δ .

4.2 Our Lifted Formulation

The following theorem forms the basis of our lifted setup.

Theorem 4.2.1. *Suppose $f : \mathbb{R} \rightarrow \mathbb{C}$ is piecewise smooth and compactly supported in $[-1, 1]$.*

Let $g \in L^2([-a, a])$ be supported in $[-a, a] \subset [-1, 1]$ for some $a < 1$, with $\|g\|_{L^2} = 1$. Then

for all $\omega \in \mathbb{R}$,

$$|\mathcal{F}[f \cdot S_\ell g](\omega)| = \frac{1}{2} \left| \sum_{m \in \mathbb{Z}} e^{-\pi i \ell m} \widehat{f}\left(\frac{m}{2}\right) \widehat{g}\left(\frac{m}{2} - \omega\right) \right|$$

for all shifts $\ell \in [a - 1, 1 - a]$.

Proof. Denote by $S_\ell g$ the right shift of g by ℓ . The short-time Fourier transform (STFT)

[42] of f given g , at a shift ℓ and frequency ω , is defined by

$$\mathcal{F}[f \cdot S_\ell g](\omega) = \int_{-\infty}^{\infty} f(t) g(t - \ell) e^{-2\pi i \omega t} dt.$$

The squared magnitude of the Fourier transform above is called a spectrogram measurement:

$$|\mathcal{F}[f \cdot S_\ell g](\omega)|^2 = \left| \int_{-\infty}^{\infty} f(t) g(t - \ell) e^{-2\pi i \omega t} dt \right|^2 = |\langle f, h \rangle|^2$$

where $h(t) := \overline{g(t - \ell)} e^{2\pi i \omega t}$. We calculate

$$\begin{aligned} \widehat{h}(k) &= \int_{-\infty}^{\infty} h(t) e^{-2\pi i k t} dt \\ &= \int_{-\infty}^{\infty} \overline{g(t - \ell)} e^{2\pi i \omega t} e^{-2\pi i k t} dt \\ &= \int_{-\infty}^{\infty} \overline{g(\tau)} e^{2\pi i \omega(\tau + \ell)} e^{-2\pi i k(\tau + \ell)} d\tau \\ &= e^{2\pi i \ell(\omega - k)} \int_{-\infty}^{\infty} \overline{g(\tau)} e^{-2\pi i(\omega - k)\tau} d\tau. \end{aligned}$$

So, we have

$$\widehat{h}(k) = e^{2\pi il(\omega-k)} \mathcal{F} \left[\overline{g(\cdot)} \right] (\omega - k).$$

Now, by Plancherel's Theorem, we have

$$\begin{aligned} |\langle f, h \rangle|^2 &= \left| \langle \widehat{f}, \widehat{h} \rangle \right|^2 = \left| \int_{-\infty}^{\infty} \widehat{f}(k) \overline{\widehat{h}(k)} dk \right|^2 \\ &= \left| \int_{-\infty}^{\infty} \widehat{f}(k) e^{-2\pi il(\omega-k)} \overline{\mathcal{F} \left[\overline{g(\cdot)} \right] (\omega - k)} dk \right|^2 \\ &= \left| \int_{-\infty}^{\infty} \widehat{f}(k) e^{2\pi ilk} \overline{\mathcal{F} \left[\overline{g(\cdot)} \right] (\omega - k)} dk \right|^2 \\ &= \left| \int_{-\infty}^{\infty} \widehat{f}(\omega - \eta) e^{-2\pi il\eta} \overline{\mathcal{F} \left[\overline{g(\cdot)} \right] (\eta)} d\eta \right|^2 \\ &= \left| \int_{-\infty}^{\infty} \widehat{f}(\omega - \eta) \widehat{g}(-\eta) e^{-2\pi il\eta} d\eta \right|^2, \end{aligned}$$

where in the last equality we have used the following Fourier transform property:

$$\overline{\mathcal{F} \left[\overline{g(\cdot)} \right] (\eta)} = \widehat{g}(-\eta).$$

And so, applying Shannon's Sampling Theorem [54] to \widehat{f} , we see that

$$\begin{aligned} |\mathcal{F}[f \cdot S_{\ell}g](\omega)|^2 &= \left| \int_{-\infty}^{\infty} \widehat{f}(\omega - \eta) \widehat{g}(-\eta) e^{-2\pi il\eta} d\eta \right|^2 \\ &= \left| \int_{-\infty}^{\infty} \widehat{g}(-\eta) \sum_{m \in \mathbb{Z}} \widehat{f}\left(\frac{m}{2}\right) \operatorname{sinc} \pi(m - 2(\omega - \eta)) e^{-2\pi il\eta} d\eta \right|^2 \\ &= \left| \sum_{m \in \mathbb{Z}} \widehat{f}\left(\frac{m}{2}\right) \int_{-\infty}^{\infty} \widehat{g}(-\eta) e^{-2\pi il\eta} \operatorname{sinc} \pi(m - 2(\omega - \eta)) d\eta \right|^2 \\ &= \left| \sum_{m \in \mathbb{Z}} \widehat{f}\left(\frac{m}{2}\right) \int_{-\infty}^{\infty} \widehat{g}(\eta) e^{2\pi il\eta} \operatorname{sinc} \pi(m + 2(-\omega - \eta)) d\eta \right|^2 \end{aligned}$$

$$= \left| \sum_{m \in \mathbb{Z}} \hat{f}\left(\frac{m}{2}\right) \left[\hat{g}(\cdot) e^{-2\pi i \ell(\cdot)} * \text{sinc} \pi(m + 2(\cdot)) \right](-\omega) \right|^2,$$

where $*$ denotes the convolution operator:

$$(p * q)(t) := \int_{\mathbb{R}} p(x) q(t - x) dx \quad \forall (p, q, t) \in L^2(\mathbb{R}) \times L^2(\mathbb{R}) \times \mathbb{R}.$$

The Convolution Theorem states

$$\mathcal{F}[f * g] = \hat{f} \cdot \hat{g} \implies f * g = \mathcal{F}^{-1}[\hat{f} \cdot \hat{g}].$$

To apply the Convolution Theorem, we calculate the Fourier transforms

$$\mathcal{F}\left[\hat{g}(\cdot) e^{-2\pi i \ell(\cdot)}\right](\xi) = \hat{g}(\xi + \ell) = g(-\ell - \xi),$$

and

$$\mathcal{F}[\text{sinc} \pi(m + 2(\cdot))](\xi) = \mathcal{F}\left[\frac{\sin \pi(m + 2x)}{\pi(m + 2x)}\right](\xi) = \frac{e^{\pi i m \xi}}{2} \chi_{(-1,1)}(\xi).$$

Thus, the spectrogram measurements may be expressed as

$$\begin{aligned} |\mathcal{F}[f \cdot S_{\ell}g](\omega)|^2 &= \left| \sum_{m \in \mathbb{Z}} \hat{f}\left(\frac{m}{2}\right) \mathcal{F}^{-1}\left[g(-\ell - (\cdot)) \frac{e^{\pi i m(\cdot)}}{2} \chi_{(-1,1)}(\cdot)\right](-\omega) \right|^2 \\ &= \frac{1}{4} \left| \sum_{m \in \mathbb{Z}} \hat{f}\left(\frac{m}{2}\right) \int_{-\infty}^{\infty} g(-\ell - x) e^{\pi i m x} \chi_{(-1,1)}(x) e^{-2\pi i x \omega} dx \right|^2 \\ &= \frac{1}{4} \left| \sum_{m \in \mathbb{Z}} \hat{f}\left(\frac{m}{2}\right) \int_{-1}^1 g(-\ell - x) e^{\pi i m x} e^{-2\pi i x \omega} dx \right|^2 \end{aligned}$$

$$\begin{aligned}
&= \frac{1}{4} \left| \sum_{m \in \mathbb{Z}} \widehat{f}\left(\frac{m}{2}\right) \int_{-\ell+1}^{-\ell-1} g(u) e^{\pi i(-\ell-u)(m-2\omega)} du \right|^2 \\
&= \frac{1}{4} \left| \sum_{m \in \mathbb{Z}} \widehat{f}\left(\frac{m}{2}\right) e^{-\pi i \ell(m-2\omega)} \int_{-\ell-1}^{-\ell+1} g(u) e^{-2\pi i u\left(\frac{m}{2}-\omega\right)} du \right|^2.
\end{aligned}$$

Since ℓ is such that $[-\ell-1, -\ell+1] \cap [-a, a] = [-a, a]$, we have

$$\begin{aligned}
|\mathcal{F}[f \cdot S_\ell g](\omega)|^2 &= \frac{1}{4} \left| \sum_{m \in \mathbb{Z}} \widehat{f}\left(\frac{m}{2}\right) e^{-\pi i \ell(m-2\omega)} \int_{-a}^a g(u) e^{-2\pi i u\left(\frac{m}{2}-\omega\right)} du \right|^2 \\
&= \frac{1}{4} \left| \sum_{m \in \mathbb{Z}} \widehat{f}\left(\frac{m}{2}\right) e^{-\pi i \ell(m-2\omega)} \int_{-\infty}^{\infty} g(u) e^{-2\pi i u\left(\frac{m}{2}-\omega\right)} du \right|^2 \\
&= \frac{1}{4} \left| \sum_{m \in \mathbb{Z}} e^{-\pi i \ell m} \widehat{f}\left(\frac{m}{2}\right) \widehat{g}\left(\frac{m}{2}-\omega\right) \right|^2.
\end{aligned}$$

We have now proven the theorem. □

Using Theorem 4.2.1 we may now write

$$|\mathcal{F}[f \cdot S_\ell g](\omega)|^2 = \frac{1}{4} \sum_{k \in \mathbb{Z}} \sum_{j \in \mathbb{Z}} v_k \overline{v_j}$$

where $v_n := e^{-\pi i \ell n} \widehat{f}\left(\frac{n}{2}\right) \widehat{g}\left(\frac{n}{2}-\omega\right)$.

4.2.1 Obtaining a Truncated, Finite Lifted Linear System

If \widehat{g} decays quickly we may truncate the sums above for a given frequency ω with minimal error. To that end, we pick the indices j and k so that $\left|\frac{k}{2}-\omega\right| \leq \delta$ and $\left|\frac{j}{2}-\omega\right| \leq \delta$ for some

fixed $\delta \in \mathbb{N}$. If we denote

$$S_\omega = \{(j, k) \in \mathbb{Z} \times \mathbb{Z} \mid |k - 2\omega| \leq 2\delta \text{ and } |j - 2\omega| \leq 2\delta\},$$

then

$$|\mathcal{F}[f \cdot S_\ell g](\omega)|^2 = \frac{1}{4} \sum_{(j,k) \in S_\omega} v_k \bar{v}_j + \text{error}.$$

We may write

$$\sum_{|j-2\omega| \leq 2\delta} e^{\pi i \ell j} \overline{\widehat{f}\left(\frac{j}{2}\right) \widehat{g}\left(\frac{j}{2} - \omega\right)} = e^{2\pi i \ell \omega} \mathbf{x}_\ell^* \mathbf{y}_\omega$$

where $\mathbf{x}_\ell \in \mathbb{C}^{4\delta+1}$ and $\mathbf{y}_\omega \in \mathbb{C}^{4\delta+1}$ are the vectors

$$\mathbf{x}_\ell = \begin{pmatrix} e^{\pi i \ell (2\delta)} \widehat{g}(-\delta) \\ e^{\pi i \ell (2\delta-1)} \widehat{g}\left(\frac{1}{2} - \delta\right) \\ \vdots \\ e^{\pi i \ell \cdot 0} \widehat{g}(0) \\ \vdots \\ e^{\pi i \ell (1-2\delta)} \widehat{g}\left(\delta - \frac{1}{2}\right) \\ e^{\pi i \ell (-2\delta)} \widehat{g}(\delta) \end{pmatrix}, \quad \mathbf{y}_\omega = \begin{pmatrix} \overline{\widehat{f}(\omega - \delta)} \\ \overline{\widehat{f}\left(\omega - \delta + \frac{1}{2}\right)} \\ \vdots \\ \overline{\widehat{f}(\omega)} \\ \vdots \\ \overline{\widehat{f}\left(\omega + \delta - \frac{1}{2}\right)} \\ \overline{\widehat{f}(\omega + \delta)} \end{pmatrix}.$$

This notation allows us to write our measurements in a lifted form:

$$|\mathcal{F}[f \cdot S_\ell g](\omega)|^2 \approx \frac{1}{4} \overline{e^{2\pi i \ell \omega} \mathbf{x}_\ell^* \mathbf{y}_\omega} \cdot e^{2\pi i \ell \omega} \mathbf{x}_\ell^* \mathbf{y}_\omega = \frac{1}{4} \mathbf{x}_\ell^* \mathbf{y}_\omega \mathbf{y}_\omega^* \mathbf{x}_\ell.$$

Here, $\mathbf{y}_\omega \mathbf{y}_\omega^*$ is the rank-one matrix

$$\begin{bmatrix} |\widehat{f}(\omega - \delta)|^2 & \cdots & \overline{\widehat{f}(\omega - \delta)} \widehat{f}(\omega) & \cdots & \overline{\widehat{f}(\omega - \delta)} \widehat{f}(\omega + \delta) \\ \vdots & \ddots & \vdots & \vdots & \vdots \\ \overline{\widehat{f}(\omega)} \widehat{f}(\omega - \delta) & \cdots & |\widehat{f}(\omega)|^2 & \cdots & \overline{\widehat{f}(\omega)} \widehat{f}(\omega + \delta) \\ \vdots & \vdots & \vdots & \ddots & \vdots \\ \overline{\widehat{f}(\omega + \delta)} \widehat{f}(\omega - \delta) & \cdots & \overline{\widehat{f}(\omega + \delta)} \widehat{f}(\omega) & \cdots & |\widehat{f}(\omega + \delta)|^2 \end{bmatrix}.$$

For each $\mathbf{x}_\ell \in \mathbb{C}^{4\delta+1}$, rewrite it as

$$\mathbf{x}_\ell = \left(m_{-\delta}^\ell, m_{-\delta+\frac{1}{2}}^\ell, \dots, m_{\delta-\frac{1}{2}}^\ell, m_\delta^\ell \right)^T$$

so that $m_k^\ell = e^{-\pi i \ell (2k)} \widehat{g}(k)$. Then construct the Toeplitz matrix $X_\ell \in \mathbb{C}^{N \times N}$ as

$$\begin{bmatrix} m_0^\ell & m_{\frac{1}{2}}^\ell & \cdots & m_\delta^\ell & 0 & 0 & \cdots & 0 \\ m_{-\frac{1}{2}}^\ell & m_0^\ell & \cdots & m_{\delta-\frac{1}{2}}^\ell & m_\delta^\ell & 0 & \cdots & 0 \\ \vdots & \vdots \\ 0 & 0 & \cdots & 0 & m_{-\delta}^\ell & m_{-\delta+\frac{1}{2}}^\ell & \cdots & m_{\frac{1}{2}}^\ell \\ 0 & 0 & \cdots & 0 & 0 & m_{-\delta}^\ell & \cdots & m_0^\ell \end{bmatrix}$$

where N is the number of frequencies ω being considered. Then we construct the block matrix $G \in \mathbb{C}^{NK \times N}$ as

$$G = \begin{pmatrix} X_{\ell_1} \\ X_{\ell_2} \\ \vdots \\ X_{\ell_K} \end{pmatrix}$$

where K is the number of shifts of the window g .

Let $H \in \mathbb{C}^{N \times N}$ be defined as

$$H_{i,j} = \begin{cases} \overline{\widehat{f}\left(\frac{i-2n-1}{2}\right)} \widehat{f}\left(\frac{j-2n-1}{2}\right), & \text{if } |i-j| \leq 2\delta, \\ 0, & \text{otherwise,} \end{cases}$$

where $n = \frac{N-1}{4}$. Note that H is composed of overlapping segments of the rank-one matrices $\mathbf{y}_\omega \mathbf{y}_\omega^*$ for $\omega \in \{-n, \dots, n\}$. Thus, our measurements can be written as

$$\mathbf{b} \approx \text{diag}(GHG^*), \quad (4.2.1)$$

where \mathbf{b} is defined in (4.1.2). By consistently vectorizing (4.2.1), we can obtain a simple linear system which can be inverted to learn \mathbf{h} , a vectorized version of H . In particular, we have

$$\mathbf{b} \approx M\mathbf{h}, \quad (4.2.2)$$

where the matrix $M \in \mathbb{C}^{NK \times N^2}$ can be computed by, e.g., passing the canonical basis elements for $\mathbb{C}^{N \times N}$ through (4.2.1). We solve the linear system (4.2.2) as a least squares problem; experiments have shown that M is of rank NK . The process of recovering the

Fourier coefficients of f from \mathbf{h} is known as angular synchronization, and is described in detail in [36].

4.3 Numerical Results

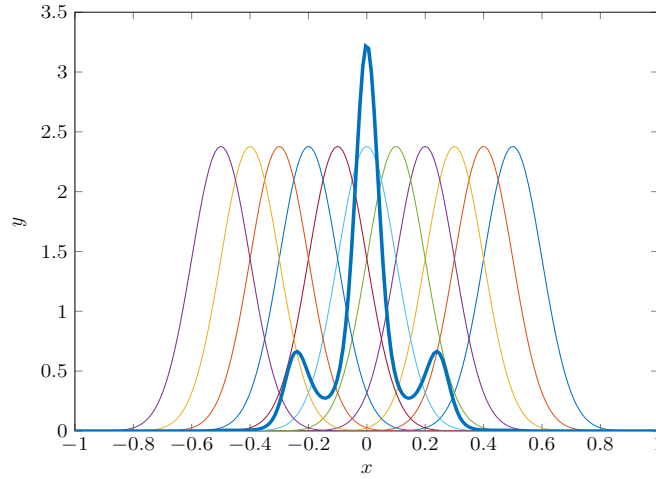


Figure 4.3.1: Modulated Gaussian signal and 11 shifts of a Gaussian window.

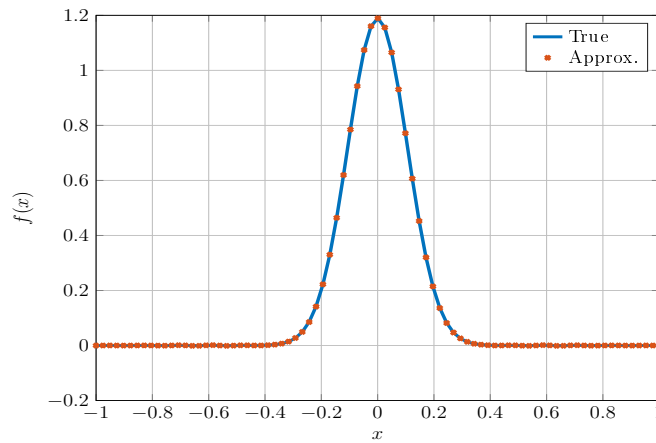


Figure 4.3.2: True Gaussian signal and its reconstruction.

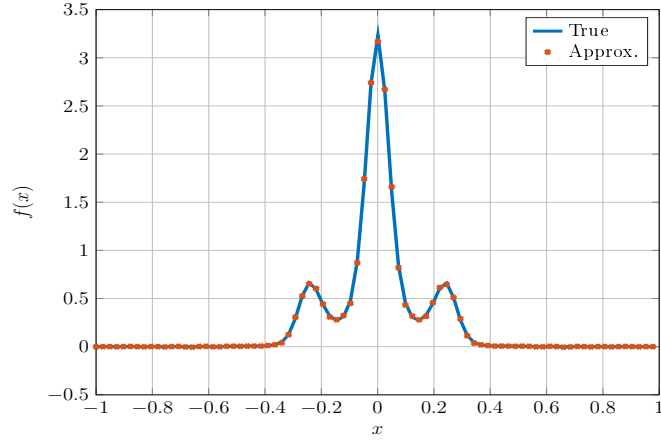


Figure 4.3.3: True modulated Gaussian signal and its reconstruction.

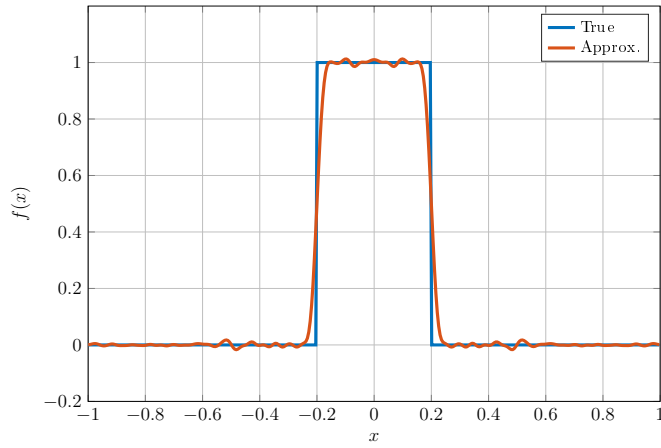


Figure 4.3.4: Characteristic function and its reconstruction.

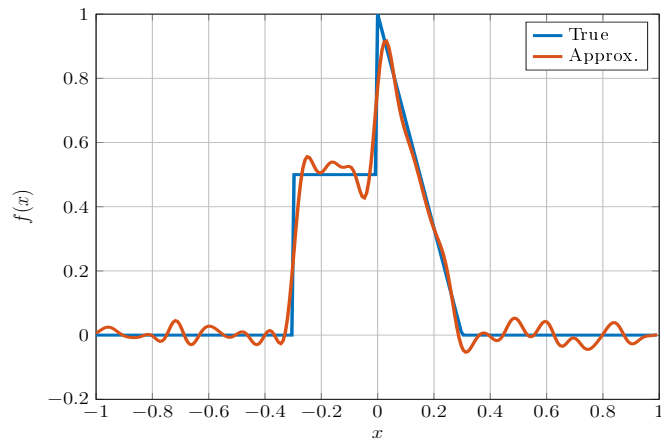


Figure 4.3.5: Piecewise continuous function and its reconstruction.

We test the phase retrieval algorithm above for four different choices of signal f . The first is a Gaussian signal

$$f(x) = \frac{1}{24} e^{-25\left(\frac{4x}{3}\right)^2} \chi_{[-1,1]}(x).$$

The second is an oscillatory Gaussian

$$f(x) = \frac{1}{4} e^{-8\pi x^2} \cos(24x) \chi_{[-1,1]}(x).$$

The third is a characteristic function

$$f(x) = \chi_{\left[-\frac{1}{5}, \frac{1}{5}\right]}(x).$$

The fourth is a piecewise continuous function

$$f(x) = \frac{1}{2} \chi_{\left[-\frac{3}{10}, 0\right]}(x) + \left(1 - \frac{10}{3}x\right) \chi_{\left[0, \frac{3}{10}\right]}(x).$$

In the first two experiments, the window used is the Gaussian

$$g(x) = c \cdot e^{-16\pi x^2} \chi_{\left[-\frac{1}{2}, \frac{1}{2}\right]}(x)$$

where c is a constant chosen so that $\|g\|_{L^2} = 1$. We use a total of 11 shifts of g . Since g is supported on $\left[-\frac{1}{2}, \frac{1}{2}\right]$, any two consecutive shifts are separated by $\frac{0.5}{11}$ (see Figure 4.3.1). We choose 61 values of ω from $[-15, 15]$ sampled in half-steps, and set $\delta = 7$. The reconstructions in physical space are shown at selected grid points in Figures 4.3.2 and 4.3.3. The relative ℓ^2 error in physical space is 1.47×10^{-3} for the first experiment and 1.872×10^{-2} for the second.

In the third and fourth experiments (in which the signals are discontinuous), the window used is the (thinner) Gaussian

$$g(x) = c \cdot e^{-32\pi x^2} \chi_{\left[-\frac{1}{2}, \frac{1}{2}\right]}(x).$$

For the recovery of the characteristic function, we use a total of 21 shifts of g , and choose 293 values of ω from $[-73, 73]$ sampled in half-steps, and set $\delta = 10$. The reconstruction in physical space for the third experiment is shown in Figure 4.3.4. The relative ℓ^2 error in physical space is 1.509×10^{-1} .

For the recovery of the piecewise continuous function, we use a total of 41 shifts of g , and choose 121 values of ω from $[-30, 30]$ sampled in half-steps, and set $\delta = 10$. The reconstruction in physical space for the fourth experiment is shown in Figure 4.3.5. The relative ℓ^2 error in physical space is 1.343×10^{-1} .

4.4 Future Work

While this paper addresses the 1D problem, the extension of this method to the 2D setting is an appealing avenue for future research. Indeed, preliminary results indicate that the underlying discrete method that forms the basis for this paper extends to two dimensions without too much difficulty.

Furthermore, empirical results suggest that the method proposed here demonstrates robustness to noise, although we defer a detailed analysis (and derivation of an associated robust recovery guarantee) to future work.

APPENDIX

Proof of Lemma 1.3.1

Proof. Let $\mathbf{x} \in \mathbb{C}^{d \times 1}$ and $\ell, \omega \in [d]_0$ be arbitrary. We have

$$\begin{aligned}
(F_d \widehat{\mathbf{x}})_\omega &= \sum_{k=0}^{d-1} \widehat{x}_k e^{-\frac{2\pi i k \omega}{d}} = \sum_{k=0}^{d-1} \sum_{n=0}^{d-1} x_n e^{-\frac{2\pi i n k}{d}} e^{-\frac{2\pi i k \omega}{d}} \\
&= \sum_{k=0}^{d-1} \sum_{n=0}^{d-1} x_{-n} e^{\frac{2\pi i k(n-\omega)}{d}} = dx_{-\omega} = (d\widetilde{\mathbf{x}})_\omega, \\
(F_d(W_\ell \mathbf{x}))_\omega &= \sum_{k=0}^{d-1} \left(x_k e^{\frac{2\pi i k \ell}{d}} \right) e^{-\frac{2\pi i k \omega}{d}} = \sum_{k=0}^{d-1} x_k e^{-\frac{2\pi i k(\omega-\ell)}{d}} \\
&= \widehat{\mathbf{x}}_{\omega-\ell} = (S_{-\ell} \widehat{\mathbf{x}})_\omega, \\
(F_d(S_\ell \mathbf{x}))_\omega &= \sum_{k=0}^{d-1} x_{k+\ell} e^{-\frac{2\pi i k \omega}{d}} = \sum_{k=0}^{d-1} x_{k+\ell} e^{-\frac{2\pi i(k+\ell)\omega}{d}} e^{-\frac{2\pi i(-\ell)\omega}{d}} \\
&= e^{\frac{2\pi i \ell \omega}{d}} \widehat{x}_\omega = (W_\ell \widehat{\mathbf{x}})_\omega, \\
(W_{-\ell} F_d(S_\ell \widetilde{\mathbf{x}}))_\omega &= e^{-\frac{2\pi i \ell \omega}{d}} (W_\ell \widehat{\widetilde{\mathbf{x}}})_\omega = (\widehat{\widetilde{\mathbf{x}}})_\omega = \sum_{k=0}^{d-1} \widetilde{x}_k e^{-\frac{2\pi i k \omega}{d}} \\
&= \sum_{k=0}^{d-1} \overline{\widetilde{x}_k e^{\frac{2\pi i k \omega}{d}}} = \sum_{k=0}^{d-1} \overline{x_{-k} e^{\frac{2\pi i k \omega}{d}}} = (\widetilde{\widetilde{\mathbf{x}}})_\omega, \\
(\widetilde{S_\ell \mathbf{x}})_\omega &= \overline{(S_\ell \mathbf{x})_\omega} = \overline{(S_\ell \mathbf{x})_{-\omega}} = \overline{x_{\ell-\omega}} \\
&= \overline{\widetilde{x}_{\omega-\ell}} = (S_{-\ell} \widetilde{\widetilde{\mathbf{x}}})_\omega, \\
(F_d \widetilde{\mathbf{x}})_\omega &= \sum_{k=0}^{d-1} \widetilde{x}_k e^{-\frac{2\pi i k \omega}{d}} = \sum_{k=0}^{d-1} x_k e^{\frac{2\pi i k \omega}{d}} \\
&= \sum_{k=0}^{d-1} \overline{x_{-k} e^{-\frac{2\pi i k \omega}{d}}} = \overline{(F_d \widehat{\mathbf{x}})_\omega}, \\
(\widetilde{\widetilde{\mathbf{x}}})_\omega &= (\widehat{\mathbf{x}})_{-\omega} = \sum_{n=0}^{d-1} x_n e^{\frac{2\pi i n \omega}{d}} = \sum_{n=0}^{d-1} x_{-n} e^{-\frac{2\pi i n \omega}{d}} = (F_d \widehat{\mathbf{x}})_\omega.
\end{aligned}$$

□

Proof of Lemma 2.0.1

Proof. Let $d \in \mathbb{N}$ and suppose $s \in \mathbb{N}$ divides d . Then for any $\mathbf{u} \in \mathbb{C}^{d \times 1}$ and $\omega \in \left[\frac{d}{s}\right]_0$,

$$\begin{aligned}
 \left(F_{\frac{d}{s}}(Z_s \mathbf{u})\right)_\omega &= \sum_{n=0}^{\frac{d}{s}-1} (Z_s \mathbf{u})_n e^{-\frac{2\pi i n \omega}{d/s}} \\
 &= \sum_{n=0}^{\frac{d}{s}-1} u_{ns} e^{-\frac{2\pi i n \omega}{d/s}} \\
 &= \frac{1}{d} \sum_{n=0}^{\frac{d}{s}-1} \left(\sum_{r=0}^{d-1} \hat{u}_r e^{\frac{2\pi i r n s}{d}} \right) e^{-\frac{2\pi i \omega n s}{d}} \\
 &= \frac{1}{d} \sum_{r=0}^{d-1} \hat{u}_r \sum_{n=0}^{\frac{d}{s}-1} e^{\frac{2\pi i n (r-\omega)}{d/s}} \\
 &= \frac{1}{s} \sum_{r=0}^{s-1} \hat{u}_{\omega+r\frac{d}{s}} \\
 &= \frac{1}{s} \sum_{r=0}^{s-1} \hat{u}_{\omega-r\frac{d}{s}}.
 \end{aligned}$$

□

Proof of Lemma 2.0.2

Proof. Let $\mathbf{x} \in \mathbb{C}^{d \times 1}$ and $\alpha, \omega \in [d]_0$ be arbitrary. Observe that

$$\begin{aligned}
 (F_d(\mathbf{x} \circ S_\omega \bar{\mathbf{x}}))_\alpha &= \frac{1}{d} (\hat{\mathbf{x}} *_d F_d(S_\omega \bar{\mathbf{x}}))_\alpha && \text{(by Lemma 1.3.2)} \\
 &= \frac{1}{d} \left(\hat{\mathbf{x}} *_d (W_\omega \hat{\bar{\mathbf{x}}}) \right)_\alpha && \text{(by Lemma 1.3.1(3))} \\
 &= \frac{1}{d} \sum_{n=0}^{d-1} \hat{x}_n (W_\omega \hat{\bar{\mathbf{x}}})_{\alpha-n} && \text{(by definition of } *_d) \\
 &= \frac{1}{d} \sum_{n=0}^{d-1} \hat{x}_n \hat{\bar{x}}_{\alpha-n} e^{\frac{2\pi i \omega (\alpha-n)}{d}} && \text{(by definition of } W_\omega)
 \end{aligned}$$

$$\begin{aligned}
&= \frac{1}{d} e^{\frac{2\pi i \omega \alpha}{d}} \sum_{n=0}^{d-1} \widehat{x}_n \widetilde{x}_{n-\alpha} e^{\frac{-2\pi i \omega n}{d}} && \text{(by definition of } \widetilde{\cdot} \text{)} \\
&= \frac{1}{d} e^{\frac{2\pi i \omega \alpha}{d}} \sum_{n=0}^{d-1} \widehat{x}_n \widetilde{x}_{n-\alpha} e^{\frac{-2\pi i \omega n}{d}} && \text{(by Lemma 1.3.1(6,7))} \\
&= \frac{1}{d} e^{\frac{2\pi i \omega \alpha}{d}} \left(F_d \left(\widehat{\mathbf{x}} \circ S_{-\alpha} \widetilde{\mathbf{x}} \right) \right)_{\omega}.
\end{aligned}$$

□

REFERENCES

REFERENCES

- [1] R. Alaifari, I. Daubechies, P. Grohs, and R. Yin. Stable Phase Retrieval in Infinite Dimensions. *Foundations of Computational Mathematics*, 2018.
- [2] Céline Aubel and Helmut Bölcskei. Vandermonde matrices with nodes in the unit disk and the large sieve. *Applied and Computational Harmonic Analysis*, 2017.
- [3] Radu Balan. Frames and phaseless reconstruction. *Finite Frame Theory: A Complete Introduction to Overcompleteness*, 93:175, 2016.
- [4] Radu Balan, Pete Casazza, and Dan Edidin. On signal reconstruction without phase. *Applied and Computational Harmonic Analysis*, 20(3):345–356, 2006.
- [5] Radu Balan and Dongmian Zou. On Lipschitz analysis and Lipschitz synthesis for the phase retrieval problem. *Linear Algebra and its Applications*, 496(Supplement C):152 – 181, 2016.
- [6] Afonso S Bandeira, Yutong Chen, and Dustin G Mixon. Phase retrieval from power spectra of masked signals. *Information and Inference: a Journal of the IMA*, 3(2):83–102, 2014.
- [7] Heinz H Bauschke, Patrick L Combettes, and D Russell Luke. Phase retrieval, error reduction algorithm, and Fienup variants: A view from convex optimization. *Journal of the Optical Society of America. A, Optics, Image science, and Vision*, 19(7):1334–1345, 2002.
- [8] Stephen Becker, Emmanuel J. Candès, and Michael Grant. Templates for convex cone problems with applications to sparse signal recovery. *Mathematical Programming Computation*, 3(3):165–218, Aug. 2011.
- [9] Stephen Becker, Emmanuel J. Candès, and Michael Grant. TFOCS: Templates for first-order conic solvers, version 1.3.1. <http://cvxr.com/tfocs>, Sep. 2014.
- [10] Tamir Bendory, Yonina C Eldar, and Nicolas Boumal. Non-convex phase retrieval from STFT measurements. *IEEE Transactions on Information Theory*, 64(1):467–484, 2018.
- [11] Oliver Bunk, Ana Diaz, Franz Pfeiffer, Christian David, Bernd Schmitt, Dillip K Satapathy, and Johannes Van der Veen. Diffractive imaging for periodic samples: Retrieving one-dimensional concentration profiles across microfluidic channels. *Acta crystallographica. Section A, Foundations of crystallography*, 63:306–14, 08 2007.

- [12] Jameson Cahill, Peter Casazza, and Ingrid Daubechies. Phase retrieval in infinite-dimensional Hilbert spaces. *Trans. Amer. Math. Soc., Ser. B*, 3(3):63–76, 2016.
- [13] E. J. Candès, X. Li, and M. Soltanolkotabi. Phase retrieval via Wirtinger Flow: Theory and algorithms. *IEEE Transactions on Information Theory*, 61(4):1985–2007, April 2015.
- [14] Emmanuel J Candès, Yonina C Eldar, Thomas Strohmer, and Vladislav Voroninski. Phase retrieval via matrix completion. *SIAM review*, 57(2):225–251, 2015.
- [15] Emmanuel J Candès, Xiaodong Li, and Mahdi Soltanolkotabi. Phase retrieval from coded diffraction patterns. *Applied and Computational Harmonic Analysis*, 39(2):277–299, Sept. 2015.
- [16] Emmanuel J Candès, Thomas Strohmer, and Vladislav Voroninski. Phaselift: Exact and stable signal recovery from magnitude measurements via convex programming. *Commun. Pur. Appl. Math.*, 66(8):1241–1274, 2013.
- [17] Henry N. Chapman. Phase retrieval x-ray microscopy by Wigner-distribution deconvolution. *Ultramicroscopy*, 66(3):153–172, 1996.
- [18] JV Corbett. The Pauli problem, state reconstruction and quantum-real numbers. *Reports on Mathematical Physics*, 57(1):53–68, 2006.
- [19] Martin Dierolf, Andreas Menzel, Pierre Thibault, Philipp Schneider, Cameron M. Kewish, Roger Wepf, Oliver Bunk, and Franz Pfeiffer. Ptychographic x-ray computed tomography at the nanoscale. *Nature*, 467(7314):436–439, Sep 2010.
- [20] Yonina C Eldar, Pavel Sidorenko, Dustin G Mixon, Shaby Barel, and Oren Cohen. Sparse phase retrieval from short-time Fourier measurements. *IEEE Signal Process. Lett.*, 22(5):638–642, 2015.
- [21] C Fienup and J Dainty. Phase retrieval and image reconstruction for astronomy. *Image Recovery: Theory and Application*, pages 231–275, 1987.
- [22] J. R. Fienup. Reconstruction of an object from the modulus of its Fourier transform. *Opt. Lett.*, 3(1):27–29, Jul 1978.
- [23] J. R. Fienup. Phase retrieval algorithms: a comparison. *Appl. Opt.*, 21(15):2758–2769, Aug 1982.
- [24] R.W. Gerchberg and A Saxton W. O. A practical algorithm for the determination of phase from image and diffraction plane pictures. *Optik*, 35:237–250, 11 1971.

- [25] Michael Grant and Stephen Boyd. Graph implementations for nonsmooth convex programs. In V. Blondel, S. Boyd, and H. Kimura, editors, *Recent Advances in Learning and Control*, Lecture Notes in Control and Information Sciences, pages 95–110. Springer-Verlag Limited, 2008. http://stanford.edu/~boyd/graph_dcp.html.
- [26] Michael Grant and Stephen Boyd. CVX: Matlab software for disciplined convex programming, version 2.1. <http://cvxr.com/cvx>, March 2014.
- [27] P. Grohs and M. Rathmair. Stable Gabor Phase Retrieval and Spectral Clustering. *Communications on Pure and Applied Mathematics*, 2018.
- [28] David Gross, Felix Kraemer, and Richard Kueng. Improved recovery guarantees for phase retrieval from coded diffraction patterns. *Applied and Computational Harmonic Analysis*, 42(1):37–64, 2017.
- [29] Robert W. Harrison. Phase problem in crystallography. *J. Opt. Soc. Am. A*, 10(5):1046–1055, May 1993.
- [30] R. Hegerl and W. Hoppe. Dynamische theorie der kristallstrukturanalyse durch elektronenbeugung im inhomogenen primärstrahlwellenfeld. *Berichte der Bunsengesellschaft für physikalische Chemie*, 74(11):1148–1154, 1970.
- [31] W. Hoppe. Beugung im inhomogenen primärstrahlwellenfeld. i. prinzip einer phasenmessung von elektronenbeugungsinterferenzen. *Acta Crystallographica Section A*, 25:495–501, jul 1969.
- [32] A.M.J. Huiser, A.J.J. Drenth, and H.A. Ferwerda. On phase retrieval in electron microscopy from image and diffraction pattern. *Optik (Jena)*, 45:303–316, 07 1976.
- [33] IARPA. Rapid Analysis of Various Emerging Nanoelectronics (RAVEN). <https://www.iarpa.gov/index.php/research-programs/raven/raven-baa>, Jan. 2016.
- [34] Mark Iwen, Yang Wang, and Aditya Viswanathan. BlockPR: Matlab software for phase retrieval using block circulant measurement constructions and angular synchronization, version 2.0. <https://bitbucket.org/charms/blockpr>, April 2016.
- [35] Mark A. Iwen, Sami Merhi, and Michael Perlmutter. Lower Lipschitz bounds for phase retrieval from locally supported measurements. *Applied and Computational Harmonic Analysis*, 2019.
- [36] Mark A. Iwen, Brian Preskitt, Rayan Saab, and Aditya Viswanathan. Phase retrieval from local measurements: Improved robustness via eigenvector-based angular synchronization. *Applied and Computational Harmonic Analysis*, 2018.

- [37] Mark A. Iwen, Aditya Viswanathan, and Yang Wang. Fast phase retrieval from local correlation measurements. *SIAM Journal on Imaging Sciences*, 9(4):1655–1688, 2016.
- [38] Kishore Jaganathan, Yonina C Eldar, and Babak Hassibi. STFT phase retrieval: Uniqueness guarantees and recovery algorithms. *IEEE J. Sel. Topics Signal Process.*, 10(4):770–781, 2016.
- [39] Steven G Johnson. Saddle-point integration of C^∞ “bump” functions. 2015. preprint, arXiv:1508.04376.
- [40] Shuyang Ling and Thomas Strohmer. Self-calibration and biconvex compressive sensing. *Inverse Problems*, 31(11):115002, sep 2015.
- [41] Andrew M. Maiden and John M. Rodenburg. An improved ptychographical phase retrieval algorithm for diffractive imaging. *Ultramicroscopy*, 109(10):1256–1262, 2009.
- [42] Stephane Mallat. *A Wavelet Tour of Signal Processing, The Sparse Way*. Academic Press, 3rd. edition, 2008.
- [43] Stefano Marchesini, Yu-Chao Tu, and Hau-tieng Wu. Alternating projection, ptychographic imaging and phase synchronization. *Appl. Comput. Harmon. Anal.*, 41(3):815–851, 2016.
- [44] Sami Merhi, Aditya Viswanathan, and Mark Iwen. Recovery of compactly supported functions from spectrogram measurements via lifting. In *2017 International Conference on Sampling Theory and Applications (SampTA) (SampTA2017)*, Tallinn, Estonia, July 2017.
- [45] R. P. Millane. Phase retrieval in crystallography and optics. *J. Opt. Soc. Am. A*, 7(3):394–411, Mar 1990.
- [46] S Nawab, T Quatieri, and Jae Lim. Signal reconstruction from short-time Fourier transform magnitude. *IEEE Trans. Acoust., Speech, Signal Process.*, 31(4):986–998, 1983.
- [47] Goetz E Pfander and Palina Salanevich. Robust phase retrieval algorithm for time-frequency structured measurements. 2016. preprint, arXiv:1611.02540.
- [48] Brian Preskitt. *Phase Retrieval from Locally Supported Measurements*. PhD thesis, UC San Diego, 2018.
- [49] J. Rodenburg and R. Bates. The theory of super-resolution electron microscopy via Wigner-distribution deconvolution. *Philosophical Transactions of the Royal Society of London. Series A: Physical and Engineering Sciences*, 339(1655), Jun 1992.

- [50] J. Rodenburg, B. McCallum, and P. Nellist. Experimental tests on double-resolution coherent imaging via stem. *Ultramicroscopy*, 48(3):304–314, 1993.
- [51] J. M. Rodenburg and H. M. L. Faulkner. A phase retrieval algorithm for shifting illumination. *Applied Physics Letters*, 85(20):4795–4797, 2004.
- [52] JM Rodenburg. Ptychography and related diffractive imaging methods. *Advances in Imaging and Electron Physics*, 150:87–184, 2008.
- [53] Palina Salanevich and Götz E Pfander. Polarization based phase retrieval for time-frequency structured measurements. In *Proc. 2015 Int. Conf. Sampling Theory and Applications (SampTA)*, pages 187–191, 2015.
- [54] E. Stade. *Fourier Analysis*. Pure and Applied Mathematics: A Wiley Series of Texts, Monographs and Tracts. Wiley, 2011.
- [55] Thomas Strohmer and Jared Tanner. Implementations of Shannon’s sampling theorem, a time-frequency approach. *Sampling Theory Signal Image Process.*, 4(1):1–17, 2005.
- [56] Nicolas Sturmel and Laurent Daudet. Signal reconstruction from STFT magnitude: A state of the art. In *Int. Conf. Digital Audio Effects (DAFx)*, pages 375–386, 2011.
- [57] Gaurav Thakur. Reconstruction of bandlimited functions from unsigned samples. *J. Fourier Anal. Appl.*, 17(4):720–732, 2011.
- [58] I. Waldspurger. Phase retrieval with random Gaussian sensing vectors by alternating projections. *IEEE Transactions on Information Theory*, 64(5):3301–3312, May 2018.
- [59] Adriaan Walther. The question of phase retrieval in optics. *Journal of Modern Optics*, 10(1):41–49, 1963.
- [60] Guoan Zheng, Roarke Horstmeyer, and Changhui Yang. Wide-field, high-resolution Fourier ptychographic microscopy. *Nature photonics*, 7(9):739, 2013.